Effect of Atmospheric Pressure Plasma Treatment on Surface Characteristics and Adhesive Bond Quality of Peel Ply Prepared Composites

Ashley C. Tracey

A dissertation
submitted in partial fulfillment of the
requirements for the degree of

Doctor of Philosophy

University of Washington

2014

Reading Committee:

Brian D. Flinn, Chair
Guozhong Cao
Dwayne D. Arola
Marcus A. (Tony) Belcher

Program Authorized to Offer Degree:

Materials Science and Engineering

University of Washington

Abstract

Effect of Atmospheric Pressure Plasma Treatment on Surface Characteristics and Adhesive Bond Quality of Peel Ply Prepared Composites

Ashley C. Tracey

Chair of the Supervisory Committee:
Dr. Brian D. Flinn, Research Associate Professor
Materials Science and Engineering

The purpose of this research was to investigate if atmospheric pressure plasma treatment could modify peel ply prepared composite surfaces to create strong adhesive bonds. Two peel ply surface preparation composite systems previously shown to create weak bonds (low fracture energy and adhesion failure) that were potential candidates for plasma treatment were Toray T800/3900-2 carbon fiber reinforced polymer (CFRP) prepared with Precision Fabrics Group, Inc. (PFG) 52006 nylon peel ply and Hexcel T300/F155 CFRP prepared with PFG 60001 polyester peel ply. It was hypothesized that atmospheric pressure plasma treatment could functionalize and/or remove peel ply remnants on the CFRP surfaces to improve adhesion.

Surface characterization measurements and double cantilever beam (DCB) testing were used to determine the effects of atmospheric pressure plasma treatment on surface characteristics and bond quality of peel ply prepared CFRP composites. Previous research showed that Toray T800/3900-2 carbon fiber reinforced epoxy composites prepared with PFG 52006 peel ply and bonded with Cytec MetlBond 1515-3M structural film adhesive failed in adhesion at low fracture energies when tested in the DCB configuration. Previous research also showed that DCB samples made of Hexcel T300/F155 carbon fiber reinforced epoxy composites prepared with PFG 60001 peel ply and bonded with Henkel Hysol EA 9696 structural film adhesive failed in

adhesion at low fracture energies. Recent research suggested that plasma treatment could be able to activate these "un-bondable" surfaces and result in good adhesive bonds. Nylon peel ply prepared 177 °C cure and polyester peel ply prepared 127 °C cure CFRP laminates were treated with atmospheric pressure plasma after peel ply removal prior to bonding.

Atmospheric pressure plasma treatment was capable of significantly increasing fracture energies and changing failure modes. For Toray T800/3900-2 laminates prepared with PFG 52006 and bonded with MetlBond 1515-3M, plasma treatment increased fracture energies from < 200 J/m^2 to > 460 J/m^2. Atmospheric pressure plasma treatment also increased fracture energies of Hexcel T300/F155 laminates prepared with PFG 60001 and bonded with EA 9696 from < 280 J/m^2 to > 1500 J/m^2. It was demonstrated that atmospheric pressure plasma treatment was able to transform poor bonding surfaces into acceptable ones by reversing the negative effects of incorrect peel ply usage.

To determine if the primary reason for adhesion was functionalization or removal, a number of experiments were performed. Surface characteristics of peel ply only and plasma treated samples were determined using contact angle (CA) measurements, FTIR spectroscopy, X-ray photoelectron spectroscopy (XPS), and scanning electron microscopy (SEM). CA was used to assess solid surface energy that was useful to determine wetting of the adhesive on the adherend, one requirement of adhesion. FTIR and XPS were used to analyze composite surface chemistry, including the identification of functional groups that were a product of atmospheric pressure plasma treatment, as well as contaminants that could inhibit adhesive bonding. SEM was used to capture surface morphology to identify peel ply remnants and whether these remnants were physically removed or modified due to plasma treatment. This research supported that atmospheric pressure plasma treatment resulted in adhesion primarily due to functionalization of

peel ply remnants, though a removal mechanism was not eliminated. It was also shown that surface energy exhibited potential for predicting adhesion. Lastly, this research indicated that plasma treatment is a robust surface preparation, as strong bonds were observed up to 30 days after treatment.

TABLE OF CONTENTS

LIST OF FIGURES

LIST OF TABLES

Dedication

To my family and friends, without whom this would not have been possible.

CHAPTER 1: INTRODUCTION

1.1 Motivation

Structural joints, though necessary in the design of structures, unavoidably form localized stresses due to discontinuities. One way to minimize these stresses is to use adhesively bonded joints rather than mechanically fastened joints. In comparison to mechanical fasteners, bonding reduces stress concentrations, reduces weight, and eliminates the need for sealants to protect against environmental damage. Additionally, bonded joints can be designed to take advantage of the ductile response to loading of the adhesive.[1] With composite content increasing in aircraft such as the Boeing 787 and Airbus A350, structural adhesive bonds are being used to increase the design space. Though there are many advantages of bonding, commercially available technology to measure adhesive bond quality without destroying the bond is lacking. As such, bonds currently must be certified through strict process control.

There are three basic bonding processes: cocuring, cobonding, and secondary bonding. The bonding of uncured materials is termed cocuring. An example of this is the curing of a composite laminate. As long as the material is fresh, cocures typically result in strong bonds because the polymer matrix is able to crosslink and form chemical bonds between lamina. Cobonding occurs when one adherend is uncured and the other adherend is fully cured (crosslinked) prior to bonding. Cobonding is thus more sensitive to surface characteristics of the cured adherend because there is a lack of uncured polymer at the surface to bond with the uncured polymer. Secondary bonding occurs when both adherends are cured prior to bonding. This type of bond is sensitive to the surface characteristics of both adherends as there is an absence of uncured polymer at the surfaces to bond with the uncured adhesive. Adhesive joints, particularly those

that are cobonded or secondarily bonded, are highly sensitive to the manufacturing process, including bonding technique, mating of parts, and environmental effects on the adhesive itself (i.e. moisture).[2] Scientists state that adhesive bonding predominantly depends on the formation of primary chemical bonds and less on mechanical factors.[1,3] Jesson and Watts, however, point out that though speculation in the literature is that primary bonds may form between the two phases, there is no unambiguous analytical evidence that supports this claim.[4] These authors attribute adhesion mostly to van der Waals bonding and some Lewis acid-base interactions.[4] Whatever the mechanism of adhesion or type of bonding, it is obvious that adhesive bonds depend on the chemistry of the interface and control of surface chemistry is critical to bond quality.[1,5] Thus, the most important step in cobonding and secondary bonding is surface preparation, which prevents or removes contaminants that can adversely affect bonding while also creating chemically active sites to maximize bond strength.

Multiple surface preparations for composite materials exist and will be discussed in a later section. Some combinations of composite adherend, surface preparation, and adhesive result in strong bonds whereas others do not. This research aims to understand how a previously poor bonding surface can become a good bonding surface after atmospheric pressure plasma treatment.

1.2 Research Plan

The overall goal of this research was to investigate if atmospheric pressure plasma treatment could modify Toray T800/3900-2 CFRP prepared with PFG 52006 to create a strong bond with MetlBond 1515-3M film adhesive. This required the analysis of two peel ply surface preparation composite systems previously shown to create weak bonds (low fracture energy and adhesion failure).[6] These systems were 177 °C (350 °F) cure Toray T800/3900-2 CFRP prepared with PFG 52006 nylon peel ply and 127 °C (260 °F) cure Hexcel T300/F155 CFRP prepared with

PFG 60001 polyester peel ply. Toray T800/3900-2 laminates were bonded with MetlBond 1515-3M and Hexcel T300/F155 laminates were bonded with Hysol EA 9696. It was hypothesized that atmospheric pressure plasma treatment could functionalize and/or remove peel ply remnants left on the CFRP surfaces upon peel ply removal to improve adhesion of these laminates.

The main difference between the Toray T800/3900-2 and the Hexcel T300/F155 surfaces was the amount of peel ply residue transfer. As will be shown, the incompatible PFG 52006 peel ply surface on the Toray T800/3900-2 composite was difficult to characterize, whereas the incompatible PFG 60001 peel ply surface on the Hexcel T300/F155 composite was easily identified. Examination and characterization of both material systems with and without subsequent atmospheric pressure plasma treatment in addition to other experiments revealed how plasma treatment was shown to change a poor bonding surface to an acceptable one.

1.2.1 Document Organization

This chapter introduced motivation for this project – determining if atmospheric pressure plasma treatment of nylon peel ply prepared Toray T800/3900-2 composites removes and/or functionalizes the surface to improve adhesion with MetlBond 1515-3M film adhesive.

The remainder of this dissertation is divided into six additional chapters. Chapter 2 discusses relevant background information for composite surface preparation and bonding. Chapter 3 outlines the research proposal. Chapter 4 details the experimental procedure. Chapter 5 discusses results and Chapters 6 and 7 are overall conclusions and future work, respectively.

CHAPTER 2: BACKGROUND

2.1 Epoxy Composite Fundamentals

The materials examined during this research were carbon fiber (woven and unidirectional) reinforced epoxy matrix composites. Surface preparation was performed on the epoxy rich surfaces to promote adhesion. The studied surface preparation methods included combinations of peel ply and atmospheric pressure plasma treatment. A basic comprehension of epoxy chemistry and the cure reaction thereof is helpful to understand how the surfaces are changed due to surface preparation and how this would encourage adhesion.

2.1.1 Basic Epoxy Chemistry and Curing

An epoxy resin is a thermosetting polymer comprised of covalently crosslinked chains that form a three-dimensional network structure (Figure 1). [7,8] An epoxy linkage is formed when an epoxide functional group is reacted with a curing agent. To explain the curing mechanism, a basic model system will be referenced. Diglycidyl ether of bisphenol-A (DGEBA) has two reactive epoxide sites. The epoxides are the triangular ring structures composed of two carbon atoms and one oxygen atom shown in Figure 2. Diethylenetriamine (DETA) is a common curing agent that has five amino hydrogens available with which the epoxides can react (Figure 2). [9]

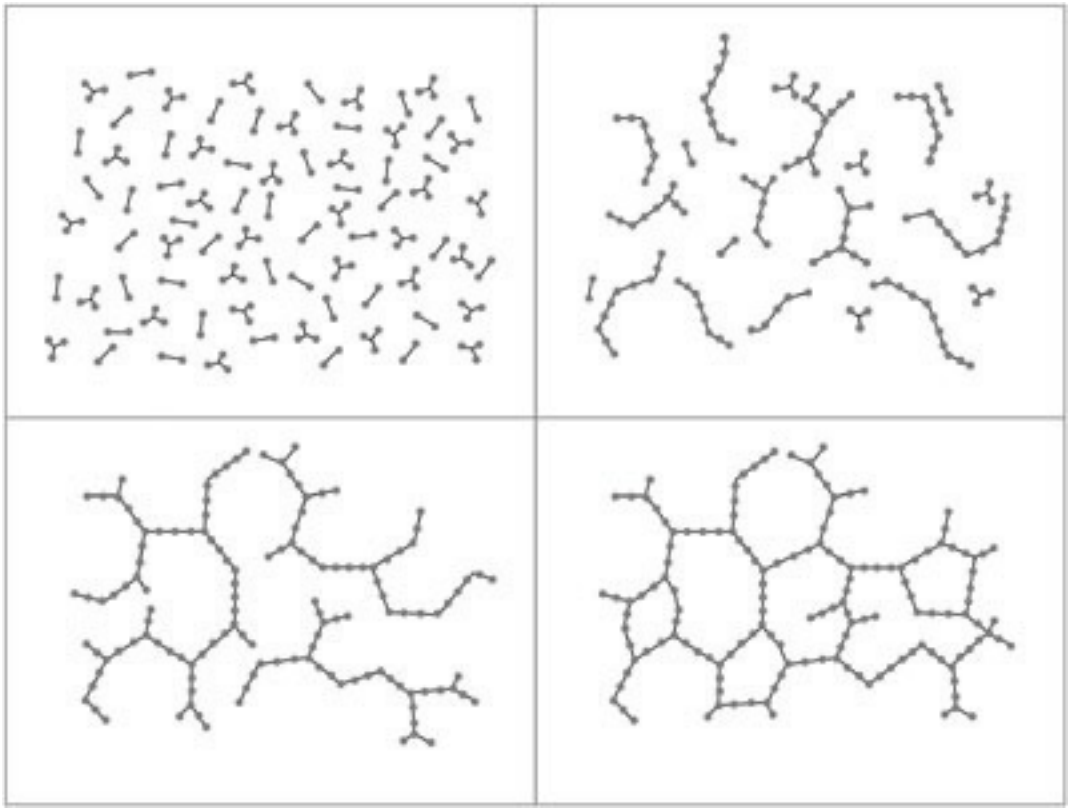

Figure 1. Two-dimensional schematic showing the cure of a thermoset, starting with monomers and ultimately yielding a crosslinked network structure. [10]

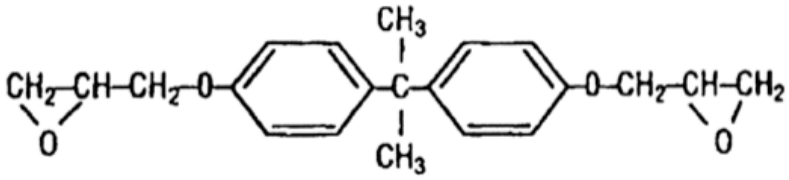

(a)

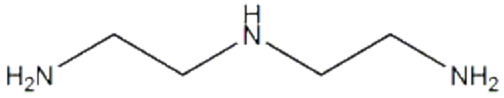

(b)

Figure 2. (a) DGEBA and (b) DETA molecules. [9,11]

During the cure of an epoxy, the epoxide ring opens and reacts with an amine to form a secondary amine with a pendant hydroxyl. [12] The secondary amine can then react with another

epoxide to form a tertiary amine. [12] This reaction is shown in Figure 3. The epoxide could also react with the pendant hydroxyl, though reaction with the amine is preferential. [13]

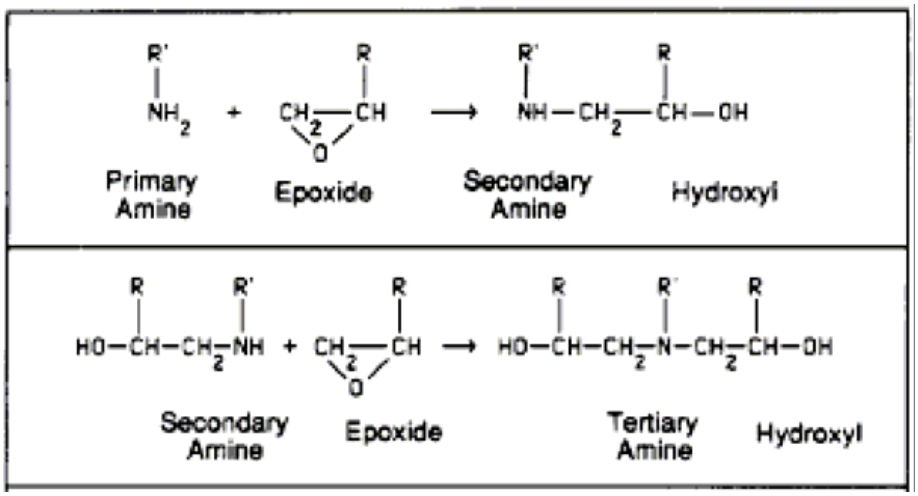

Figure 3. Epoxy cure reaction. [12]

2.2 Surface Preparation Methods

Several composite surface preparation methods exist to improve adhesion of polymer composites. Some of these surface preparations include peel ply, abrasive methods (sanding, grit blasting), and energetic methods (laser ablation, plasma treatment, corona discharge). [2,11,14,15,16,17,18,19,20,21] The surface preparations of interest for this research were peel ply and atmospheric pressure plasma treatment, and combinations thereof.

2.2.1 Peel Ply

A peel ply is a polymer fabric, such as polyester or nylon. It is the last layer applied to a composite part before cure and is removed directly before bonding. During cure, resin from the composite infiltrates the peel ply fabric. A cross section of peel ply preparation on a composite surface is shown in Figure 4. [6] Removal of the peel ply subsequently destroys this mechanical

bond formed during cure, resulting in a textured surface free of gross environmental contamination. Peel ply is an attractive surface preparation method because it typically creates repeatable and consistent surfaces. Figure 5 shows an electron micrograph of a peel ply prepared composite surface.

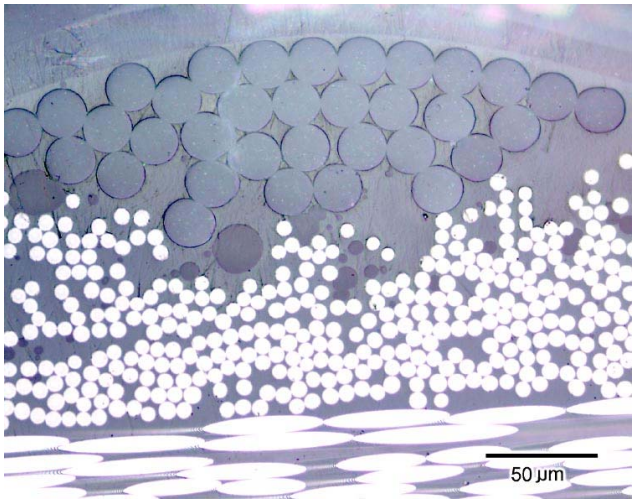

Figure 4. Cross section image of a peel ply prepared composite, where the larger diameter dark gray circles are peel ply fibers and the smaller diameter white circles are carbon fibers. [6]

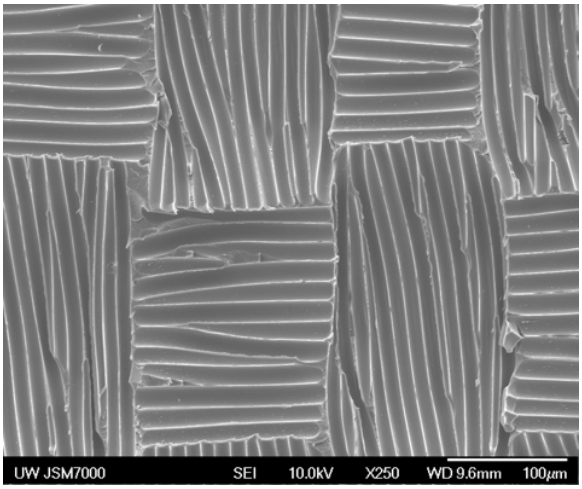

Figure 5. Electron micrograph of a peel ply prepared surface.

Though peel ply is attractive due to its consistency and repeatability, there exists some opposition to the use of peel ply, especially nylon peel plies, without subsequent abrasive techniques. [22] This is because peel ply material changes the surface characteristics of the composite. Upon removal of peel ply from a cured composite, the resultant surface is an interphase that is a function of both the peel ply and resin materials. Peel ply prepared composites can also leave behind physical remnants from the peel ply on the surface. Previous XPS analyses of peel ply prepared epoxy composite surfaces support this claim. [23] XPS results showed different concentrations of carbon, oxygen, nitrogen, and silicon based on different peel ply surface preparation methods. [23] Control epoxy surfaces (i.e., composites cured without peel ply) had the highest concentration of carbon while polyester peel ply prepared surfaces showed the largest concentration of oxygen, and nylon prepared surfaces had the greatest nitrogen concentration while super release blue (SRB; a polyester peel ply with siloxane release coating to aid in peel ply removal) surfaces had the highest silicon concentration. [23] Each combination of composite, surface preparation, and adhesive must be validated together as a system to ensure an optimum bond. [22] Additional research confirmed by SEM that peel ply residue was transferred onto epoxy composite surfaces after peel ply removal. [6] This research suggested that poor bonding was the result of either chemical incompatibility or the thickness of the remnants/interphase from peel ply removal. [6]

Other studies also support the material system specificity of peel ply surface preparation. [22,23,24,25] For example, previous research showed that different peel ply types applied to CFRP adherends resulted in different failure modes and Mode I strain energy release rates (G_{IC}) when bonded with MetlBond 1515-3M film adhesive. [23] **Table 1** shows the failure modes and G_{IC} values for polyester, nylon, and SRB peel ply preparations. [23] The images are of mating halves

of bonded specimens. The Mode I strain energy release rate (G_{IC}) and failure modes were determined using the DCB test configuration. [23] Failure modes for composites are defined by ASTM D5573 (Figure 6) and can be classified generally as failure of adhesion, cohesive failure of the substrate (interlaminar and intralaminar), and cohesive failure of the adhesive. [26] Cohesive failure modes are desired, whereas adhesion failure modes are not. Failure modes will be discussed in further detail in a following section. Toray T800/3900-2 CFRP adherends prepared with nylon and SRB peel plies failed in adhesion at low fracture energies when bonded with MetlBond 1515-3M film adhesive. The same CFRP prepared with polyester peel ply and bonded with the same adhesive failed cohesively within the adhesive at fracture energies more than eight times those observed for nylon and SRB prepared surfaces.

Table 1. DCB fracture surfaces of peel ply surfaces bonded with MB1515-3M adhesive. [23]

	Polyester Prepared	Nylon Prepared	SRB Prepared
		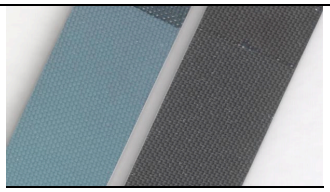	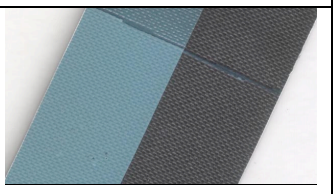
Failure Mode	Cohesive	Adhesion	Adhesion
G_{IC}	812±35 J/m^2	122±15 J/m^2	< 94 J/m^2

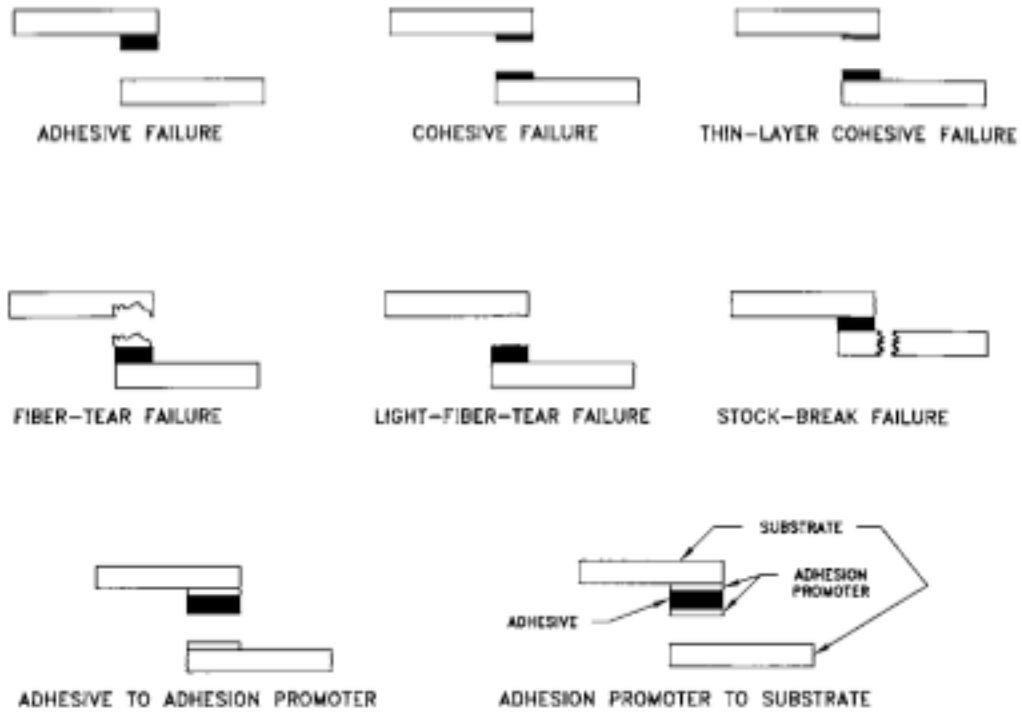

Figure 6. ASTM D5573 composite failure modes. [26]

This research also showed that the same adherends (Toray T800/3900-2) prepared with polyester, nylon, and SRB peel plies and bonded with AF 555M epoxy film adhesive failed similarly for polyester and SRB preparation as those bonded with MetlBond 1515-3M epoxy film adhesive, but differently for those prepared with nylon peel ply. [23] The adherends prepared with nylon peel ply and bonded with AF 555M film adhesive exhibited cohesive and interlaminar failure modes and higher fracture energies than adherends bonded with MetlBond 1515-3M. [23] This suggested that there is a chemical incompatibility between the nylon peel ply CFRP surface and MetlBond 1515-3M, as adherends bonded with both epoxy adhesives were prepared the same way.

2.2.2 Plasma Treatment

In situations where the incorrect peel ply might be used, additional surface preparation, such as abrasive or energetic techniques, are required to produce an acceptable surface for bonding. One type of energetic technique that shows real potential is atmospheric pressure plasma treatment. In addition to eliminating downstream wastes from subsequent surface preparation, plasma treatment can be automated, thus reducing process variability and increasing both reliability and processing rates. [27] Atmospheric pressure plasma is of particular interest to the aerospace industry because it does not require a vacuum chamber to control pressure for consistent surface treatment. [28] Therefore, costly and size prohibiting vacuum systems are unnecessary leading to more versatile processing.

Plasma is a partially ionized gas composed of unbound electrons, electrically charged ions, and neutral atoms and molecules, molecular fragments, and excited molecules. [28,29,30] Plasma is a chemically active medium [28] capable of altering the surface energy of a material. **Figure 7** shows a relative comparison for solids, liquids, gases, and plasmas in terms of chemical species, energy, and temperature. [30] Unlike solids, liquids, and gases, which mostly carry energy in the form of heat or kinetic energy, plasma also carries energy due to the splitting of electrons from nuclei generating ions and free electrons. [31] Thus, plasma can be highly energetic and simultaneously low temperature. [31]

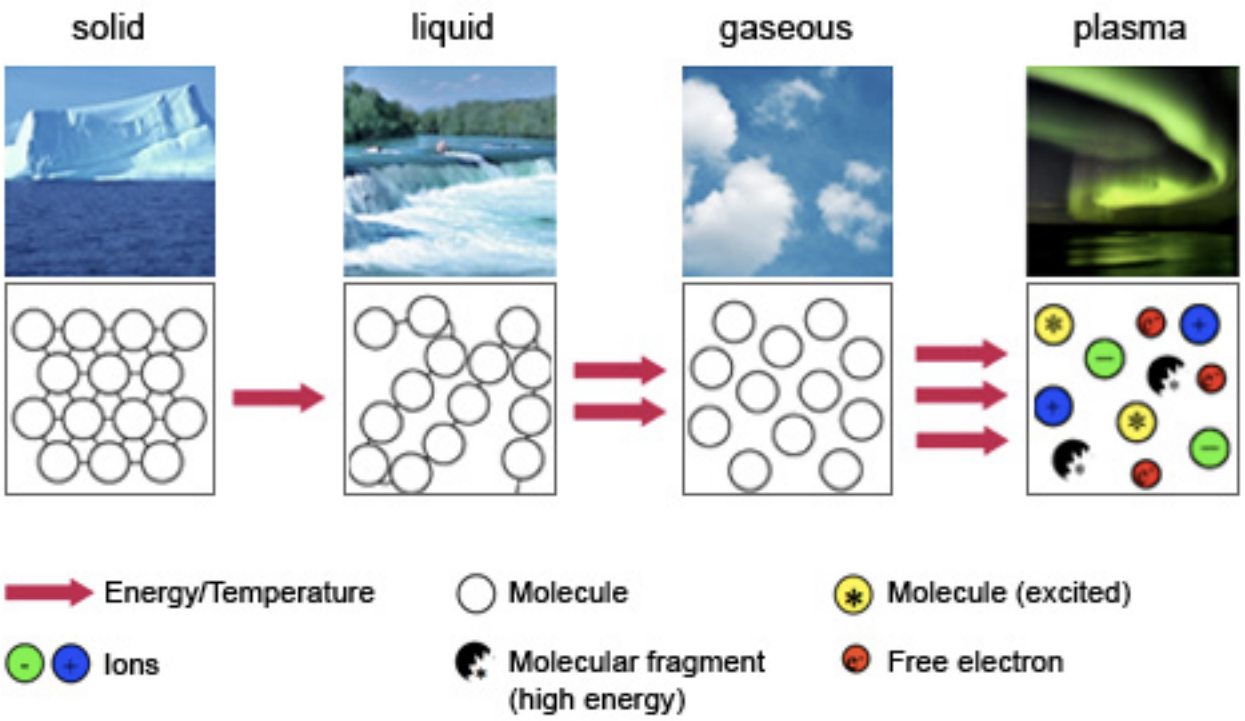

Figure 7. Comparison of solids, liquids, gases, and plasmas. [30]

Plasma can be thermal (high temperature) or non-thermal (cold/low temperature). [31,32] Thermal plasmas have high electron densities. [32] Inelastic collisions between electrons and heavy particles are responsible for creating the plasma reactive species, while elastic collisions are responsible for heating the heavy particles. [32] Examples of thermal plasmas include flames, arc plasma, and nuclear explosions. [31,32] Thermal plasma is destructive and thus not applicable as a surface treatment method for polymers. [31] Non-thermal plasma, however, finds application as a polymer processing technique and has been used extensively throughout literature, especially for thermoplastic surface preparation. [33,34,35,36] Contrary to thermal plasmas, non-thermal plasmas have lower electron densities. [32] Inelastic collisions between electrons and heavy particles are responsible for creating the plasma reactive species and heavy particles are only heated slightly by elastic collisions. [32] One type of non-thermal plasma that has been applied with success to

both thermoplastics and thermosets and is thus the focus of this research is atmospheric pressure plasma.

To create atmospheric pressure plasma, sufficient electric current is passed through a gas at ambient conditions. [28] This initiates the ionization process, which is the gain or loss of electrons by the gas molecules. [28] The resultant plasma can interact with a surface causing the following effects: (1) ablation or etching, (2) removal of organics, (3) crosslinking of surface species, and (4) reconstructing of surface chemistry. [28] The bombardment of a polymer surface with free radicals, electrons, ions, and radiation can break covalent bonds in the polymer backbone, creating lower molecular weight polymer chains. [28] As the chains get smaller, volatile monomers and oligomers are vaporized and carried away with the exhaust. [28] This is the process of ablation, which results in removal of organics. When an inert gas is used, there are no free radicals in the plasma for the broken bonds to interact with, so free radicals on the polymer chains react with each other, resulting in crosslinking of the surface. [28] In both cases, the surface chemistry is altered. Surface reconstruction occurs after free radical effects that are initiated by highly reactive species in a high-density atmospheric pressure plasma. [28] This creates polar functional groups on the surface that are generally believed to encourage adhesion between the substrate and an adhesive, including as-tooled (cured against a fluorinated release film) carbon and glass fiber toughened epoxy composites. [28,34,35,37]

There are five key variables of atmospheric pressure plasma believed to affect adhesion capabilities. [28] These are (1) substrate material, (2) pretreatment of the substrate, (3) power density of the surface post-treatment (power setting relative to discharge assembly length, raster speed, and power level), (4) chemistry of surface treatment (types and proportions of gas chemistries), and (5) adhesive/paint/ink chemistry. [28]

Atmospheric pressure plasma treatment has been applied to numerous polymer substrates and published throughout the literature. One study showed that atmospheric pressure plasma treatment of polyethylene terephthalate, polyamide 6, polyvinylidene fluoride, high-density polyethylene, and polypropylene resulted in increased bond strength and changed failure modes from predominantly adhesion failure to only cohesive or substrate failure. [33] Lap shear samples were bonded with a two-part polyurethane resin and XPS results showed the formation of different oxygen containing functional groups on the surface of treated substrates relative to untreated substrates. [33] The authors speculated that the formation of these additional functional groups on the surface were "probably the most significant contribution to the adhesion improvements." [33]

A study on polyolefins (high-density polyethylene, low-density polyethylene, and polypropylene) showed improved wetting and surface energy increases after atmospheric pressure plasma treatment. [34] They suggested the resulting introduction of polar functional groups (carboxyl, carbonyl, hydroxyl, and amide) may have improved adhesion properties of polyolefins. [34] Another study on polypropylene bonded with polyurethane showed that atmospheric plasma treatment increased apparent shear strength and resulted in cohesive failure modes. [35] Untreated polypropylene bonded with polyurethane failed in adhesion at lower shear strengths. [35] The authors attributed the increase in bond quality to chemical moieties with polar components, specifically with electron-donor character (e.g. amine, imine, ketone, ester, alcohol functionalities), as measured by contact angles (surface energy), FTIR, and XPS. [35] Another study used static-secondary ion mass spectrometry (static-SIMS) to examine atmospheric pressure air plasma treatment of polypropylene films. [36] The researchers found that the detected

ions reflected the formation of oxygen functional groups both on pendant groups and within the polymer chain. [36]

More recent studies on atmospheric pressure plasma applied to composites have also shown promising results. One study showed an increase in apparent shear strength of bonded carbon fiber epoxy composite substrates with an increase in the number of atmospheric plasma treatment scans, and thus increase in oxygen functional groups on the surface (Figure 8). [19] The composite resin system was a semi-interpenetrating network made of a multifunctional epoxy and reactive thermoplastic modifier to increase toughness. [19] Single lap shear (SLS) specimens were bonded with Henkel Hysol EA 9394 epoxy paste adhesive. [19] The researchers also found that hydrophilicity increased with the number of plasma scans and that this increase correlated well with previous studies that attributed the greater hydrophilicity to the addition of polar functional groups onto the surface, such as hydroxyls, carboxyls, and peroxides. [19] This increase in hydrophilicity due to the addition of polar groups was also supported by both XPS and FTIR results. [19]

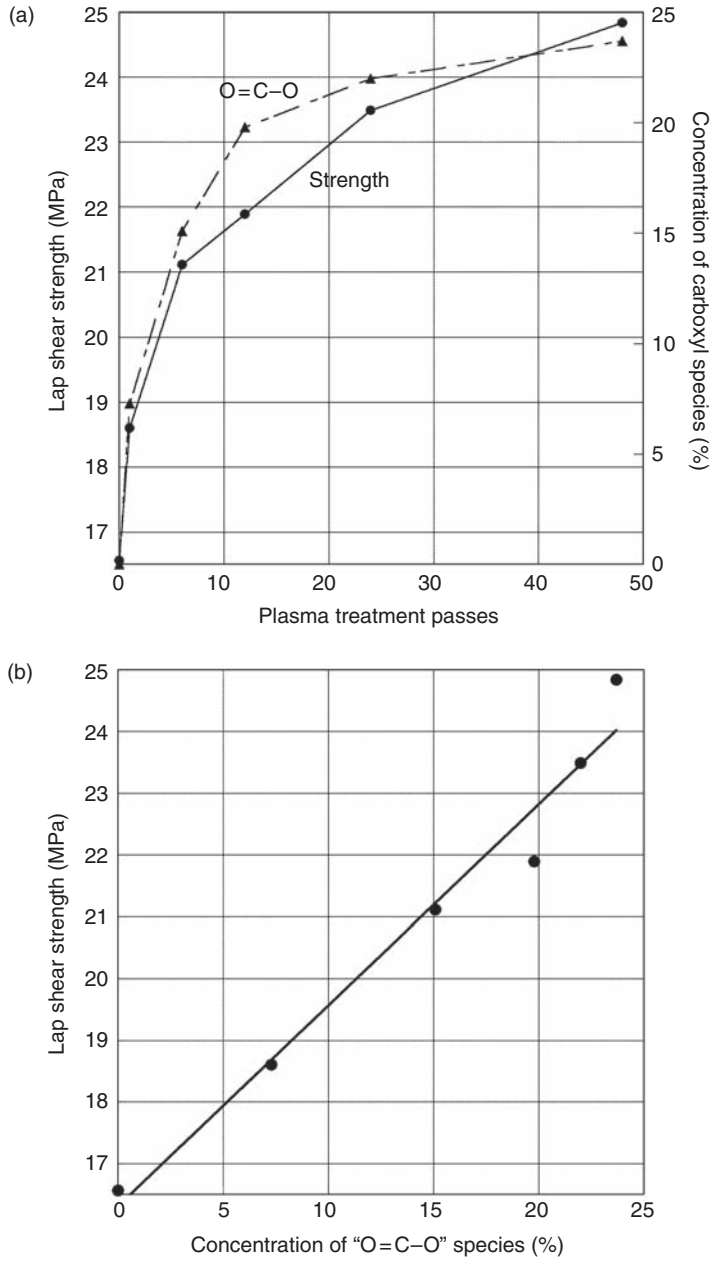

Figure 8. (a) Lap shear strength as a function of number of plasma treatment passes and concentration of carboxyl groups, and (b) relationship between lap shear strength and carboxyl group concentration. [19]

An additional study on glass fiber and carbon fiber reinforced epoxy matrix composites showed that atmospheric pressure plasma treated samples displayed cohesive and interlaminar failure

modes when tested in the DCB configuration and bonded with a modified epoxy adhesive (Henkel Hysol EA 9696). [37] They suggested that atmospheric pressure plasma promoted the integration of oxygen functional groups, such as hydroxyls, esters, and acids, onto the surface and that these functional groups cause the formation of strong interfacial bonding. [37] They also suggested that the presence of oxygen functional groups could be quantified with polar surface energy. [37]

At the Universidad Rey Juan Carlos, one researcher studied how atmospheric pressure plasma treatment modified the surface of composite materials prepared with various release agents. [31] He examined two carbon fiber epoxy prepreg systems (Cytec-Cycom 977-2/HTS and Hexcel Hexply 8552/AS4) prepared with various releases (release film, solvent based release agent, and released nylon peel ply). [31] He subsequently treated the surface with either atmospheric pressure plasma or abraded the surface and compared these techniques as a means for contamination removal, and surface activation. [31] Serrano showed that atmospheric pressure plasma treatment significantly increased the atomic concentration of oxygen on the surfaces and decreased the concentration of contaminants (Si, F) on the Cytec-Cycom 977-2/HTS composite surfaces that were prepared initially with the release film and release agent. [31] He also observed a slight increase in surface roughness. [31] This change in surface characteristics caused a significant increase in fracture energy (DCB test) and strength (SLS test) as well as nearly 100% cohesive failure for DCB specimens. [31] G_{IC} measurements of plasma treated surfaces were comparable to abraded surfaces. [31] Samples were bonded with Henkel Hysol EA 9695 epoxy film adhesive. [31] Serrano attributed this improved bond quality to increased surface wettability due to partial removal of contaminants and increased concentration of oxygen containing groups. [31]

Similar results were observed for Hexcel Hexply carbon fiber epoxy composite surfaces that were prepared with release film, release agent, and released nylon peel ply. [31] However, for the released nylon peel ply prepared surface, a flatter surface was observed after atmospheric pressure plasma (Figure 9) and the author suggested that the roughness due to the peel ply imprint in addition to the surface activation and cleaning created a surface that was responsible for improved adhesion performance. [31]

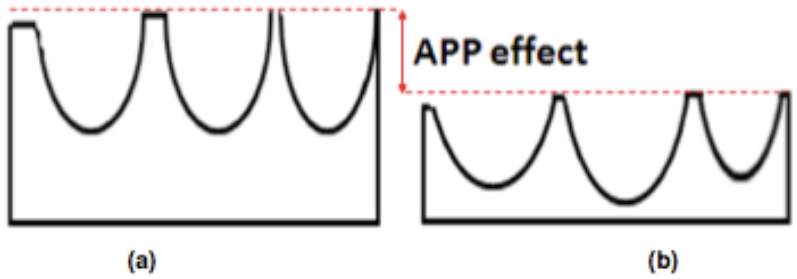

Figure 9. Schematic of a side-view of the released nylon peel ply surface (a) before and (b) after atmospheric pressure plasma treatment**. [31]**

Another study also showed atmospheric pressure plasma treatment increased the surface energy of Zinc Chromate primer coated aluminum substrates and suggested there was "conclusive evidence" that plasma treatment increased the surface energy of some low energy polymer surfaces. [38] They stated that the increase in surface energy was generally attributed to the increased concentration of surface functional groups, such as amines and imines. [38]

Studies on the influence of atmospheric pressure plasma treatment on bond quality suggested this technique would remove contaminants and increase active bonding sites on polymer surfaces, such as composites potentially prepared with an incorrect peel ply material. Note that the peel plies studied in this research were not released like the one studied by Serrano.

2.3 Surface Analysis Techniques

The specificity of composite and adhesive materials on bond quality is true for other surface preparations aside from peel ply and plasma. Surface characteristics and bond quality can change depending on type of abrasive paper/cloth, grit blast media material or size, and laser preparation parameters used. [14,15,17,19] Because of this specificity, a model to guide bonding based on surface preparation, materials properties, and surface characterization is desired. There are many characterization techniques available, including X-ray photoelectron spectroscopy (XPS), time of flight secondary ion mass spectroscopy (TOF-SIMS), surface energy measurements (e.g. inverse gas chromatography (IGC), contact angle (CA) measurements), Fourier transform infrared (FTIR) spectroscopy, scanning electron microscopy (SEM), and energy dispersive spectroscopy (EDS). Though these are known as surface characterization techniques, it should be noted that each technique has different interaction volumes yielding surface information from various depths into the material. The interaction volume of the above listed techniques as well as other surface analysis techniques are shown in Figure 10. [39]

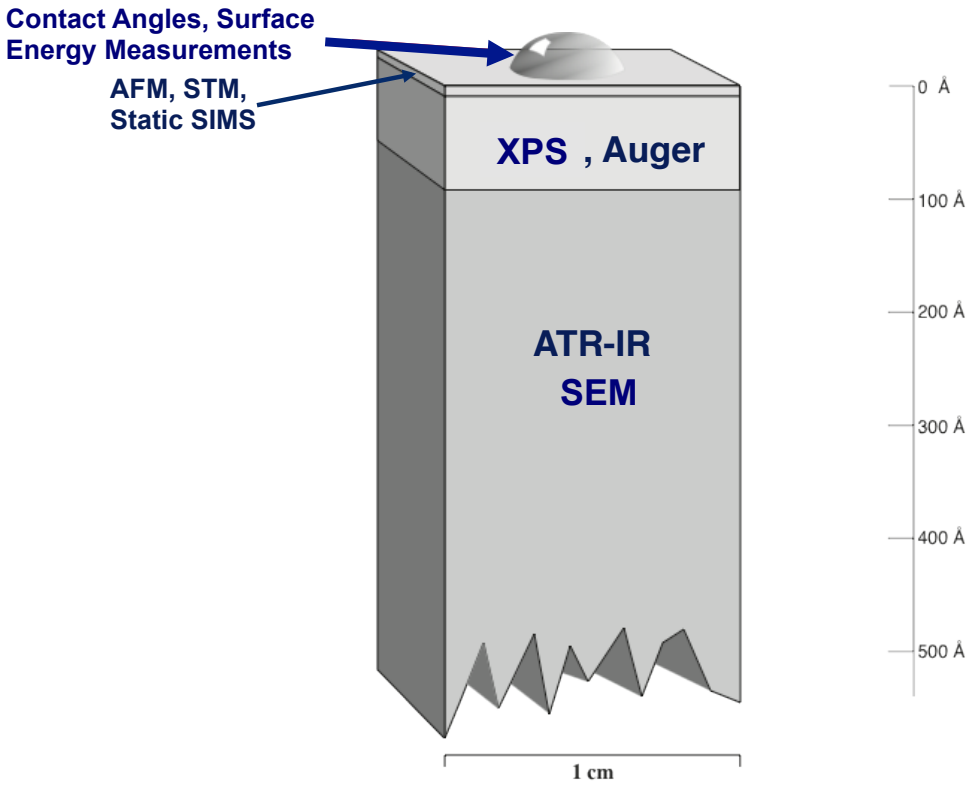

Figure 10. Interaction volume comparison for surface analysis methods. [39]

2.3.1 X-ray Photoelectron Spectroscopy

XPS is an electron spectroscopy considered by many to be the "workhorse" of surface chemical analysis. [4] The sample is placed under ultra-high vacuum conditions and irradiated with low energy X-rays, causing the sample to emit photoelectrons (Figure 11). [4] The photoelectrons are analyzed by energy and plots of intensity as a function of electron binding energy are generated, providing chemical information about the surface, excluding the detection of hydrogen. [40] An example XPS spectrum of a glass fiber reinforced composite is shown in Figure 12. [40] The spectrum shows photopeaks for carbon and oxygen, as well as Auger peaks from carbon and oxygen. [40] The carbon peaks come from the ionization of C 1s core level electrons, as shown in Figure 13. [40]

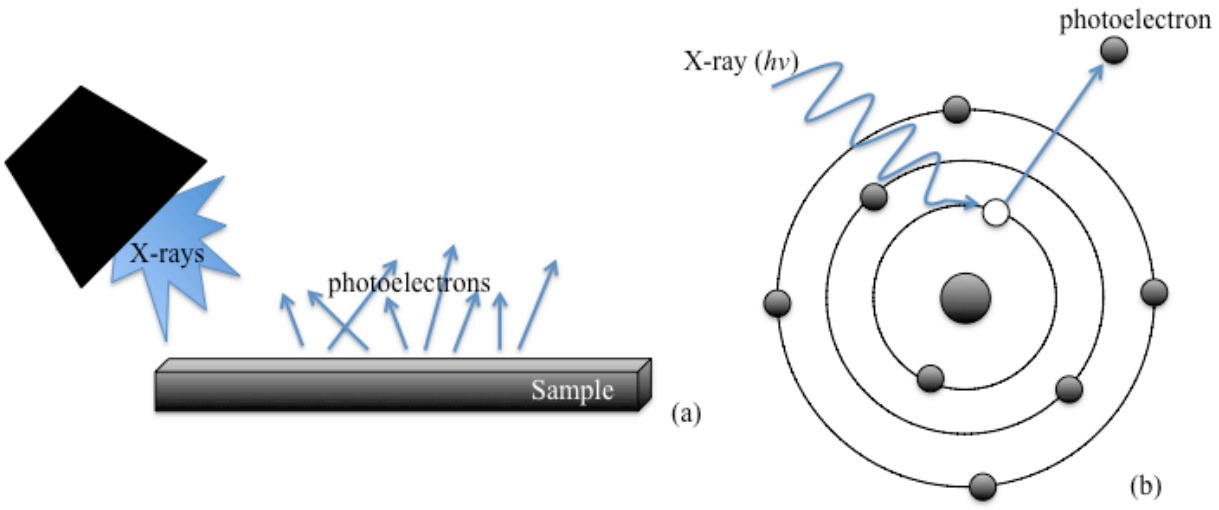

Figure 11. Schematics of (a) a surface irradiated with X-ray photons resulting in emission of photoelectrons and (b) an atom ejecting a core-level electron as a result of energy transfer from the X-ray photon.

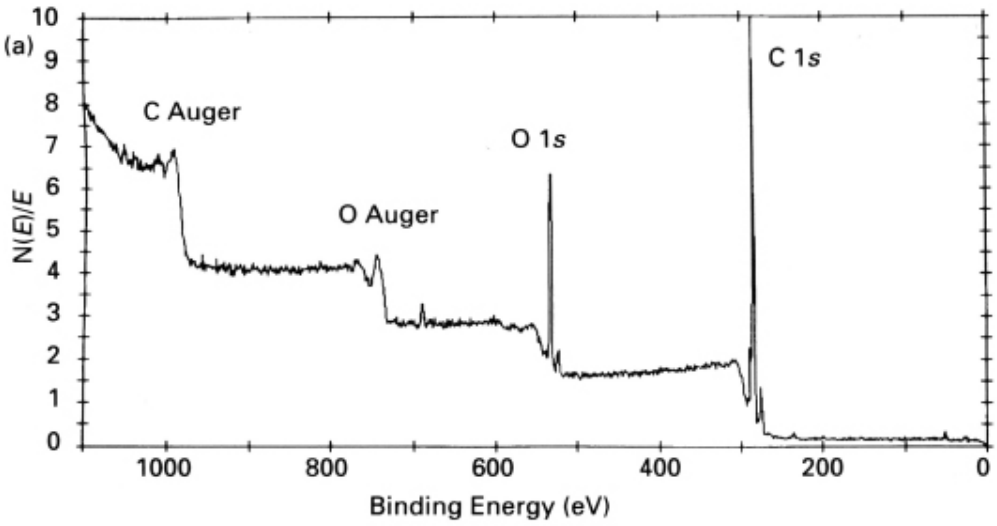

Figure 12. XPS survey spectrum of glass fiber reinforced composite, showing carbon and oxygen peaks. [40]

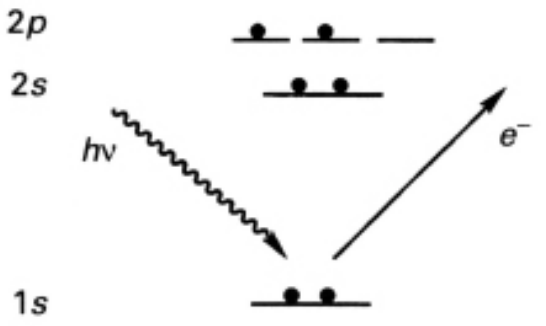

Figure 13. The photoionization process for the C 1s electron. [40]

Because binding energy is a function of the type of atom and its chemical environment, compositional information about the surface, as well as information about structure and oxidation states, of the surface can be determined from these plots. The basic theory behind XPS can be described using the Einstein equation:

$$E_B = hv - KE - w \quad [1]$$

In Equation [1], E_B is the binding energy of the electron emitted from the sample surface, hv is the energy of the X-ray beam, KE is the kinetic energy of the emitted electron, and w is the work function of the spectrometer. The energy of the X-ray beam is a known value, the kinetic energy is measured by the spectrometer, and the work function can be determined for any given spectrometer. The work function of a spectrometer corrects for the electrostatic environment where the electron is formed and measured. [41] Binding energy can be calculated from this information.

Because binding energies of core electrons are shifted depending on what atoms are surrounding the particular atom that ejected the electrons, chemical functionality and oxidation states can be determined by collecting high-resolution spectra. [40] An example of a binding energy shift is shown in Table 2, where corresponding binding energies and oxidation states for various sulfur

compounds are listed. [40] Modern XPS spectrometers have the ability to produce monochromatic X-rays, which minimizes the energy distribution enabling the acquisition of such high-resolution spectra. [40]

Table 2. Binding energies and oxidation states for sulfur compounds (2p energy level). **[40]**

Sample	Binding Energy (eV)	State
ZnS	163.4	-2
S_8	164.1	0
Na_2SO_3	166.6	+4
SO_2	167.5	+4
Na_2SO_4	169.5	+6

Resolving peaks from high-resolution spectra from composite samples would likely be more difficult as both fibers and matrix materials can be composed of many elements in a variety of chemical functional groups. [40] One such example is that of an organic matrix material, which was composed of an ester-based resin, carboxyl functional groups, and alcohol-type carbons. [40] These groups resulted in a complex high-resolution C 1s spectrum that required a four-peak fit. [40] This is important when analyzing samples with XPS as both peak over- and under-fitting is possible, which can severely change the results obtained. This is especially true for composites, where proprietary matrix and fiber chemistries can be complex.

XPS is a powerful tool for the analysis of solid surfaces due to the inability of electrons to deeply penetrate the material, only yielding information from surfaces down to a few atomic layers (2-5 nm). [41] The electron escape depth varies with the binding energy of the ejected photoelectron,

meaning that high binding energy (low kinetic energy) electrons originate closer to the surface than low binding energy (high kinetic energy) electrons (Figure 14). [40]

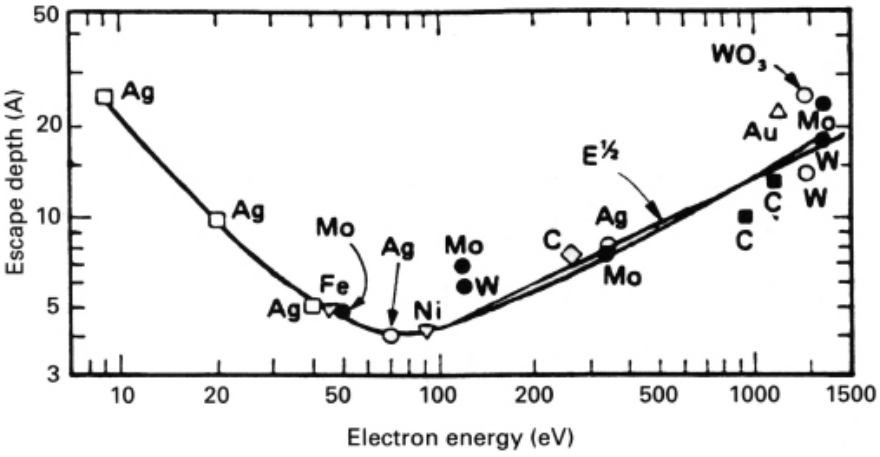

Figure 14. Escape depth as a function of electron kinetic energy. **[40]**

XPS is a type of electron spectroscopy that can provide not only compositional information about the surface examined but also information about structure and oxidation states. Previous research showed XPS to be successful in detecting surface preparation such as different peel ply materials applied to the same composite. [23] It has also been shown to be useful to determine oxygen functional groups from plasma treatment of polymer materials. [33] It can provide surface chemistry information that has potential use for understanding the relationship between surface preparation and adhesion.

2.3.2 Time of Flight Secondary Ion Mass Spectrometry

TOF-SIMS is a mass spectrometry of ionized particles emitted from a surface. When a surface is bombarded with energetic primary particles, secondary particles are emitted (Figure 15). [42,43] Typically, primary particles are atomic ion sources (e.g. Ga^+, Ar^+, Cs^+, Au^+ and Bi^+) or cluster sources (e.g. C_{60}^+, Au^{3+}, Bi_3^+ and Ar_n^+ ($100 < n < 1500$ atoms)). [4]

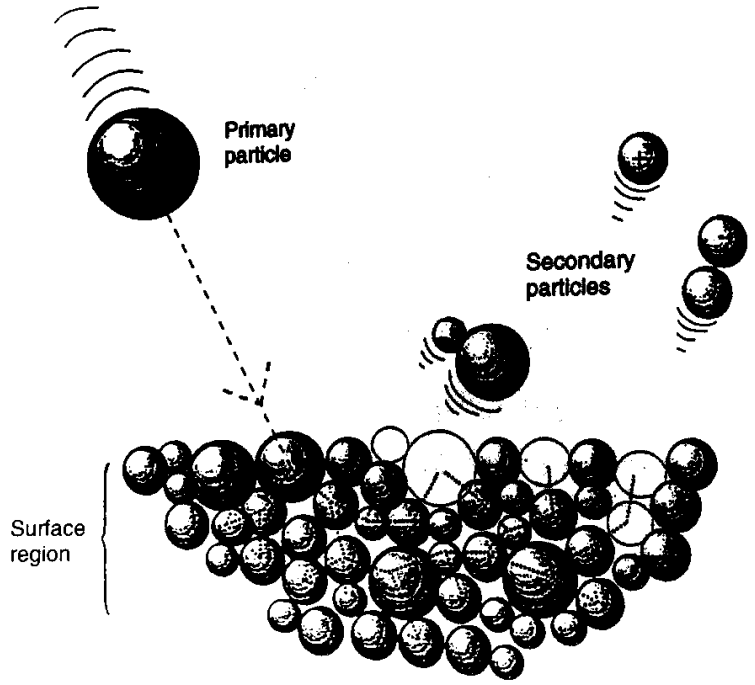

Figure 15. Schematic of SIMS process. [43]

When a surface is bombarded with primary particles, the surface layer of atoms is stripped off, mostly as neutral atoms but also as ions that are accelerated towards a detector. These ions are accelerated by an electric field into a field-free drift tube. Ideally, these ions all have the same kinetic energy when they enter the tube. [3,41] Kinetic energy is a function of mass (m) and velocity (v), as shown by Equation [2].

$$E_k = \frac{1}{2}mv^2 \qquad [2]$$

Thus, lighter particles will have greater average velocities and arrive at the detector before heavier particles. For a one-meter drift tube, flight times are in the micro-second range. [41]

SIMS has proven useful for determining atomic and molecular composition of solid surfaces, including thermosetting polymers. [41] It has also been proven useful for the analysis of composite

materials prepared for secondary bonding, [42] in particular for the detection of oxygen containing functional groups due to plasma treatment of polymers. [36]

2.3.3 Scanning Electron Microscopy and Energy Dispersive Spectroscopy

SEM can be used to produce images of surfaces of various types of materials, including organics and inorganics, on a nanometer to micrometer scale. [44] An electron beam is used to excite secondary electrons from the surface generating a topographical image of the sample surface. These secondary electrons are emitted from a depth of 50-500 angstroms from the specimen. [41,45] Since SEM can be used to produce high magnification images of a composite surface, it can be helpful to understand the surface topography produced from various surface preparations. In addition to secondary electrons, SEM can be used to detect backscattered electrons, Auger electrons and X-rays. When SEM is used to detect X-rays, EDS can be used for elemental analysis. Because all the polymers of this study are composed of carbon backbones, EDS does not add value. This is because EDS cannot differentiate between polymer surface preparations applied to a polymer substrate, which is necessary for this research. Though EDS will not be useful for analyzing the polymer surface chemistries examined here, SEM can be used for imaging surfaces, which could yield useful morphological information.

2.3.4 Surface Energy Measurements

Surface energy is a measure of the energy associated with unsatisfied bonds at the surface, and has units of free energy per unit area. [46] Surface energy measurements are sensitive to the surface layer of the substrate being measured and are perhaps the most surface sensitive technique currently available. Surface energy measurements include CA and IGC. There are various CA measurement devices and methods available. When measuring the CA of a liquid

droplet on a surface, the traditional sessile drop method (e.g. goniometry) or a ballistic drop deposition technique (Brighton Surface Analyst) can be utilized. The Wilhelmy plate method also measures the CA of a liquid but instead of using droplets, the CA of a meniscus on a slide is measured as the slide is brought into contact with a liquid. [47,48]

Goniometry is used to measure the CA from a side-view of a sessile drop. CAs of multiple fluids dispensed onto a composite substrate are measured. From this data, the surface energy of the composite substrate can be calculated. Surface energy can therefore be used to characterize a surface, specifically its ability to be wetted by a liquid with known surface energy, such as an adhesive. Wetting of the adherend by the adhesive is necessary for adhesion, though not sufficient for predicting adhesion. [20,23,49] Wetting is necessary because in order for adhesion to occur, the adhesive and adherend must be in intimate contact, which occurs when the adhesive wets the adherend. Surface energy can be used to explain why epoxies will wet high-energy surfaces, such as metals, "but offer weak adhesion on many untreated polymeric substrates, such as polyethylene, polypropylene, and the fluorocarbons." [50] Figure 16 displays the relationship of parameters that influence the shape a liquid drop assumes on a solid surface. These values are related by Young's equation, shown by Equation [3].

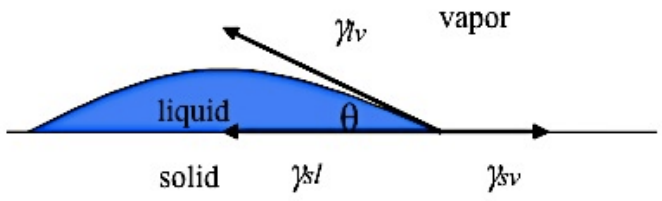

Figure 16. Relationship between solid surface energy (γ_{sv}), solid-liquid surface energy (γ_{sl}), liquid surface tension (γ_{lv}), and CA measurement.

$$\gamma_{sl} = \gamma_{sv} - \gamma_{lv}\cos\theta \quad [3]$$

In Equation [3], γ_{sl} is the surface energy at the interface of the solid and liquid, γ_{sv} is the solid surface energy, γ_{lv} is the liquid surface energy, commonly known as surface tension, and θ is the CA the droplet makes with the solid surface. By measuring the CA of at least two fluids, the surface energy of a solid can be calculated. For this research, the surface energy is expressed by two components (polar and dispersive) using Owens-Wendt's model, [49] which is given by Equation [4].

$$\gamma = \gamma^p + \gamma^d \quad [4]$$

In Equation [4], γ is the total surface energy and γ^p and γ^d are the polar and dispersive components, respectively. [49] The polar component accounts for hydrogen bonding and dipole-dipole interactions. [49] The dispersive component accounts for dispersion interactions. [49] This model allows for the generation of wettability envelopes, a two-dimensional graphical representation of surface wetting.

There are other surface energy models, including the Zisman method and the van Oss-Chaudhury-Good method. [51,52,53] The Zisman method is used to calculate critical surface free energy, which is defined for a solid as the value equal to that of a liquid that when in contact with the solid has a CA of exactly 0° (critical wetting). [51,53] This approach does not partition the surface energy and thus wettability envelopes cannot be generated. The van Oss-Chaudhury-Good method (acid-base method) partitions the surface energy into three components (acid, base, and dispersion). [51,52] This could be attractive for the generation of three-dimensional wettability envelopes; however, there are some consistency issues suggesting further development of the model is necessary. [54] When the method is inverted (i.e. solid surface characteristics used to

derive surface tension of probe liquids), the model did not hold, giving inconsistent values for surface tension. [54]

Additional techniques exist for measurement of contact angles and surface energy. One such technique measures the CA of a ballistically deposited drop from a top view. The only commercial device used to do this is the Brighton Surface Analyst (BSA). Twenty 69 nL drops are deposited rapidly on a surface by the BSA tool forming one 1.38 μL drop. The CA is measured by fitting the volume of the drop to its diameter, assuming a spherical drop. This relationship to measure CA from drop dimensions is given by Equation [5].

$$\frac{d^3}{V} = \frac{24\sin^3\theta}{\pi[2 - 3\cos\theta + \cos^3\theta]} \quad [5]$$

In Equation [5], d is the diameter of the drop, V is its volume and θ is the CA. Because the Surface Analyst is currently only set up for the analysis of water droplets, it cannot be used to determine surface energy, as at least two fluids are necessary.

Similar to CA drop measurements is the Wilhelmy plate method, however instead of measuring the CA of a liquid droplet on a surface, the CA of a meniscus is measured as a plate comes in contact with a liquid bath. [48] When a flat plate is immersed into a liquid, the force to keep the plate in place is a function of the weight of the plate, buoyancy forces, and surface tension. [55] Equation [6] describes this relationship. [47,56]

$$\gamma\cos\theta = \frac{\Delta W}{p} \quad [6]$$

In Equation [6], γ is the surface tension of the liquid, θ is the CA, ΔW is the change in weight of the plate when it is in contact with the liquid compared to when it is not touching the liquid and p is the wetted perimeter of the plate. [47,56]

Of CA measurement methods available, the Wilhelmy plate method is typically preferred for the measurement of advancing and receding CAs. [48] On an ideal surface, the advancing and receding CAs would be equal. [48] Generally, most, if not all, surfaces are non-ideal. [48] The advancing CA is greater than and the receding CA is less than the equilibrium CA. [55] On polymeric surfaces, the advancing angle is more sensitive to the surface components that are low energy, while the receding angle is more sensitive to the higher energy components. [48] By measuring advancing and receding CAs, a hysteresis is obtained that describes the heterogeneity of the surface in question. To measure advancing and receding angles using the sessile drop method, one would apply a drop to the surface and then tilt that surface to the point right before the drop would slide down the surface. The advancing angle is measured on the downhill side and the receding angle is measured at the uphill side of the droplet. Tilting the plate to the correct angle to measure accurate advancing and receding angle could prove to be difficult, which may account for why the Wilhelmy plate method is generally preferred. When plunging the plate into the liquid, the measured CA is the advancing angle, whereas the receding CA is measured when withdrawing the plate from the liquid (Figure 17). [55]

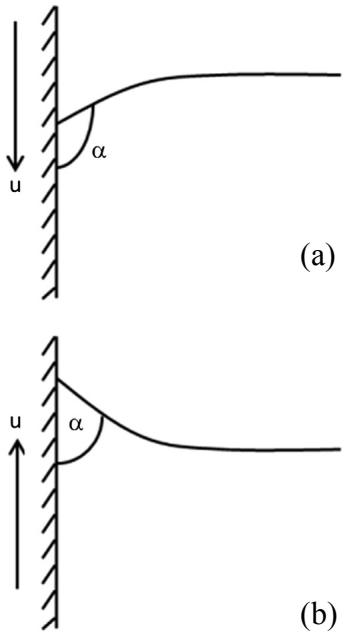

Figure 17. Nature of (a) dynamic advancing contact angle, and (b) dynamic receding contact angle, where u is the velocity of the plate and α is the contact angle. **[55]**

Similar to the force balance of the plate in the static condition, a force balance can be expressed for the dynamic condition, as shown by Equation [7]. [57]

$$F = \gamma p \cos\theta - \rho_L g A h \qquad [7]$$

In Equation [7], F is the force exerted on the solid, γ is the surface tension of the liquid, p is the wetted perimeter of the solid, θ is the CA, ρ_L is the net density of the liquid, g is the force due to gravity, A is the cross-sectional area of the solid, and h is the depth of immersion into the liquid of the solid. [57] The first term in Equation [7] accounts for the surface tension forces that act along the wetted perimeter while the second term accounts for buoyancy of the liquid that has been displaced. [57] When measuring advancing and receding angles, it is important to be aware of variables that can affect the measurements, such as plate velocity. [55]

Yet another technique to determine surface energy of a solid surface is IGC. IGC uses the same idea as analytical gas chromatography, except it uses known gases on an unknown solid to determine its surface energy instead of using a known solid to separate unknown gases. [4] Measuring the retention time of the gas as it passes over the surface, creating intermolecular bonds between the gas and the surface, affords surface energy information. Some claim that IGC is able to identify a range of surface energies, highlighting the heterogeneity of surface energy. [58] Others claim that gas molecules preferentially probe the high-energy sites resulting in higher surface energy calculations compared to CA measurements that are representative of the average surface energies. [4]

The preceding text has described relationships between liquids, gases, and ideal solids. As stated previously, solid surfaces are rarely, if ever, ideal so it is important to account for reasons as to why these surfaces would not be ideal and to use CA measurements and surface energy measurements heuristically with this understanding. One reason solid polymeric surfaces are not ideal is because they are often chemically heterogeneous. Another reason is surface morphology and texture. As discussed previously, the use of peel ply is a common surface preparation for composites to be secondarily bonded. When a peel ply is removed from a composite surface, it leaves an imprint of the peel ply fabric on the surface. This imprint is not only affected by the individual picks of the polymer that compose the fabric, but also by the curvature of the fabric defined by the yarn warp and weft as they cross over and under each other.

The effect of roughness on CA measurements is supported by well-known experiments conducted by Busscher, Mori, and Oliver. [59,60,61] During the mid-1900s, Wenzel conducted the first quantitative theoretical analysis of the effects of roughness on CA measurements. [61] The Wenzel equation shows the relationship between surface roughness, and CA (Equation [8]). [62]

$$\cos\theta_W = r\cos\theta \quad [8]$$

In Equation [8], θ_W is the CA obtained on the rough surface, r is the roughness factor (ratio between actual and projected surface area), and θ is the CA on the same surface without roughness.[62] The theory, supported by two studies, was later seen to lack validity because the studies never directly measured the roughness factor, and it thus seemed to be valid only for special cases "under certain geometrical restrictions."[61] Future studies by Oliver showed that factors aside from surface roughening, such as surface chemistry and changes made to the morphology of surface layer, affect the wetting hysteresis.[61] However, surface roughening still does account for a large portion of this hysteresis. For example, Oliver demonstrated that for extremely oriented roughness, the liquid drops formed on a surface are non-circular in shape.[61] More recent research has also shown non-circular drops to form on peel ply prepared composite surfaces due to the imprint left on the surface upon peel ply removal.[63] The non-circular drops lead to different CA measurements at different peel ply orientations.[63] Due to this discovery, CA measurements for this research were always measured at the same peel ply orientation for comparable data.

2.3.5 Fourier Transform Infrared (FTIR) Spectroscopy

Infrared spectroscopy is used to identify chemical bonds present in a material. For this research, a portable Agilent Technologies ExoScan configured with a diffuse reflectance sampling interface was utilized. Figure 18 shows an IR beam path for diffuse reflectance.

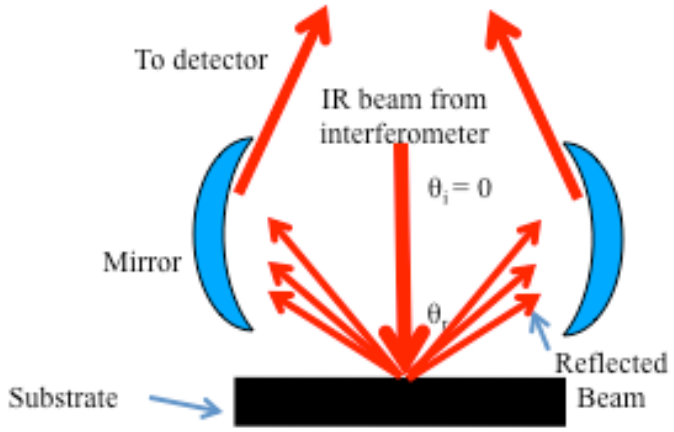

Figure 18. An IR beam path for diffuse reflectance.

For IR spectroscopy to be useful, the materials under examination must be IR active. The first requirement for this is that the frequency of the radiation must match that of one of the normal vibrational modes of the molecules in the material. [41] A normal mode is defined as the number of possible vibrations (vibrational degrees of freedom) within a N-atom molecule (3N-6 or 3N-5). [41] These types of vibrations include stretching vibrations: symmetric and asymmetric, and bending vibrations: in-plane rocking, in-plane scissoring, out-of-plane wagging, and out-of-plane twisting. [41] Secondly, the vibration of the molecule must cause a change in the molecular dipole moment. [41] This means that certain molecules, such as H_2 or O_2, that have dipole moments of zero due to their inherent symmetry, are not IR active. Because the polymers under examination for this research (epoxy, polyester, nylon, etc.) as well as common contaminants such as siloxane and other organics meet these criteria, FTIR is a powerful tool for determining the surface chemistry of peel ply prepared composites and surface contamination. [64]

IR spectroscopy outputs spectra of wavenumber vs. intensity, which enables identification of chemical bonds present in a material. However, analysis of these spectra can be difficult, especially when chemistries are complex. Sometimes a different number of peaks are observed

than would normally be expected. The observation of fewer peaks can occur due to the following: (1) the dipole does not change for a certain vibration due to the symmetry of the molecule, (2) two or more vibrational energies are the same or very close in value, (3) the absorption energy is undetectable because it is so low, and (4) the vibrational energy does not fall within the wavelength range of the instrument.[41] Phantom peaks may be observed due to the following: (1) overtone peaks can occur at two or three times the energy of the fundamental peak, and (2) combination peaks can occur when a photon excites two vibrational modes simultaneously, rather than one.[41]

Diffuse reflectance is used for the analysis of materials with rough surfaces and occurs when the angle of incidence of the IR beam is fixed and the angles of reflection take values from 0-360° (Figure 18).[64] One disadvantage of reflectance techniques is that depth of penetration into the sample is unknown.[64] This is because penetration depth depends pathlength, which is difficult to determine as sample properties, surface properties, and the angle of incident light affect pathlength.[64] This makes quantitative analysis difficult, as pathlength is an important variable for determining sample absorbance.[64] In general, however, penetration depths are 1-10μm, which makes reflectance techniques surface sensitive as much of the spectrum signal comes from the surface.[64]

It should also be noted that carbon fibers absorb infrared light over a broad range of wavenumbers.[65,66] This means that the signal can be different depending on the fiber direction with respect to the incident IR beam or the detector geometry. This suggests that peel ply prepared surfaces may have different IR absorbance due to how close the reinforcing carbon fibers within the composite are to the surface of the composite. Other reinforcing fibers, such as glass or Kevlar, could also affect the IR signal and require examination.

Overall, IR spectroscopy is a powerful tool, requiring little acquisition time. It is a surface sensitive technique that can provide information about polymer materials. In particular, diffuse reflectance is capable of analyzing polymer composites prepared for adhesive bonding as it can successfully interrogate rough surfaces.

2.4 Mechanisms of Adhesion

Surface analysis can provide insight as to what factors contribute to adhesion. This research aims to study the surfaces of composites prepared for adhesive bonding in terms of surface energy (CA) and surface chemistry (FTIR and XPS). The data collected from CA, FTIR, and XPS measurements can then be related to bond data; however, an understanding of adhesion theory is necessary to do this.

There are many theories of adhesion recognized by the science community, all of which require intimate contact between the adherend and adhesive. This can be described by surface wetting, which is measured with CA and surface energy. In order for adhesion to occur, the adhesive must wet the adherend. If this requirement is not fulfilled, adequate bonding cannot happen due to the formation of stress regions that develop along the interface at small air pockets. [50] Insufficient wetting can be a result of contaminants on the surface or the inability of the adhesive to displace the air on the adherend surface forming voids. Realistically, perfect wetting is unlikely to occur. One proposed depiction of the actual contact between adherend and adhesive is represented in Figure 19.

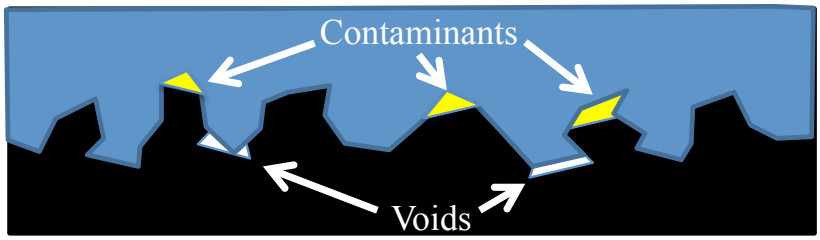

Figure 19. Conceptual representation of contact between adhesive and adherend.

Adhesion theories can be used to understand or predict wetting of an adherend by an adhesive. These theories include adsorption (acid-base), mechanical, electrostatic, and diffusion. Adsorption theory states that adhesion occurs "from the adsorption of adhesive molecules onto the substrate and the resulting attractive forces, usually designated as secondary or van der Waals forces." [50] Mechanical theory recognizes that true surfaces are not actually flat, but comprised of many peaks and valleys. It states that for adhesion to occur, the adhesive must spread into the valleys, displace the entrapped air, and "lock-on mechanically to the substrate." [50] Electrostatic theory states that adhesion occurs because electrostatic forces are formed at the interface of adhesive and adherend. [67] Diffusion theory is based on adhesion resulting from the molecules of both adhesive and adherend diffusing into each other when brought into contact. This yields the formation of an interphase, rather than an interface [67] The term interphase was coined over forty years ago by Sharpe and refers to a three-dimensional region that is either chemically or mechanically altered between adjacent phases. [4] Figure 20 shows a schematic representation of these theories.

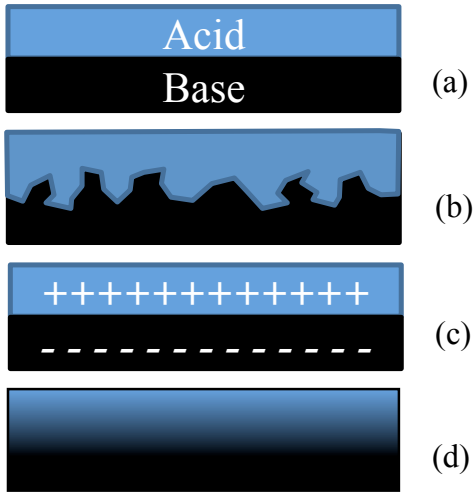

Figure 20. Schematic drawings of (a) adsorption, (b) mechanical interlocking, (c) electrostatic, and (d) diffusion theories.

Just as adhesion theories are important, defects that could inhibit adhesion are equally meaningful to consider. One such consideration is the weak boundary layer theory, which suggests that true interfacial failure rarely occurs, but rather "usually a cohesive rupture of a weak boundary layer is the real event." [50] Weak boundary layers can be attributed to the adhesive, adherend, environment, or any combination of the three. [50] A schematic of the weak boundary layer theory is shown in Figure 21. Contamination is intuitively detrimental to adhesion because the adhesive is in contact with the surface contaminant rather than the surface to be bonded (Figure 19). Research suggests that an interphase or remnants from certain peel ply surface preparations may contaminate composite surfaces and thus inhibit or otherwise prevent adhesion.

Figure 21. Schematic illustration of a weak boundary layer (shown in yellow) theory.

Adsorption, mechanical, electrostatic, and diffusion theories contribute to understanding adhesion between two dissimilar materials, though the contribution of each is not well known. Weak boundary layers or contamination may also be present causing failure to occur in a phase between both interfaces. Surface characteristics, such as surface chemistry and surface energy, must be known to apply these theories to aid in a more complete comprehension of adhesion.

2.5 Adhesive Bond Quality

Bond quality is defined by failure mode and some mechanical assessment of the bond. For this research, bond quality was measured using the double cantilever beam (DCB) test to determine failure mode and Mode I strain energy release rate (G_{IC}). [68] Mode I, II, and III failure as defined by fracture mechanics is shown in Figure 22. [69] Fracture modes for adhesively bonded composite samples include cohesive within the substrate (interlaminar and intralaminar), cohesive within the adhesive, and adhesion failure between the adherend and adhesive, as defined by Figure 23. [26]

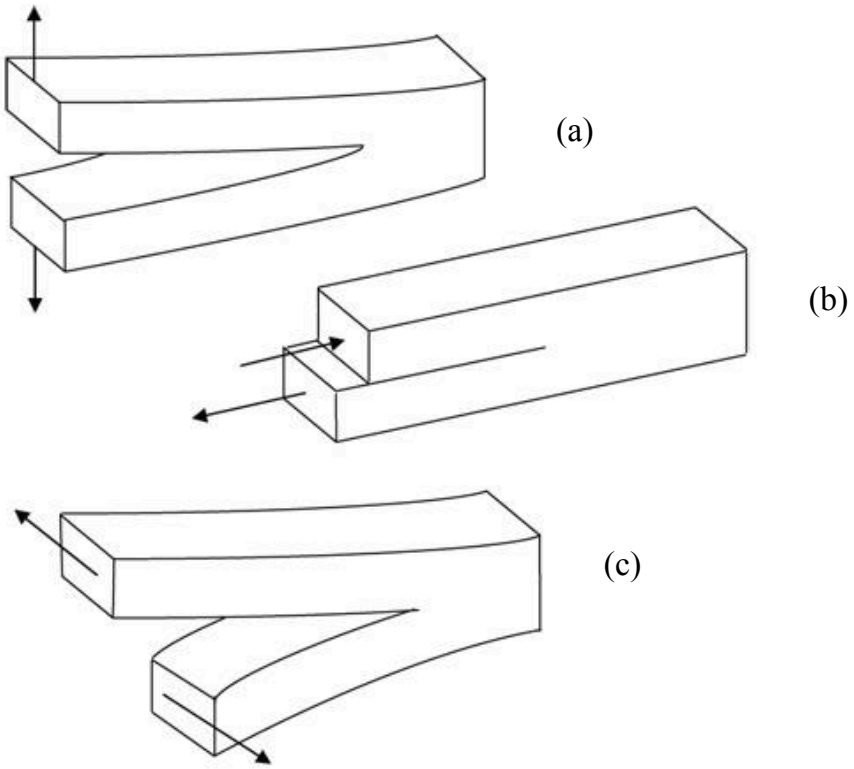

Figure 22. (a) Mode I, (b) Mode II, and (c) Mode III failure as defined by fracture mechanics. [69]

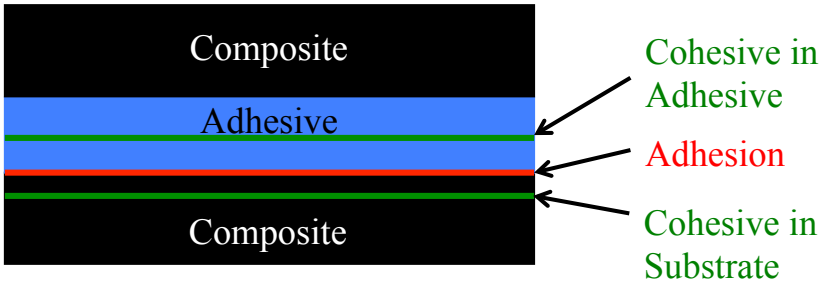

Figure 23. Adhesive bond failure modes: (a) cohesive in the adhesive, (b) adhesion and (c) cohesive in the substrate (interlaminar).

To understand how these failure modes occur, work of adhesion (W_{adh}) and work of cohesion (W_{coh}) must be defined. Work of adhesion, the energy required to separate two dissimilar surfaces, is a function of the surface energies of the individual components (γ_1, γ_2) and

intermolecular forces between the materials (γ_{12}), as defined by Equation [9]. [50] When a material breaks and forms two new surfaces, the energy consumed is defined as the work of cohesion. Thus, the work of cohesion is a function of the surface energy of the material (γ) as shown by Equation [10]. [50]

$$W_{adh} = \gamma_1 + \gamma_2 - \gamma_{12} \quad [9]$$

$$W_{coh} = 2\gamma \quad [10]$$

Assuming only influence of surface energies and ignoring effects of other energy consumption (e.g. different material moduli, plastic deformation, etc.), when the work of adhesion is greater than the work of cohesion, cohesive failure occurs either within the adherend or the adhesive. When the work of cohesion of the composite and the adhesive are both greater than the work of adhesion, adhesion failure will occur. Adhesion failure is unacceptable, as it can occur at unknown loads below that of the cohesive fracture energy of the composite or adhesive. Cohesive failure modes are acceptable because a joint can be designed to the fracture toughness of the adhesive and/or composite laminate. Typically, cohesive failures of the adhesive result in higher fracture energies than cohesive failures of the substrate while adhesion failures result in the lowest fracture energies. [70]

CHAPTER 3: RESEARCH PROPOSAL

3.1 Research Goal

It is proposed that atmospheric pressure plasma can be used to reverse the negative effects caused by incorrect peel ply use. From the literature and previous research, it is known that an interphase or remnants from peel ply preparation are left behind to varying degrees on most composite surfaces after peel ply removal. Also from literature, atmospheric pressure plasma treatment has been shown to be a viable surface preparation for composite materials. [27,37] The effect of atmospheric pressure plasma treatment on modern peel ply prepared composites, however, has not been investigated. Surface energy and surface chemistry measurements are tools that can be used to analyze surface preparations to understand why particular bond qualities are observed. From the literature, atmospheric pressure plasma treatment adds oxygen containing functional groups onto composite surfaces. XPS can be used to analyze these groups. Thus, XPS will be investigated to determine if it can be used to predict if there is a high enough concentration of oxygen functionalities on a surface for improved adhesion to occur. Also from literature, SEM can be used to observe remnants left behind from peel ply removal. Thus, SEM will also be investigated to determine if it can be used to confirm if atmospheric pressure plasma treatment removes the incompatible surface left behind from peel ply preparation.

Hypothesis: Atmospheric pressure plasma treatment of epoxy composites removes and/or functionalizes peel ply remnants/interphase to promote adhesion.

3.2 Research Scope

The scope of this research is limited to the following common aerospace material systems:

- Carbon fiber reinforced epoxy matrix composites:
    - Toray T800/3900-2
    - Hexcel T300/F155
- Epoxy adhesives:
    - Cytec MetlBond (MB) 1515-3M film adhesive
    - Henkel Hysol EA 9696 film adhesive
- Woven peel ply fabrics:
    - PFG nylon 52006
    - PFG polyester 60001

3.3 Research Objectives

To meet the goal of this research, prepared surfaces will be examined in terms of surface characteristics and bond quality. As discussed previously, bond quality is a function of the composite adherend, the adhesive, and the surface preparation as a material system. The goal of this research was to determine if and why atmospheric pressure plasma treatment can reverse the negative effects of particular composite and peel ply preparation combinations. Two composite and peel ply preparation combinations are to be examined: one that results in minimal peel ply transfer to the surface and one that results in significant peel ply transfer. These systems were chosen because both exhibit poor adhesion when certain adhesives are utilized. Thus, they were prime candidates for atmospheric pressure plasma treatment to determine if it can reverse the negative effects of peel ply surface preparation through functionalization and/or removal mechanisms.

The hypothesis that atmospheric pressure plasma treatment can reverse the negative effects of peel ply preparation on certain composite adherends was tested. The surface energy, surface chemistry, and surface morphology of the peel ply prepared composites with and without subsequent atmospheric pressure plasma treatment were characterized with CA, FTIR, XPS, and SEM in both systems of interest. Surface characterization measurements have been used to investigate peel ply prepared composites. Specifically, wettability envelopes produced from surface energy measurements have shown promise. [6] Also potentially showing promise are chemical analysis measurements including FTIR and XPS. These measurements will be compared with fracture energies and failure modes to determine if surface analysis measurements can be used to identify and potentially predict differences in bond quality.

3.3.1 Atmospheric Pressure Plasma Treatment of Peel Ply Prepared Composites: Removal and/or Functionalization of Peel Ply Interphase/Remnants

Determination of whether bonding is a product of functionalization or removal is a challenge that requires numerous experiments. One experiment examined two different material systems (composite, peel ply, adhesive) that are known to result in poor adhesion, another examined the surface as it changed with the level of plasma treatment, another examined time exposure to a constant environment, and lastly, yet another examined the interaction between the nylon peel ply material and MB 1515-3M adhesive. How each of these experiments contributed to the determination of whether plasma treatment promotes adhesion through a functionalization or removal mechanism are explained.

3.3.1.1 Composites Prepared with Peel Ply and Plasma Treatment

Assuming atmospheric pressure plasma treatment reverses the negative effects of peel ply preparation for the two systems of interest and results in adhesion, the following statements will apply:

1. If remnants or an interphase due to peel ply preparation are still present on a composite surface after plasma treatment, it is proposed that the primary reason for adhesion was chemical functionalization.
2. If remnants or an interphase due to peel ply preparation are not present after plasma treatment, it is proposed that the primary reason for adhesion was removal of the peel ply remnants/interphase, though functionalization could still apply and would not be disproven.

The absence or presence of remnants will be examined by SEM, XPS, CA, and FTIR. SEM will determine if a physical difference between peel ply only and peel ply plus plasma treated samples exist, identifying remnants on the surface. FTIR and XPS will be used to determine chemical differences at the surface. Surface energy, as determined from CA measurements and a function of both physical and chemical characteristics of a surface, will be used to determine relative differences between peel ply only and plasma treated surfaces.

3.3.1.2 Different Levels of Plasma Treatment

The purpose of this experiment was to vary the amount of plasma interaction with the surface by keeping all plasma treatment parameters constant, except raster speed. The effect of different raster speeds from 2.54 cm/s (slower means more plasma interaction with the surface) to 30.5 cm/s (faster means less plasma interaction with the surface) on bond quality and surface characteristics will be examined. These raster speeds were chosen because they span the rates

achievable by the PlasmaTreat device used in this study. Bond quality will be measured with the DCB test and failure mode percentages will be quantified by Image J software analysis. [71] Prebond surface characteristics will be quantified by SEM, XPS, FTIR, and CA measurements.

3.3.1.3 Time Exposure to a Constant Environment

An out time study will be performed to determine how plasma treated surfaces change with time. If there is a change with time, that would suggest that functional groups that were added from atmospheric pressure plasma treatment were consumed with time exposure to a constant environment. If the surfaces and bond quality do not change with time exposure to a constant environment, that would suggest the incompatible peel ply interphase was removed. This study will also provide information about the robustness of the plasma treatment process. Surfaces will be exposed to a constant environment after plasma treatment for predetermined times up to 30 days. Surfaces will be examined with CA and FTIR as screening methods. Samples that show significant changes after varying out time will be bonded and examined by XPS to determine if a difference in bond quality or surface chemistry was realized.

3.3.1.4 PFG 52006 Peel Ply and MB 1515-3M Adhesive Interaction

SEM, XPS, and CA will be used to analyze MB 1515-3M surfaces cured against PFG 52006 nylon peel ply. It is proposed that PFG 52006 will not adhere to MB 1515-3M film adhesive, as the adhesive does not adhere to the Toray 3900-2/T800 surface prepared with PFG 52006 peel ply. This will be investigated and correlation with SEM and XPS will be attempted. Atmospheric pressure plasma treatment will also be applied to PFG 52006 and then this peel ply will be cured against MB 1515-3M. SEM analysis of the adhesive and peel ply surfaces after peel ply removal should determine if the primary reason for adhesion after plasma treatment is due to functionalization or removal. Results from SEM will be confirmed with XPS to determine if

nylon is transferred to either MB 1515-3M surfaces prepared with PFG 52006 and plasma treated PFG 52006. CA will also be used to confirm if differences in surface energy exist between the two resultant MB 1515-3M surfaces. A schematic of this idea is shown in Figure 24.

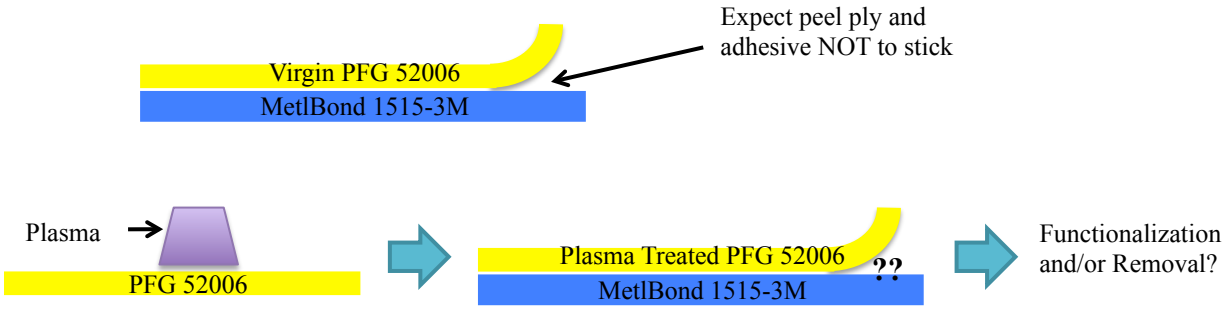

Figure 24. Schematic of peel ply interaction with MB 1515-3M film adhesive for determination of functionalization or removal.

Assuming the virgin nylon peel ply does not transfer to the MB 1515-3M surface, the following conclusions are valid for the MB 1515-3M prepared with plasma treated nylon peel ply:

1. If no peel ply transfers to the MB 1515-3M adhesive, the primary reason for adhesion of Toray 3900-2/T800 surfaces prepared with PFG 52006 and subsequent plasma treatment would likely be due to removal of the incompatible surface.
2. If peel ply transfers to the adhesive, the primary reason for adhesion would likely be due to functionalization of the incompatible surface.

3.4 Summary

This research aims to determine the primary reason for adhesion of peel ply prepared and subsequently atmospheric pressure plasma treated composites. Ultimately, this work will contribute to a fundamental understanding of adhesion, specifically how plasma treatment changes surface characteristics of peel ply prepared composites and how those surface characteristics relate to resultant bond quality. Though peel ply and atmospheric pressure plasma

treatment have been previously studied, this work is original in that it examines modern systems and aims to answer a fundamental question of how and why plasma treatment changes a peel ply prepared composite that was originally a poor bonding surface to one that results in strong bonds.

CHAPTER 4: EXPERIMENTAL

4.1 Experimental Overview

This study focused on atmospheric pressure plasma treatment of CFRP prepared with the incorrect peel ply for bonding. Incorrect peel ply was defined as one that resulted in adhesion failure when combined with a particular composite and adhesive. After peel ply removal, surfaces were plasma treated at various raster speeds. Some samples were bonded for determination of bond quality and others were measured with analytical methods to determine surface characteristics. Bond quality was measured using the DCB test to determine G_{IC} and failure mode. Surface characterization included CA, FTIR, XPS, and SEM to understand how atmospheric pressure plasma treatment changed peel ply prepared composite surfaces in terms of wetting characteristics/surface energy, surface chemistry, and morphology. This section will discuss what materials were examined, how CFRP surfaces were prepared, adhesive bonding operations, and all methodologies used to examine surface characteristics and bond quality.

4.2 Specimen Preparation and Materials

For this study, two materials systems were examined. Composite prepreg materials included Toray T800/3900-2 (177 °C [350 °F] cure) and Hexcel T300/F155 (127 °C [260 °F] cure). Surface preparations were nylon and polyester peel ply (PFG 52006 and 60001, respectively) followed by atmospheric pressure plasma treatment. Adhesives were Cytec MetlBond 1515-3M (177 °C [350 °F] cure), and Henkel Hysol EA 9696 (127 °C [260 °F] cure) epoxy film adhesives.

4.2.1 Material System 1: Toray T800/3900-2, PFG 52006, MetlBond 1515-3M

For this study, 10-ply and 4-ply panels of carbon fiber reinforced epoxy prepreg composite (Toray T800/3900-2 unidirectional tape) prepared with a nylon peel ply (PFG 52006) were

fabricated. The 10-ply panels were prepared by laying up $[0]_s$ laminates and the 4-ply panels were prepared by laying up $[0/90]_s$ CFRP laminates. All specimens were vacuum bagged and cured in an autoclave. The autoclave cure cycle for the specimens was as follows:

1. Heat to 57.2 °C (135 °F) at a rate of 1.1 °C/min (2 °F/min), increase pressure to 0.6 MPa (89 psi) at a rate of 0.1 MPa/min (20 psi/min), soak for 0 min
2. Heat to 177 °C (350 °F) at a rate of 2.8 °C/min (5 °F/min), maintain pressure of 0.6 MPa (89 psi), soak at 177 °C and 0.6 MPa for 120 min
3. Cool to 10 °C (50 °F) at a rate of 2.8 °C/min (5 °F/min), maintain pressure of 0.6 MPa (89 psi), soak for 0 min
4. Decrease pressure to 0 MPa (0 psi) at a rate of 0.1 MPa/min (20 psi/min), maintain temperature of 10 °C (50 °F), soak for 0 min

After cure, specimens were cut to the appropriate dimensions for surface analysis and DCB testing. The 10-ply panels were cut into 12.7 cm (5 in) by 15.2 cm (6 in) coupons for CA and FTIR measurements. DCB adherends were also made from the 10-ply panels and had dimensions of 38.1 cm (15 in) by 15.2 (6 in). The 4-ply panels were 15.2 cm (6 in) by 15.2 cm (6 in) and used for XPS and SEM because the laminate was thin enough to cut with a pair of scissors after treatment (while avoiding contamination from sawing/cutting with lubricants and/or water) to fit into XPS and SEM chambers.

Five plasma treatment levels were studied for the Toray T800/3900-2 CFRP with PFG 52006 peel ply preparation: (1) no plasma (control), (2) 2.54 cm/s (1 in/s), (3) 15.2 cm/s (6 in/s), (4) 22.9 cm/s (9 in/s), and (5) 30.5 cm/s (12 in/s). These conditions will be referred to as "*control 1*" for no plasma, "*high 1*" for 2.54 cm/s plasma, "*medium 1*" for 15.2 cm/s plasma, "*low 1*" for 22.9 cm/s plasma, and "*x-low 1*" for 30.5 cm/s plasma. Though the nylon peel ply surface is not

completely characterized and understood, it is considered a control here as it consistently forms a poor bonding surface for MetlBond 1515-3M adhesive.[23] These five plasma conditions were examined to determine the effect the level of plasma interaction with the surface had on bond quality and surface characteristics. The 15.2 cm/s raster speed was also chosen for the out time study.

Time exposure to a constant environment was also examined on material system 1. Time intervals chosen were within four hours of treatment (4 h), one week after treatment (168 h), approximately two weeks after treatment (408 h), and one month after treatment (720 h). These times were chosen based on a previous study.[72] All samples were treated at one plasma raster speed (15.2 cm/s [6 in/s]). After atmospheric pressure plasma treatment, samples were stored in covered aluminum trays to prevent debris from settling onto the surfaces while allowing the surfaces to interact with the constant lab environment (~55-65 %RH, ~14-17 °C) before testing at the predetermined time intervals.

Atmospheric pressure plasma treatment was performed with a PlasmaTreat model FG1001 plasma generator equipped with a model RD1004 single flume jet. Figure 25 shows the plasma flume for the PlasmaTreat system. The distance between the head of the plasma device and the substrate was fixed at 1.27 cm (0.5 in). Also fixed was a 50% overlap of each raster pass using the rotating flume. In cases when plasma treatment was used, the peel ply was removed directly before treatment. After treatment, samples for CA, FTIR, XPS, SEM, and DCB testing were wrapped in aluminum foil to protect surfaces from gross contamination while in transit to another location for bonding or surface characterization. All samples were bonded or measured with CA and FTIR within 4 hours of peel ply removal. Samples for XPS analysis were also wrapped in aluminum foil after treatment and then placed in a portable desiccator for

transportation. This was done because XPS requires ultra-high vacuum pressures and excess moisture would add additional pump down time. Samples for SEM analysis were kept wrapped in aluminum foil and inside of a desiccator until they were prepared for measurement.

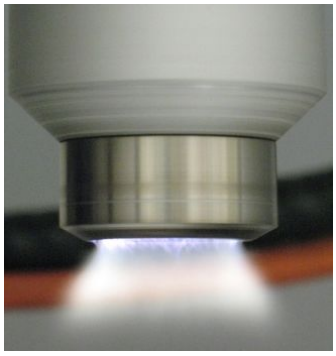

Figure 25. Plasma flume for PlasmaTreat system. [27]

4.2.2 Material System 2: Hexcel T300/F155, PFG 60001, Henkel Hysol EA 9696

Hexcel T300/F155 laminates (10-ply and 2-ply) were fabricated with polyester peel ply (PFG 60001) surface preparation. The 10-ply panels were prepared by laying up 8-ply $[0]_s$ laminates with T300/F155 plain weave (3K-70-PW) outer layers and the 2-ply panels were prepared by laying up 2 plies of T300/F155 plain weave CFRP laminates. All specimens were vacuum bagged and cured in an autoclave using the following cycle:

1. Heat to 57.2 °C (135 °F) at a rate of 1.1 °C/min (2 °F/min), increase pressure to 0.3 MPa (45 psi) at a rate of 0.1 MPa/min (20 psi/min), soak for 0 min
2. Heat to 127 °C (260 °F) at a rate of 3.9 °C/min (7 °F/min), maintain pressure of 0.3 MPa (45 psi), soak at °C and 0.3 MPa for 90 min
3. Cool to 10 °C (50 °F) at a rate of 2.8 °C/min (5 °F/min), maintain pressure of 0.3 MPa (45 psi), soak for 0 min
4. Decrease pressure to 0 MPa (0 psi) at a rate of 0.1 MPa/min (20 psi/min), maintain temperature of 10 °C (50 °F), soak for 0 min

After cure, specimens were cut to the appropriate dimensions for surface analysis measurements and DCB testing. The 10-ply panels were cut into DCB adherends as described in 4.2.1. The 2-ply panels used for surface analysis (CA, FTIR, XPS, SEM) were 15.2 cm (6 in) by 10.2 cm (4 in).

Three plasma treatment scenarios were studied for the Hexcel F155/T300 CFRP with PFG 60001 peel ply preparation: (1) no plasma (control), (2) 0.254 cm/s (0.1 in/s), and (3) 2.54 cm/s (1 in/s). These conditions will be referred to as "*control 2*" for no plasma, "*high 2*" for 0.254 cm/s plasma, and "*low 2*" for 2.54 cm/s plasma. Though the polyester peel ply surface is not completely characterized and understood, it is considered a control here as this composite resin system and peel ply preparation consistently form a poor surface for bonding with Henkel Hysol EA 9696 film adhesive. [20]

Atmospheric pressure plasma treatment was performed with the PlasmaTreat system described in 4.2.1 for the raster speeds listed. After treatment, samples were transported, bonded, and measured as described in 4.2.1.

4.2.3 MetlBond 1515-3M and PFG 52006 Interaction

To help determine if the predominant mechanism responsible for adhesion was functionalization or removal of the peel ply interphase/remnants from the Toray T800/3900-2 composite system prepared with PFG 52006 and subsequently treated with atmospheric pressure plasma, the interaction between PFG 52006 peel ply and MB 1515-3M film adhesive was examined. It was expected that the peel ply would not transfer to the adhesive, as the composite surface prepared with the peel ply does not adhere to the adhesive. This control sample was examined to verify this hypothesis. To determine if functionalization and/or removal of the peel ply interphase/remnants was responsible for improved adhesion, the peel ply was treated with

atmospheric pressure plasma per section 4.2.1 at a raster speed of 2.54 cm/s (1 in/s). The treated peel ply was cured against MB 1515-3M using the autoclave cure cycle described below. Note that 2 plies of 159 g/m^2 [0.0325 psf] areal weight film adhesive were used and the adhesive was sandwiched between phosphoric acid anodized (PAA) aluminum and the peel ply for ease of sample preparation and handling. PAA aluminum was wiped with methyl ethyl ketone to clean the surface prior to bonding.

1. Heat to 57.2 °C (135 °F) at a rate of 1.1 °C/min (2 °F/min), increase pressure to 0.3 MPa (45 psi) at a rate of 0.1 MPa/min (20 psi/min), soak for 0 min
2. Heat to 177 °C (350 °F) at a rate of 2.8 °C/min (5 °F/min), maintain pressure of 0.3 MPa (45 psi), soak at 177 °C and 0.3 MPa for 120 min
3. Cool to 10 °C (50 °F) at a rate of 2.8 °C/min (5 °F/min), maintain pressure of 0.3 MPa (45 psi), soak for 0 min
4. Decrease pressure to 0 MPa (0 psi) at a rate of 0.1 MPa/min (20 psi/min), maintain temperature of 10 °C (50 °F), soak for 0 min

Removal of the plasma treated peel ply from the cured MB 1515-3M adhesive can have 2 results: (1) transfer of peel ply to adhesive, or (2) no transfer of peel ply to surface. If there is transfer of the plasma treated peel ply to the MB 1515-3M adhesive, then that would suggest a functionalization mechanism. If there is no transfer of the plasma treated peel ply to the adhesive (i.e., the resultant surface is the same as if it were prepared with virgin PFG 52006 peel ply), then that would suggest a removal mechanism. This idea was shown schematically in Figure 24. Surfaces were analyzed with SEM, XPS, and CA to determine if peel ply transfer occurred. Also examined with SEM and XPS were virgin and plasma treated peel plies.

4.3 DCB Testing

Individual DCB adherends 15.2 cm (6 in) by 38.1 cm (15 in) in size were bonded after peel ply removal and subsequent application of atmospheric pressure plasma. A fluorinated ethylene propylene (FEP) release film crack starter was employed as shown in Figure 26.

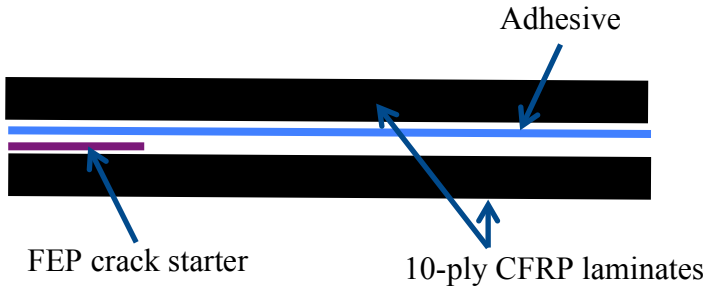

Figure 26. Cross sectional view of bonding lay-up.

After cure, the bonded assemblies were cut into individual specimens 1.27 cm (0.5 in) by 33.0 cm (13 in) in dimension. Six bondline thickness measurements were collected for each DCB specimen. Average, maximum, and minimum bondline thicknesses per sample set were reported. G_{IC} measurements and calculations were guided by ASTM D5528, where G_{IC} is a function of the area under the load-displacement curve, E, the length of the crack, A, and the width of the specimen, B, shown by Equation [11]. [68] After DCB testing, fracture surfaces were visually characterized to determine bond failure mode. In some cases, Image J software was used to determine relative percentages of each failure mode (Figure 27). Previous research has shown this to be a viable tool for failure mode quantification. [71]

$$G_{IC} = \frac{E}{A \times B} \qquad [11]$$

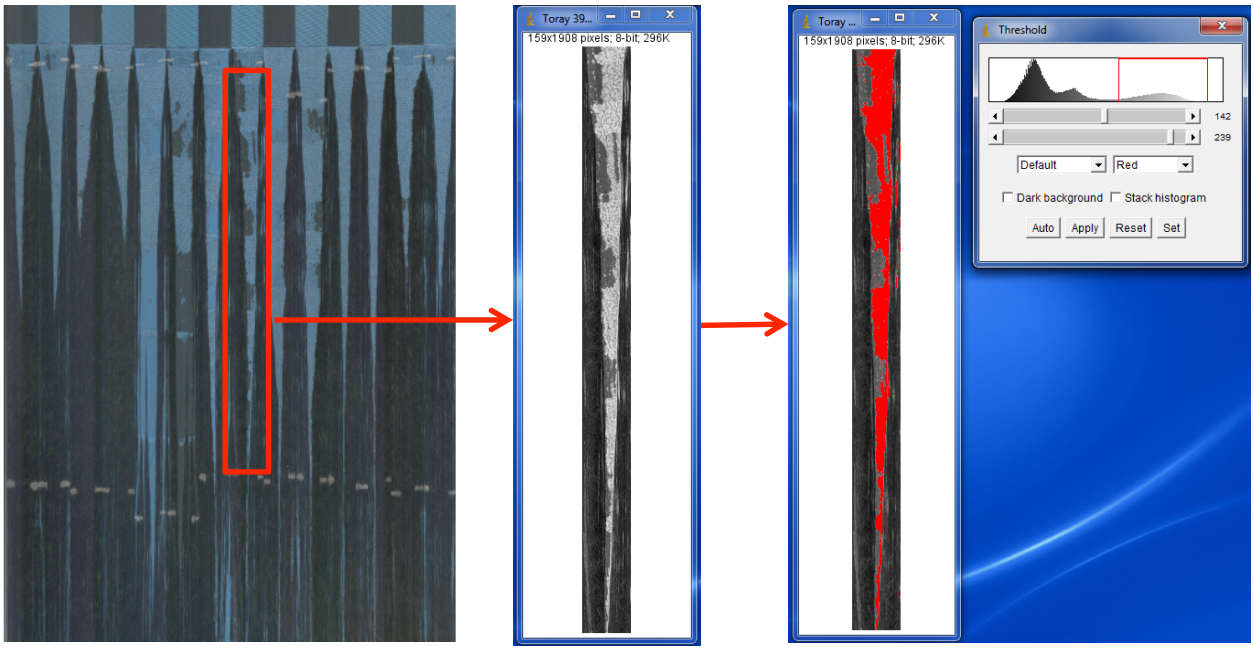

Figure 27. Example of how failure mode percentages were calculated with Image J software. Shown here is the image analysis for determination of cohesive failure on the sample (red in last image).

4.3.1 Material System 1: Toray T800/3900-2, PFG 52006, MetlBond 1515-3M

Three of the five sets of Toray T800/3900-2 laminates with various levels of plasma treatment, as well as the time exposure samples were bonded with MetlBond 1515-3M film adhesive (159 g/m^2 [0.0325 psf] areal weight). The *low 1* (22.9 cm/s) and *x-low 1* (30.5 cm/s) samples were bonded with MetlBond 1515-3M film adhesive (244 g/m^2 [0.050 psf] areal weight). The 244 g/m^2 areal weight adhesive was used for the *low 1* and *x-low 1* samples because 159 g/m^2 was no longer available. The autoclave cure cycle for the bonded assemblies was described in 4.2.3. Bondline thickness measurements are shown in Table 3 and Table 4. The thicker bondlines for *x-low 1* and *low 1* DCB specimens can be explained by the use of the heavier adhesive (Table 3).

Table 3. Material system 1 bondline thickness measurements.

Sample	Maximum (µm)	Minimum (µm)	Range (µm)	Average (µm)	Standard Deviation (µm)
control 1	191.7	119.4	72.3	148.3	12.0
x-low 1	290.0	175.7	114.3	235.6	29.7
low 1	305.6	163.1	142.4	247.2	32.9
medium 1	143.5	101.9	41.6	125.3	9.6
high 1	177.8	90.7	87.1	129.5	15.9

Table 4. Material system 1 time exposure bondline thickness measurements.

Sample	Maximum (µm)	Minimum (µm)	Range (µm)	Average (µm)	Standard Deviation (µm)
4 h	213.0	138.0	75.0	174.8	16.4
168 h	216.7	127.8	88.9	181.1	18.7
408 h	214.8	140.7	74.1	178.6	16.2
720 h	216.7	114.8	101.8	178.8	22.1

4.3.2 Material System 2: Hexcel T300/F155, PFG 60001, EA 9696

Hexcel T300/F155 laminates were bonded with Henkel Hysol EA 9696 film adhesive (146 g/m^2 [0.030 psf]). The autoclave cure cycle for the bonded assemblies was as follows:

1. Heat to 57.2 °C (135 °F) at a rate of 1.1 °C/min (2.0 °F/min), increase pressure to 0.3 MPa (45 psi) at a rate of 0.1 MPa/min (20 psi/min), soak for 0 min
2. Heat to 127 °C (260 °F) at a rate of 5.6 °C/min (10 °F/min), maintain pressure of 0.3 MPa (45 psi), soak at 121 °C and 0.3 MPa, soak for 90 min
3. Cool to 18 °C (65 °F) at a rate of 5.6 °C/min (10 °F/min), maintain pressure of 0.3 MPa (45 psi), soak for 0 min
4. Decrease pressure to 0 MPa (0 psi) at a rate of 0.1 MPa/min (20 psi/min), maintain temperature of 18 °C (65 °F), soak for 0 min

Materials System 3 bondline thickness measurements are shown in Table 5.

Table 5. Material system 2 bondline thickness measurements.

Sample	Maximum (µm)	Minimum (µm)	Range (µm)	Average (µm)	Standard Deviation (µm)
control 2	229.6	140.8	88.8	186.5	23.8
low 2	231.5	116.7	114.8	179.7	25.0
high 2	250.0	129.4	129.6	182.4	22.6

4.4 Contact Angle Measurement and Surface Energy Analysis: VCA Optima Video Goniometer

Peel ply was removed immediately before plasma treatment (or CA measurement in the case of control samples and adhesive plaques). Test coupons were placed on the goniometer stage, which was confirmed to be level prior to each analysis. Samples were measured within 4 hours of atmospheric pressure plasma treatment or peel ply removal (control samples). Fluid drops of 1 µL volume were dispensed from the syringe and placed on the test strip by raising the stage and

"catching" the drops. An image of the side-view of the drop was collected at a predetermined time of 5 seconds and CAs were measured using the goniometer software. Figure 28 shows the instrument and an example drop image showing measured CAs.

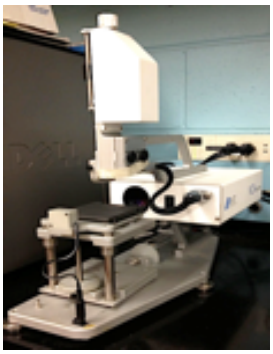

(a)

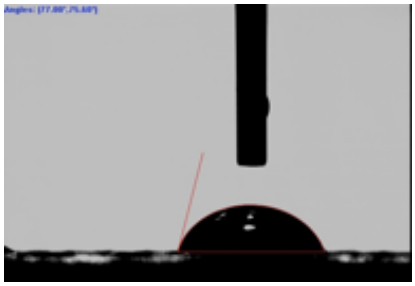

(b)

Figure 28. (a) VCA Optima Goniometer and (b) Side-view of a drop as viewed from the goniometer camera, showing CA measurement in the upper left corner of the image.

The probe fluids used for CA measurement were deionized water (DI H_2O), diiodomethane (DIM), ethylene glycol (EG), and glycerol (GLY). These fluids were chosen due to their differing polar and dispersive surface energies, as shown in Table 6. Note that superscripts "p," "d" and "tot" refer to polar, dispersive, and total, respectively.

Table 6. Polar and dispersive surface energies for CA fluids.

Fluid	**γ^p (mJ/m^2)**	**γ^d (mJ/m^2)**	**γ^{tot} (mJ/m^2)**
DI H_2O [15]	50.2	22.0	72.2
DIM [73]	0	50.8	50.8
EG [15]	19.0	29.3	48.3
GLY [15]	30	34	64

A total of 20 measurements (10 drops) were averaged for each CA value reported. Averages were used to calculate polar and dispersive surface energies of the composite from the Owens-Wendt surface energy model. [49] The surface energies were calculated using Equation [12], which is derived from Equations [3] and [4] and takes the form y = mx + b.

$$\frac{\gamma_{lv}(\cos\theta+1)}{2\sqrt{\gamma_{lv}^{p}}}=\sqrt{\gamma_{sv}^{d}}\left(\sqrt{\frac{\gamma_{lv}^{d}}{\gamma_{lv}^{p}}}\right)+\sqrt{\gamma_{sv}^{p}} \quad [12]$$

In Equation [8], γ_{lv} is the total surface energy between the liquid and the vapor (surface tension), γ^{p}_{lv} is the polar component of the surface tension, γ^{d}_{lv} is the dispersive component of the surface tension, γ^{p}_{sv} is the polar component of the solid, γ^{d}_{sv} is the dispersive component of the solid, and θ is the average CA. From Equation [12], an x-y plot was generated with x and y coordinates defined as Equations [13] and [14].

$$x=\sqrt{\frac{\gamma_{lv}^{d}}{\gamma_{lv}^{p}}} \quad [13]$$

$$y=\frac{\gamma_{lv}(\cos\theta+1)}{2\sqrt{\gamma_{lv}^{p}}} \quad [14]$$

Each fluid contributed a point to the plot. A line was fit to these points, generating a Kaelble plot, [14,74] which showed the relationship between the CAs obtained with each probe fluid. The differences in surface tensions of the probe fluids produce unique points on a Kaelble plot providing the ability to have greater confidence in calculated surface energies. [14,74] The polar surface energy of the composite was calculated to be the y-intercept of the Kaelble plot squared ($\gamma^{p}_{sv}= b^2$). The dispersive surface energy was the slope of the line squared ($\gamma^{d}_{sv}= m^2$). From this information, wettability envelope plots were created. These were generated by inputting the polar and dispersive components of the surface energy of the composite into a computer program originally written by Mark Tuttle and later edited by Brian Clark, BKCWet v 1.1. [75]

3.5 FTIR Measurement and Multivariate Analysis: Agilent Technologies ExoScan

An Agilent Technologies ExoScan FTIR was used to collect spectra from the prepared surfaces. Peel ply was removed immediately before plasma treatment (or FTIR measurement for the control samples). All samples were measured within 4 hours of plasma treatment or peel ply removal (control samples). The ExoScan, which was configured for diffuse reflectance, used one background spectrum for a series of sample spectra. Figure 29 shows an image of the instrument. The background was then ratioed to the specimen spectra. Data collection was 90 scans with 16 cm^{-1} resolution in the mid-infrared (MIR) data range (4000-650 cm^{-1}). Seven spectra were collected per sample.

Figure 29. Agilent Technologies ExoScan FTIR.

The GRAMS IQ software package from Thermo Scientific was used for multivariate analysis (MVA) of the collected FTIR spectra. MVA is a powerful tool for the examination of chemical spectra because it can help identify differences in peak locations and peak intensities that are otherwise not obvious. A partial least squares (PLS) regression method using polar surface energy was used to determine differences between spectra. Two principal components were used. Spectra required preprocessing before the PLS method was able to differentiate between sample

sets. Multiplicative scatter correction and a gap first derivative with 5 smoothing points were the preprocessing steps used. The multiplicative scatter correction was used to overcome unknown pathlength effects inherent to the diffuse reflectance technique. The derivative was used to magnify differences between spectra by amplifying changes in slope of the spectral peaks while reducing effects of baseline offsets. Smoothing points were used to reduce the influence of noise.

3.6 XPS Measurement and Peak Fitting Analysis: Surface Science Instruments S-Probe XPS

A Surface Science Instruments S-Probe XPS was used to analyze prepared composite surfaces (Figure 30). Peel ply was removed immediately before plasma treatment (or introduction into the XPS chamber in the case of control samples). Samples were roughly 1 cm (0.39 in) by 1 cm (0.39 in) in size and mounted onto a sample stage equipped with a nickel screen hovering over the sample surfaces. Because the samples were analyzed as insulators, the nickel screen was used to aid in charge neutralization by providing a grounded surface just above the sample surfaces. This, coupled with a low energy electron flood gun (5 eV electrons), was responsible for the charge neutralization of the non-conducting polymer samples. Figure 31 shows the samples loaded on the specimen holder. After three hours in the chamber, the samples were removed and placed into a test stand vacuum system. This was done because the samples outgassed so much that the system could not pump down to operating pressure.

Figure 30. Surface Science Instruments S-Probe XPS instrument.

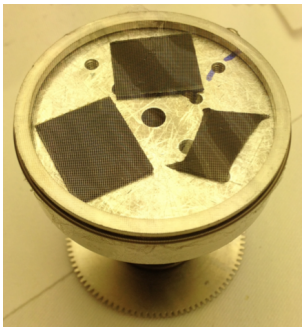

Figure 31. Samples loaded onto specimen holder.

Two days later, the samples were removed from the test stand vacuum chamber and analyzed by XPS. For all subsequent samples examined with XPS, the test stand vacuum was utilized for up to three days before introduction into the XPS chamber for analysis. The source used was monochromatized Al Kα X-rays. The takeoff angle was 55° as measured normal to the surface. Before data collection, the system was pumped down to less than 5 x 10^{-9} torr. Three survey scans (with 800 μm spot size) at 150 eV pass energy were performed on each specimen. Each survey scan was the average of 4 sweeps. These parameters yielded low resolution and high sensitivity measurements, which enabled quantitative analysis of percent concentration of

elements present on the sample. High-resolution carbon scans were also performed at 50 eV pass energy, which enabled oxidation state information.

Data analysis was completed using Hawk Data Analysis 7 software. The first step of analysis was to shift the data so the carbon 1s peak appeared at 284.6 eV. This was necessary because the low energy electron flood gun overcompensated for the charged surface resulting in a shift of the peaks to lower binding energies. From survey scans, compositional information was determined by measuring the area under each peak. A linear fit yielded the percentage of each element present on the surfaces. High-resolution spectra obtained for carbon were fit with multiple peaks to determine chemical bonds on the surfaces.

3.7 Scanning Electron Microscopy: FEI Sirion XL30 SEM

A FEI Sirion LX30 SEM was used to image composite and adhesive surfaces. Peel ply was removed immediately before plasma treatment (or introduction into the sputter coating chamber in the case of control samples). Samples were roughly 1 cm (0.39 in) by 1 cm (0.39 in). Because samples were polymeric and thus would charge in a SEM, it was necessary to sputter coat all samples with platinum before introduction into the SEM chamber. Accelerating voltages of 2-5 kV and spot sizes of 2-3 were used for analysis. Images were captured at multiple magnifications and analyzed to identify if peel ply remnants remained on composite or adhesive plaque surfaces.

CHAPTER 5: RESULTS AND DISCUSSION

5.1 Toray T800/3900-2 + PFG 52006 Nylon Peel Ply + Atmospheric Pressure Plasma + MetlBond 1515-3M

5.1.1 DCB Testing

To determine if atmospheric pressure plasma treatment could reverse the negative effects of nylon peel ply surface preparation of Toray T800/3900-2 CFRP laminates for MB 1515-3M film adhesive bonding, DCB adherends were plasma treated at various raster speeds. Multiple raster speeds were used to examine the influence of various levels of peel ply remnant/interphase removal and/or functionalization on bond performance. As shown in Figure 32, plasma treatment afforded an approximately threefold increase in G_{IC} compared to *control 1* samples, with fracture energies greater than minimally acceptable levels (i.e., cohesive capability of MetlBond 1515-3M and delamination of composite). [70] Fracture energies did not significantly vary for different levels of plasma treatment (i.e., all levels of plasma treatment drastically improved the condition of the faying surface and resultant bond performance). This improved bond quality could be attributed to an increase in polar group concentration (e.g. –COOH) on the plasma treated surfaces when compared to *control 1* surfaces. As reported by others, increased concentration of polar functional groups has been shown to promote adhesion. [34,35,37]

While bond performance did not differentiate among plasma rastering speeds, analysis of failure modes was able to reveal differences. As expected, *control 1* exhibited 100% adhesion failure (Figure 33), which correlated well to the low fracture energies. The images shown in Figure 33 are the matching halves of one DCB specimen and are generally representative of the group. Of all plasma treated samples, only *high 1* samples exhibited 0% adhesion failure (Figure 33). As shown in Figure 33, all other plasma treated samples showed mixed failure modes, including

some level of adhesion failure. The level of adhesion failure ranged from <1% for *medium 1* and *low 1* samples to up to 35% for *x-low 1* samples (Table 7). The higher fracture energies of the plasma treated samples could be explained by cohesive and interlaminar failure modes. Surface characterization measurements were utilized to understand why the difference in failure modes was observed.

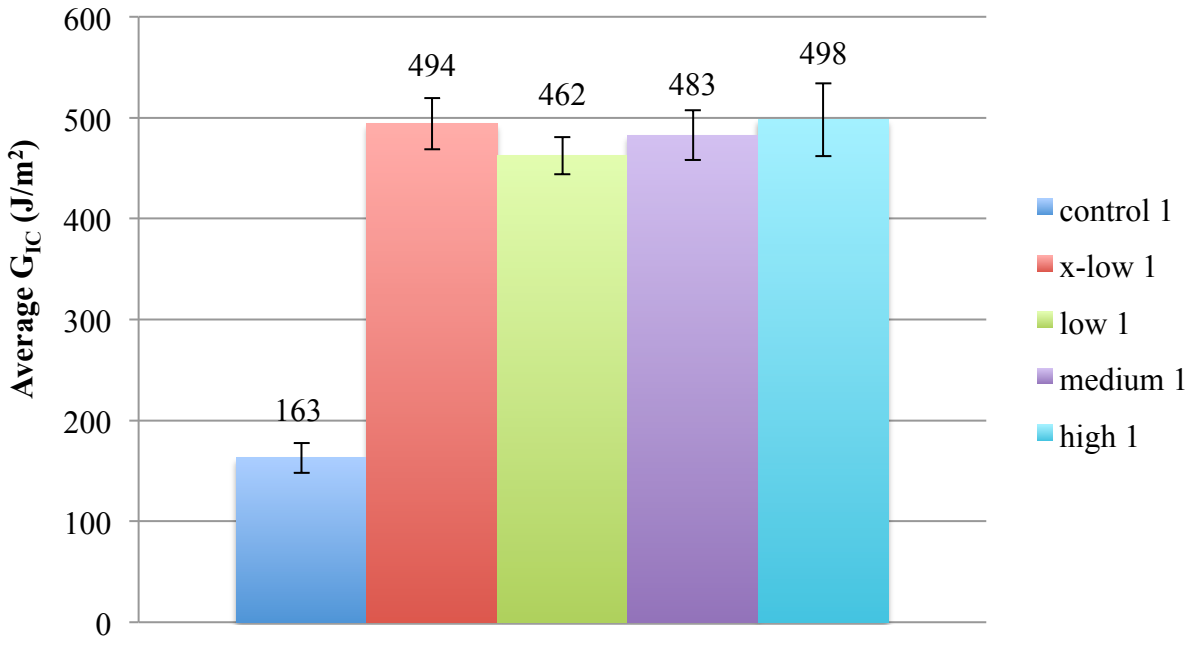

Figure 32. Average G_{IC} measurements for *control 1*, *x-low 1*, *low 1*, *medium 1*, and *high 1* samples with standard deviation error bars.

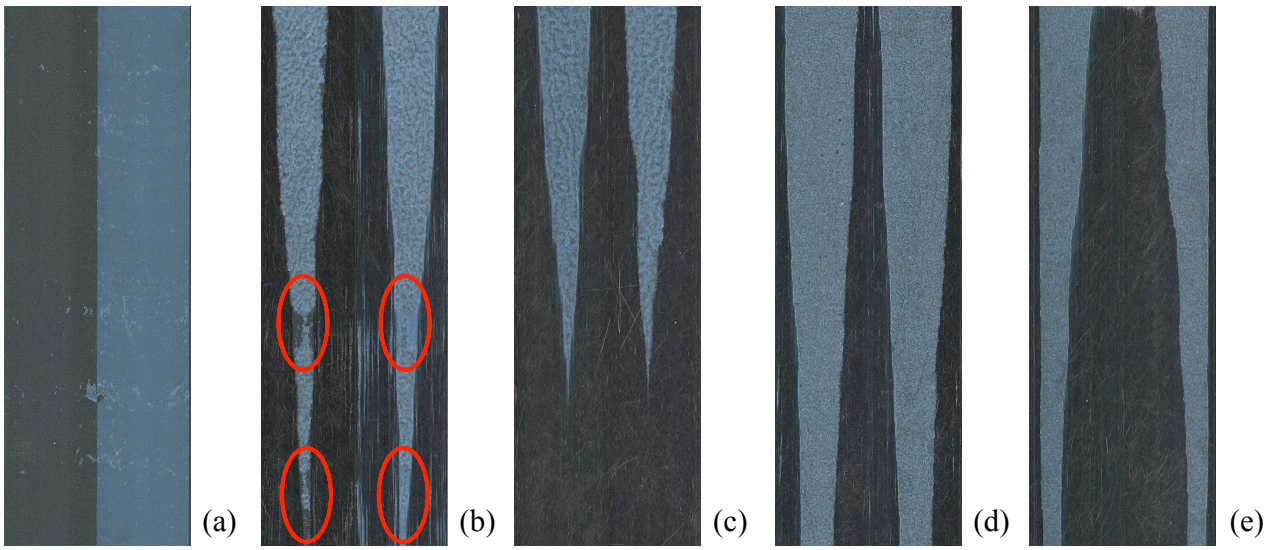

Figure 33. Representative fracture surfaces for (a) *control 1*, (b) *x-low 1* (red circles showing adhesion failure), (c) *low 1*, (d) *medium 1*, and (e) *high 1* DCB samples.

Table 7. Failure mode percentages, showing average, minimum, and maximum percentages.

Sample	Failure Modes: average [min, max] (%)		
	Cohesive	**Interlaminar**	**Adhesion**
control 1	0 [0, 0]	0 [0, 0]	100 [100, 100]
x-low 1	23 [15, 36]	64 [41, 85]	13 [1, 35]
low 1	18 [7, 38]	82 [63, 93]	< 1 [< 1, < 1]
medium 1	52 [35, 62]	48 [38, 65]	< 1 [< 1, < 1]
high 1	35 [16, 63]	65 [37, 84]	0 [0, 0]

5.1.2 Contact Angle Measurements

Contact angle measurements were significantly different for peel ply only (*control 1*) samples compared to those treated with atmospheric pressure plasma upon peel ply removal (Figure 34).

DI H_2O, EG, and GLY CAs were lower on plasma treated samples than on *control 1* specimens. DIM CAs did not change significantly regardless of plasma treatment. This could be due to the addition of polar groups, such as –OH, –COOH, –OOH, onto the surface as a result of atmospheric pressure plasma treatment.[19] XPS was used to confirm this and will be discussed in a latter section.

All liquids with a polar component wetted plasma treated peel ply surfaces more than peel ply only surfaces. For example, EG wetted out (e.g. CA was ~0°) all plasma treated surfaces but had a CA of 39° on *control 1* surfaces. DIM was the only probe fluid without a polar component and its CA remained unchanged after plasma treatment. Some differences in CA measurements were observed among the four plasma treatment raster speeds examined. *High 1* samples, which corresponded to the slowest plasma treatment raster speed, resulted in lower CAs for DI H_2O and GLY, indicating better wetting than *medium 1*, *low 1*, and *x-low 1* samples. There was not a significant difference among DI H_2O CA measurements for *medium 1*, *low 1*, or *x-low 1* samples which corresponded to faster plasma treatment raster speeds compared to *high 1* samples. However, GLY CA measurements were lower on *medium 1* samples than on *low 1* and *x-low 1* samples. There was not a significant difference between CAs measured on *low 1* and *x-low 1* surfaces.

This data suggested that the amount of atmospheric pressure plasma treatment correlated weakly with DI H_2O and GLY CA measurements. In support of this statement, the slower the raster speed, which corresponds to greater plasma interaction with the surface, the lower the CA of DI H_2O and GLY, except for *low 1* and *x-low 1* samples which were not significantly different from each other in terms of CA measurements. As previously stated, CAs were measured 5 seconds after placing the drop onto the surface. It must be noted that GLY ultimately wetted the *medium*

1 surface 30 seconds after drops were placed on the surface and reduced by about 10° after 30 seconds on the *low 1* and *x-low 1* samples.

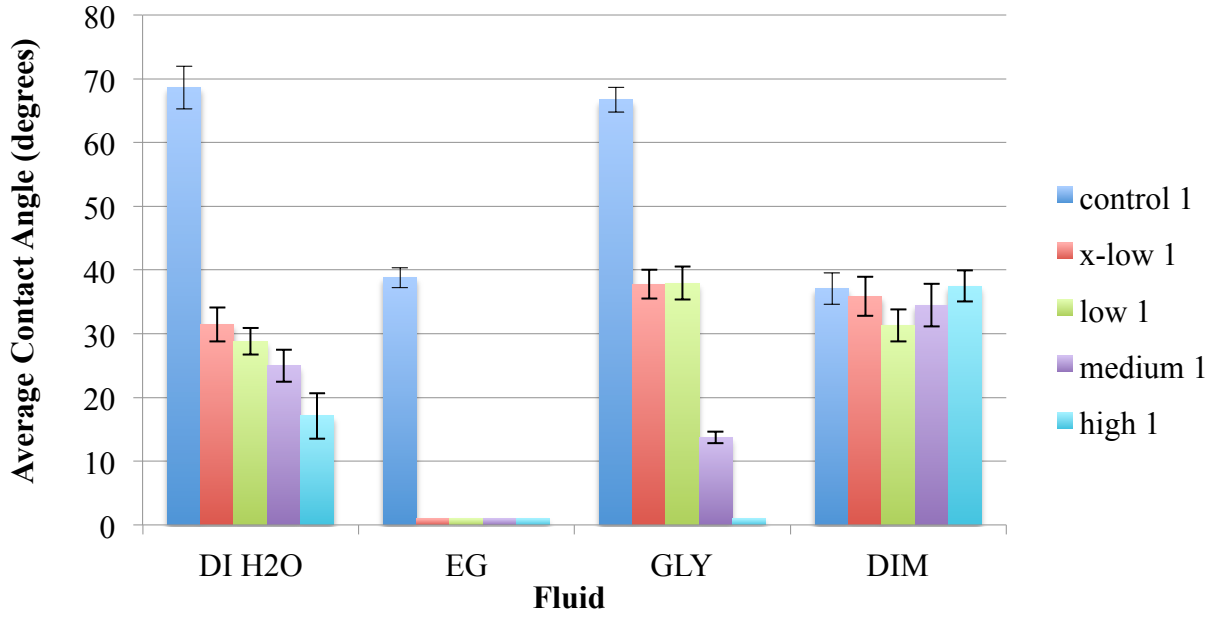

Figure 34. Average contact angle measurements on *control 1* and plasma treated samples with standard deviation error bars.

The significant difference in CA measurements translated to a considerable variation in surface energies (Figure 35). Plasma treated samples had higher polar and in turn higher total surface energies than the peel ply only sample (*control 1*). Compared to the *control 1*, plasma treatment increased total surface energy by 15.8, 17.1, 20.1, and 21.9 mJ/m^2 for *x-low 1*, *low 1*, *medium 1*, and *high 1* samples, respectively. The greater total surface energy was due to the large increase in polar surface energy. The larger polar component could be attributed to the addition of polar groups onto the surface, as stated previously. It also appeared that the polar component increased 6.2 mJ/m^2 while the dispersive component remained relatively unchanged from *x-low 1* samples to *high 1* samples. Overall, the dispersive component of the surface energy for plasma treated samples appeared lower than control samples with the difference being small (ranging 1.8 to 3.6

mJ/m^2 lower). This difference may not be significant and could be due to the use of average CA measurements to calculate surface energy. It could also be attributed to an underestimation of the surface energy from calculations. In cases where the fluid wetted the surface, a CA of 0° (and 1°, which showed no difference) was used for calculations. A ~0° CA can occur on a surface when the surface energy of the fluid is at or below the critical wetting surface energy of the solid.

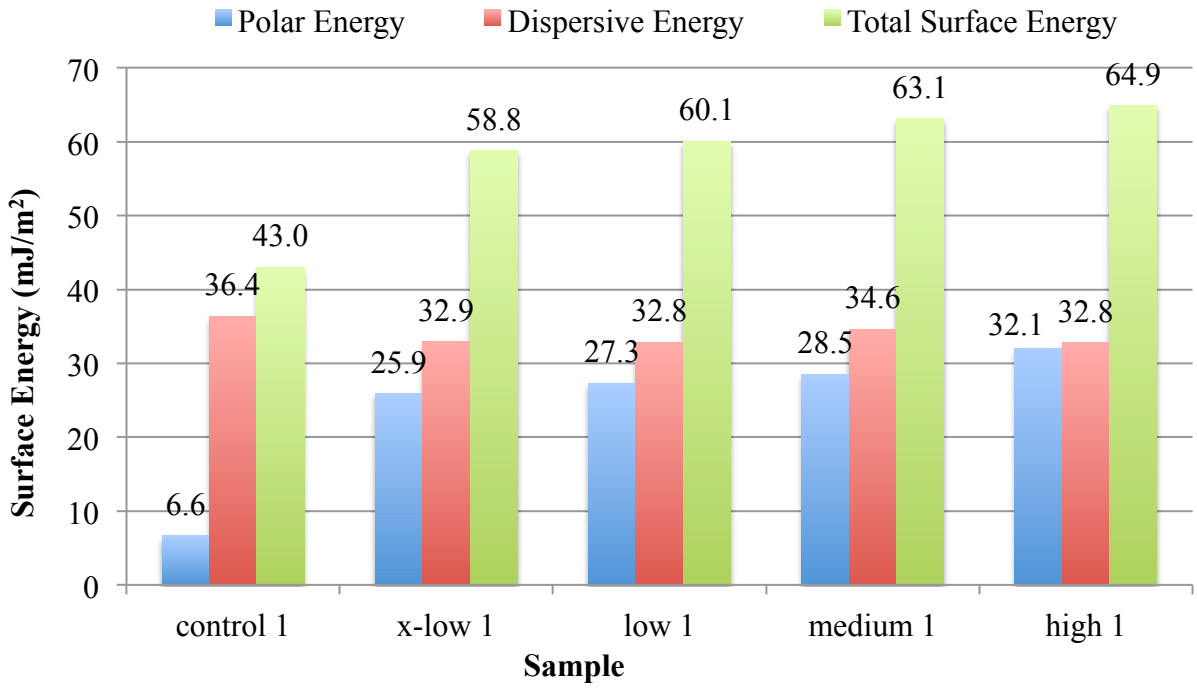

Figure 35. Surface energies for *control 1*, *x-low 1*, *low 1*, *medium 1*, and *high 1* plasma substrates.

To better understand how the increase in surface energy translates to wettability of these surfaces by an epoxy adhesive, wettability envelopes were generated for each substrate (Figure 36). The wettability envelopes may help explain why adhesion was observed for plasma treated substrates but not *control 1* surfaces. Though wetting is not sufficient to predict bonding, it is necessary for adhesion. [20,23,49] As shown in Figure 36, the surface energy of epoxy adhesives lies on the border of the *control 1* sample wettability envelope and thus certain epoxy adhesives may not be

expected to wet the nylon prepared surface. Plasma treatment increased the size of the wettability envelopes compared to the *control 1* sample, such that epoxy adhesives would be expected to wet the surface. This is likely a contributing factor as to why adhesion was observed for plasma treated surfaces but not control peel ply only adherends. However, as stated previously, wetting is not sufficient to predict bonding but is supported by this data. Though none of the plasma treated samples exhibited 100% adhesion failure like the *control 1* samples, the *medium 1*, *low 1*, and *x-low 1* samples all showed varying degrees of adhesion failure.

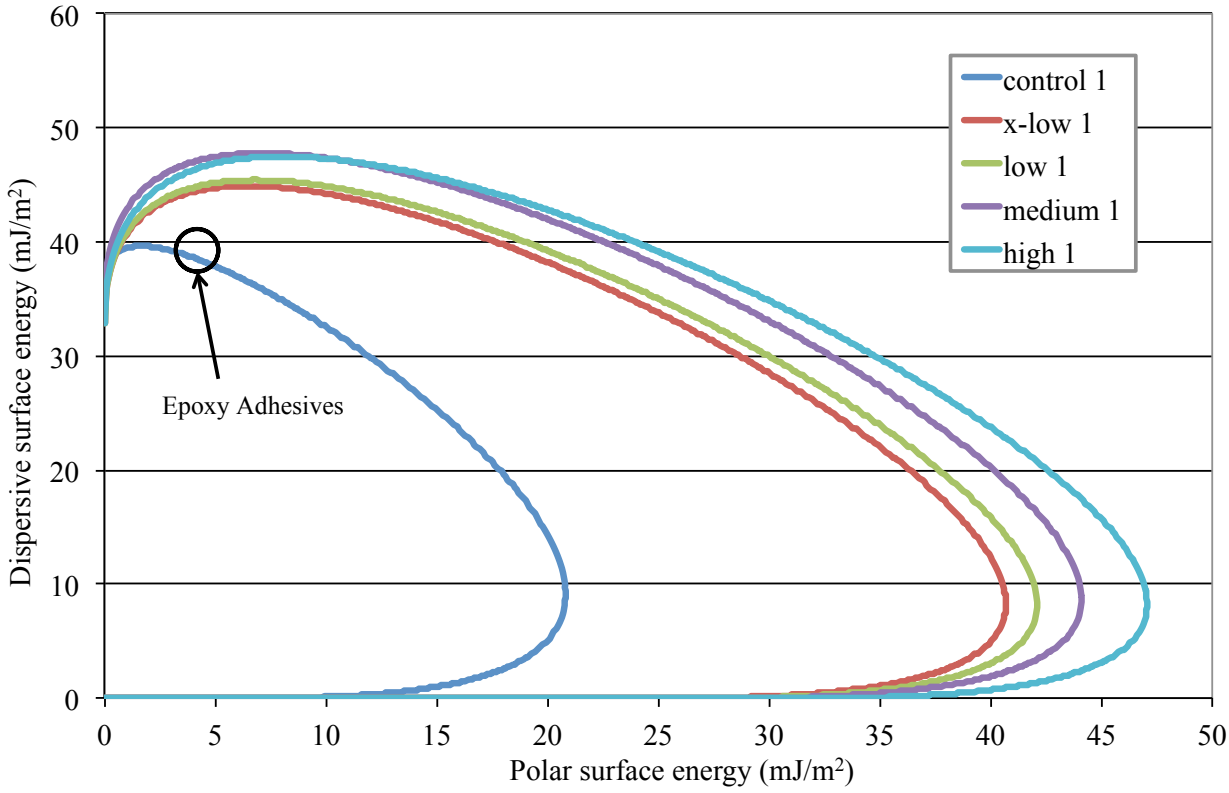

Figure 36. Wettability envelopes for *control 1*, *x-low 1*, *low 1*, *medium 1*, and *high 1* surfaces with typical epoxy adhesive surface energy. [67]

5.1.3 FTIR Measurements

Shown in Figure 37 are representative FTIR spectra from each substrate (*control 1*, *x-low 1*, *low 1*, *medium 1*, and *high 1*), as well as a virgin PFG 52006 nylon peel ply spectrum. Nylon peaks were identified on the peel ply spectrum. As observed, there are nonobvious nylon peaks on the composite samples or changing peaks in those locations. From initial inspection, FTIR spectra for all samples were not noticeably different. MVA was thus used to highlight the subtle spectral differences between sample sets. As shown in Figure 38, *control 1*, *medium 1* (with an identified potential outlier), and *high 1* samples grouped separately using 2 principal components, and thus were identified by the PLS model as different sample sets. *X-low 1* and *low 1* samples identified differently from *control 1*, *medium 1*, and *high 1* samples but were largely indistinguishable from each other, as there was significant overlap between these groupings.

The difference detected between the samples could be due to the amount of oxygen and nitrogen on the surfaces of the substrates or other factors, such as reflectivity variations. It would be expected that the sample plasma treated with the slowest raster speed (*high 1*) would have the most oxygen on the surface while the *control 1* sample would have the least. The lack of difference between the *x-low 1* and *low 1* samples could be due to the sampling depth of the instrument. Diffuse reflectance FTIR samples to a depth up to about 10 μm.[64] This results in signal from the bulk of sample, which would be the same for all samples tested. Atmospheric pressure plasma only penetrates a small depth on the order of a few nanometers.[19] Thus, the surface would need to be sufficiently altered in order for the signal from FTIR measurements to be significantly different. FTIR spectra collected from Toray 3900 epoxy plaques were subtracted from nylon peel ply prepared Toray T800/3900-2 composite surfaces but this did not result in spectra similar to nylon peel ply and no nylon peaks were revealed upon subtraction. To

determine chemical differences at the scale that peel ply preparation and plasma treatment changes the composite surface, XPS was necessary.

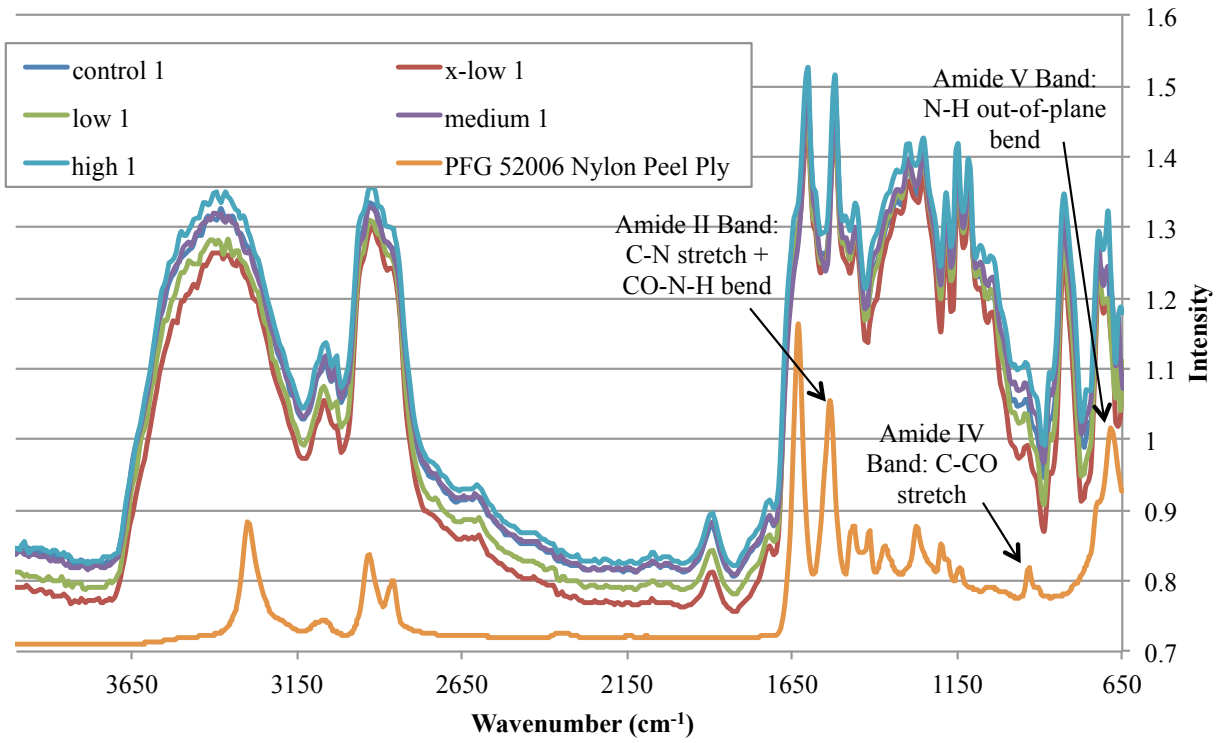

Figure 37. Representative FTIR spectra for *control 1*, *x-low 1*, *low 1*, *medium 1*, and *high 1* samples, as well as virgin 52006 nylon peel ply with nylon peaks identified. [76]

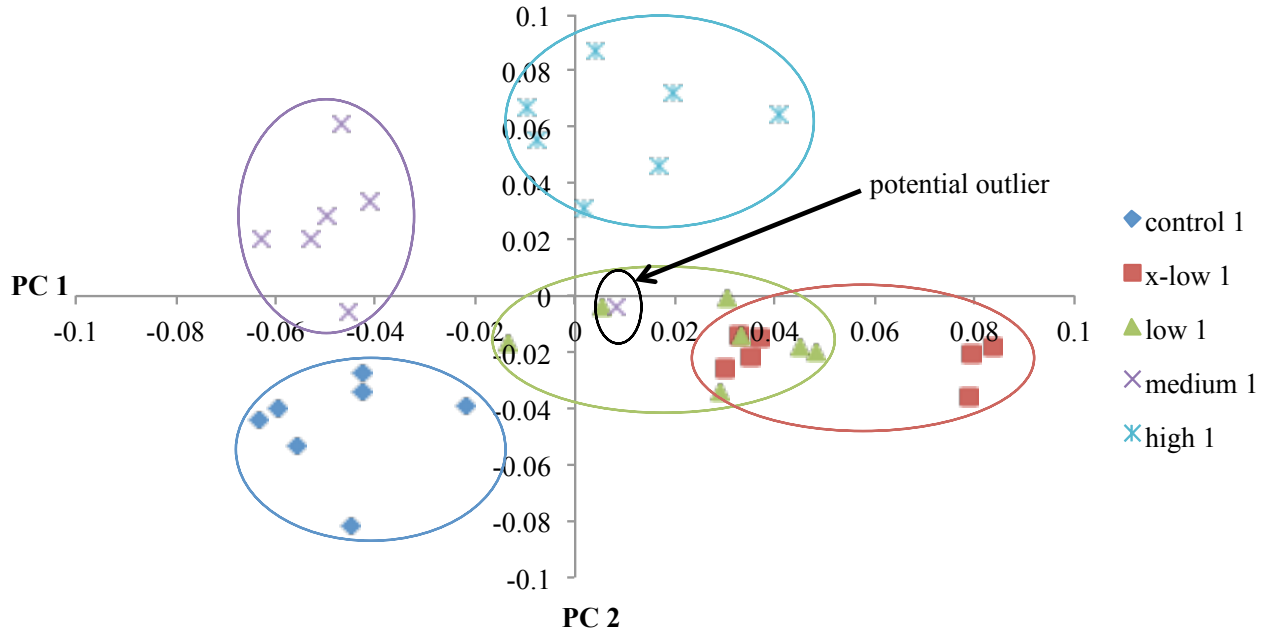

Figure 38. Scores plot from PLS analysis of *control 1*, *x-low 1*, *low 1*, *medium 1*, and *high 1* spectral data preprocessed with multiplicative scatter correction, a gap 1st derivative, and 5 smoothing points.

5.1.4 XPS Measurements

To obtain a meaningful measurement from XPS, it is important to understand where the signal originates. As mentioned previously, the spot size for the S-Probe XPS is about 800 µm. Referencing Figure 5 to this spot size suggested that the signal from XPS is an average from a rough peel ply surface. This includes signal from areas due to the peel ply imprint from yarns in both the warp and weft as well as from fractured epoxy (where the warp and weft crossed over and under each other). Thus, the data presented here would be expected to be an average of the heterogeneous peel ply surfaces.

Survey and high-resolution scans were significantly different for *control 1* and plasma treated surfaces. Atomic percentages determined from survey scans are shown in Table 8. It was

observed that the percentage of oxygen increased significantly from approximately 15% to 23% to 22% to 27% to 31% for *control 1* to *x-low 1* to *low 1* to *medium 1* to *high 1* treatments, respectively. Note that the difference in oxygen content on the *x-low 1* and *low 1* samples was insignificant. This increase in oxygen was expected as atmospheric pressure plasma was generated from air, which is composed of oxygen and nitrogen. Also shown in Table 8 was a slight decrease in nitrogen content on the surface of plasma treated surfaces compared to control surfaces, though the difference in nitrogen content between the plasma treated surfaces was not significant. This observation was not necessarily intuitive because air is mostly composed of nitrogen. Compared to epoxy surfaces (no peel ply), nylon peel ply prepared epoxy surfaces have higher concentrations of nitrogen, which can be attributed to the nitrogen present in the nylon moieties. [23] This was also confirmed by an XPS measurement of a neat epoxy Toray 3900 resin plaque (Table 8). The decrease in nitrogen from plasma treatment suggested that possibly some of the interphase created during cure of the CFRP against the nylon peel ply was actually removed by atmospheric pressure plasma.

Carbon content was shown to decrease with an increase in atmospheric pressure plasma treatment compared to *control 1* samples, also shown in Table 8. There was no significant difference, however, in carbon content on *x-low 1* and *low 1* samples. There was no trend for the sulfur content on *control 1* compared to plasma treated samples (Table 8), with the sulfur being attributed to proprietary toughenners within the epoxy matrix material or from the curing agent. The survey scan of the Toray 3900 resin suggested that at least some of the sulfur is from the curing agent, since it was present in the resin plaque. Though the simple DETA curing agent shown in Figure 2 does not contain sulfur, other curing agents that may be used in this propriety system could contain sulfur (e.g. 4,4'-diaminodiphenylsulfone [DDS]). [77] The Toray 3900 resin

examined did not contain any proprietary interlaminar tougheners but showed the largest concentration of sulfur of all samples examined with XPS. Previous research also showed possible trace amounts of sulfur on epoxy only surfaces and showed no sulfur on nylon peel ply prepared surfaces. [23] The lack of sulfur on nylon prepared samples, however, was inconsistent with the ~0.3% sulfur observed on the nylon peel ply sample here. Trace amounts of silicon were also observed on some samples (*low 1* and *x-low 1*) likely due to environmental contaminants.

Table 8. Atomic percentages of carbon, nitrogen, oxygen, and sulfur on *control 1*, *x-low 1*, *low 1*, *medium 1*, *high 1*, and Toray 3900 surfaces.

Element		**Sample**					
		control 1	***x-low 1***	***low 1***	***medium 1***	***high 1***	***Toray 3900***
C 1s	Average	74.298	68.446	68.588	64.831	61.754	77.848
	StDev	1.415	0.408	0.589	0.760	0.670	0.296
N 1s	Average	10.339	7.739	7.513	8.279	6.376	4.779
	StDev	0.890	0.466	0.366	0.850	1.164	0.437
O 1s	Average	14.997	22.656	22.323	26.559	30.665	15.252
	StDev	1.214	0.107	0.183	0.673	0.663	0.484
S 2p	Average	0.366	0.581	0.741	0.331	1.204	2.121
	StDev	0.124	0.090	0.087	0.238	0.211	0.057
Si 2s	Average	N/A	0.578	0.835	N/A	N/A	N/A
	StDev	N/A	0.293	0.111	N/A	N/A	N/A

Peak fitting of high-resolution XPS spectra confirmed the appearance of oxygen containing functional groups after plasma treatment. More specifically there were –COOH functional groups on plasma treated surfaces as shown in Figure 39-Figure 42. Note that on the *high 1* sample, the –COOH could also be identified as –COON, shown in Figure 42. This peak could be attributed to either –COOH or –COON functional groups, or represent a combination of both. More research would be necessary to determine which functional group is associated with that peak. It is sufficient to state, however, that oxygen-rich functionalities were identified as a result of plasma treatment. *Control 1* (no plasma, peel ply only) surface high-resolution peak fitting is shown in Figure 43 for comparison. No –COOH was observed on the *control 1* surface, suggesting functionalization. *Control 1* and plasma treated surfaces showed amide groups (N-C=O), which are chemically consistent with nylon and likely originate from the peel ply used. Note that the amide groups on the plasma treated surfaces could also be due to C=O bonds. Also shown is a high-resolution carbon scan for Toray 3900 epoxy resin (Figure 44). This shows that epoxy is best described by a two-peak fit, where the peaks were consistent with carbon bonds that would be expected for this epoxy (C-O, C-N, C-C, and C-H).[77] Additionally, comparison of high-resolution carbon scans for both peel ply prepared and plasma treated surfaces to the epoxy resin show that the chemistry of an epoxy was not recovered from plasma treatment, further supporting a functionalization mechanism.

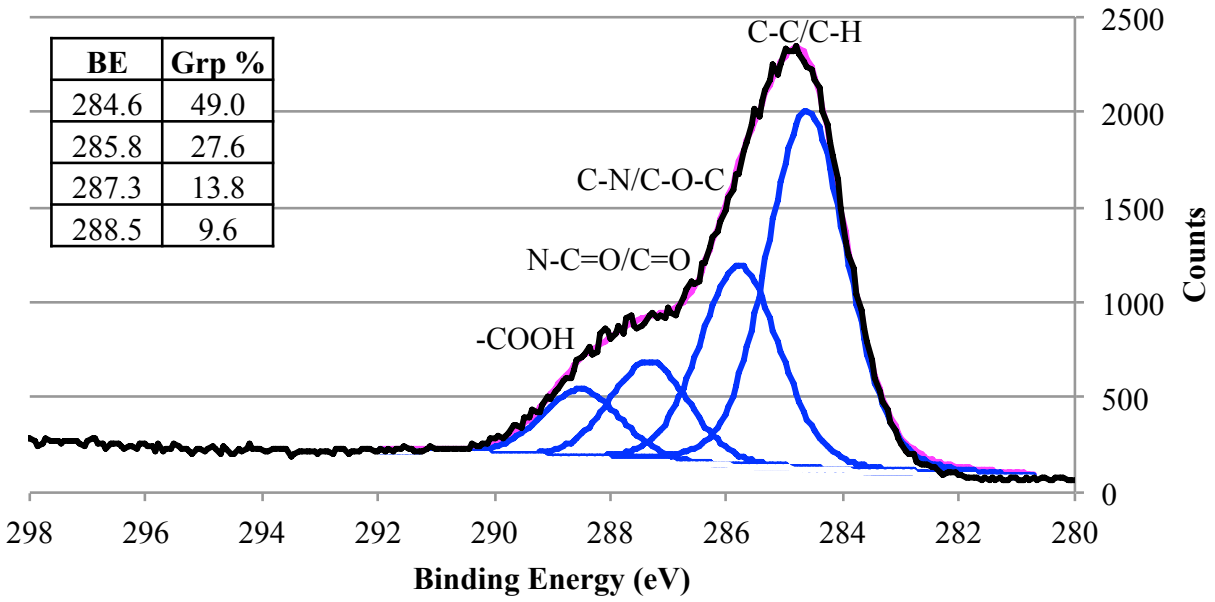

Figure 39. High-resolution carbon peak for *x-low 1* sample.

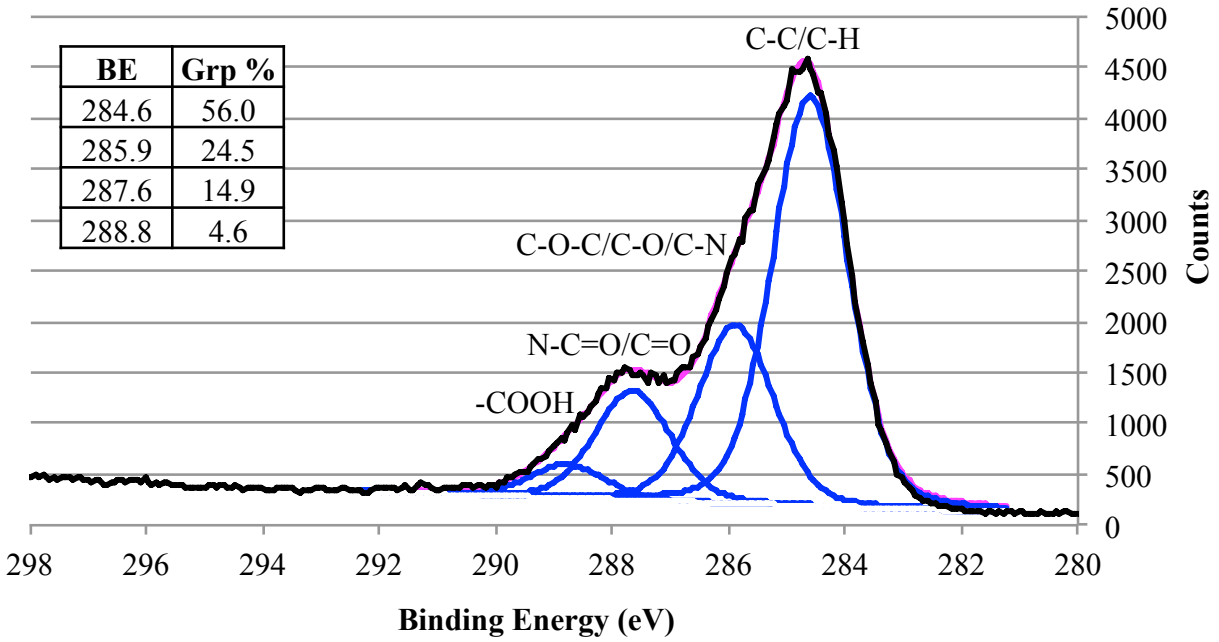

Figure 40. High-resolution carbon peak for *low 1* sample.

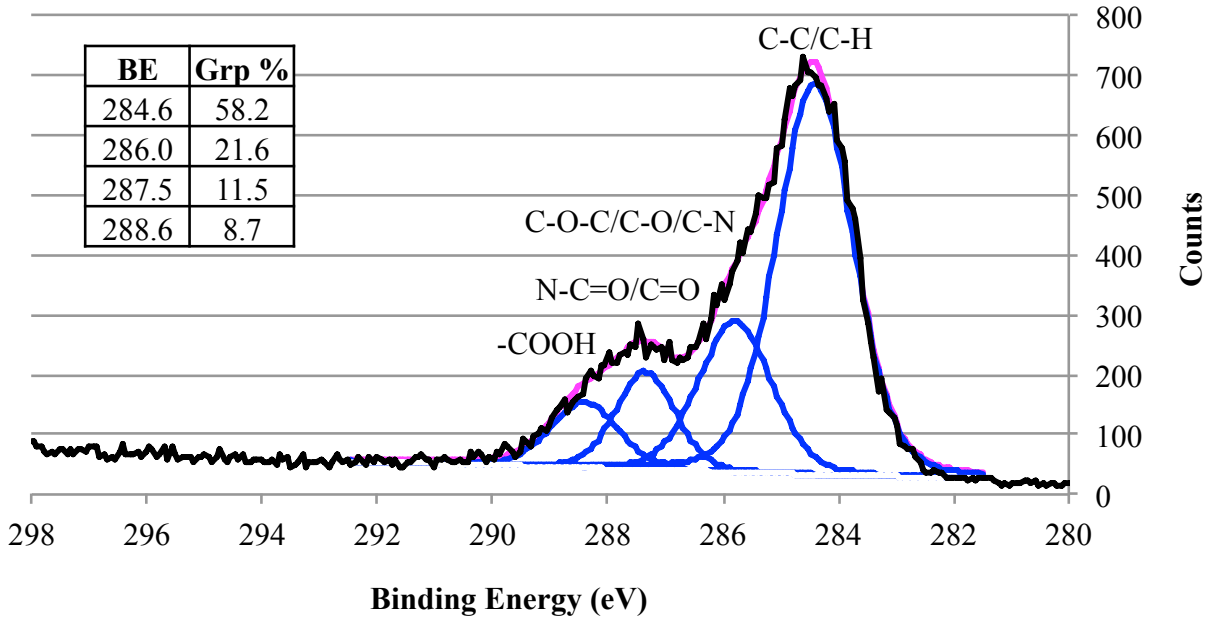

Figure 41. High-resolution carbon peak for *medium 1* sample.

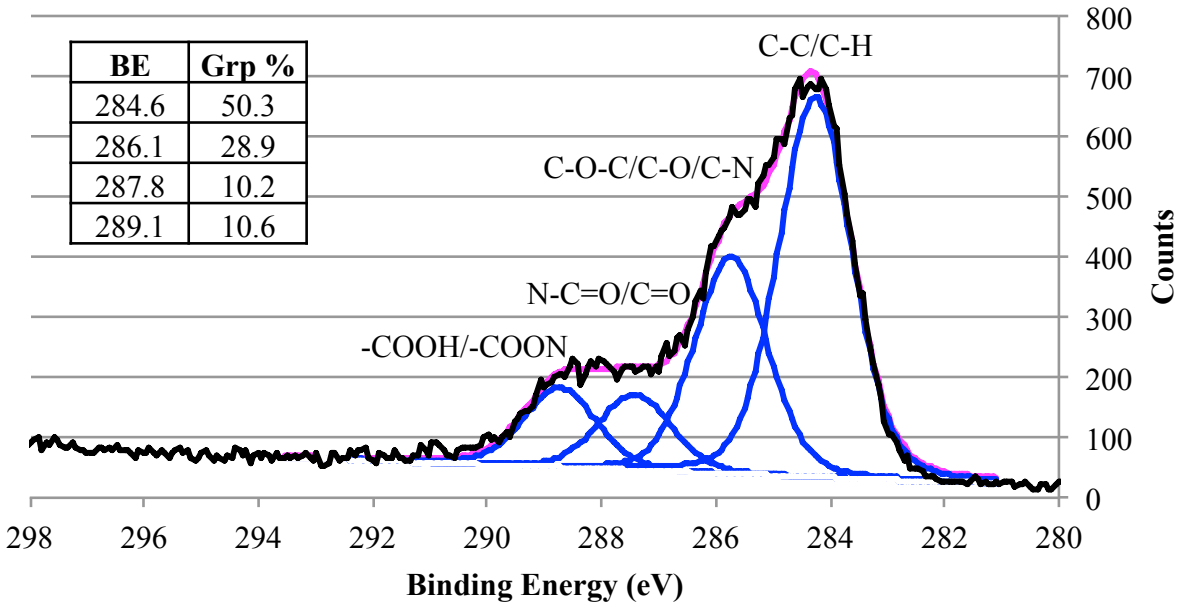

Figure 42. High-resolution carbon peak for *high 1* sample.

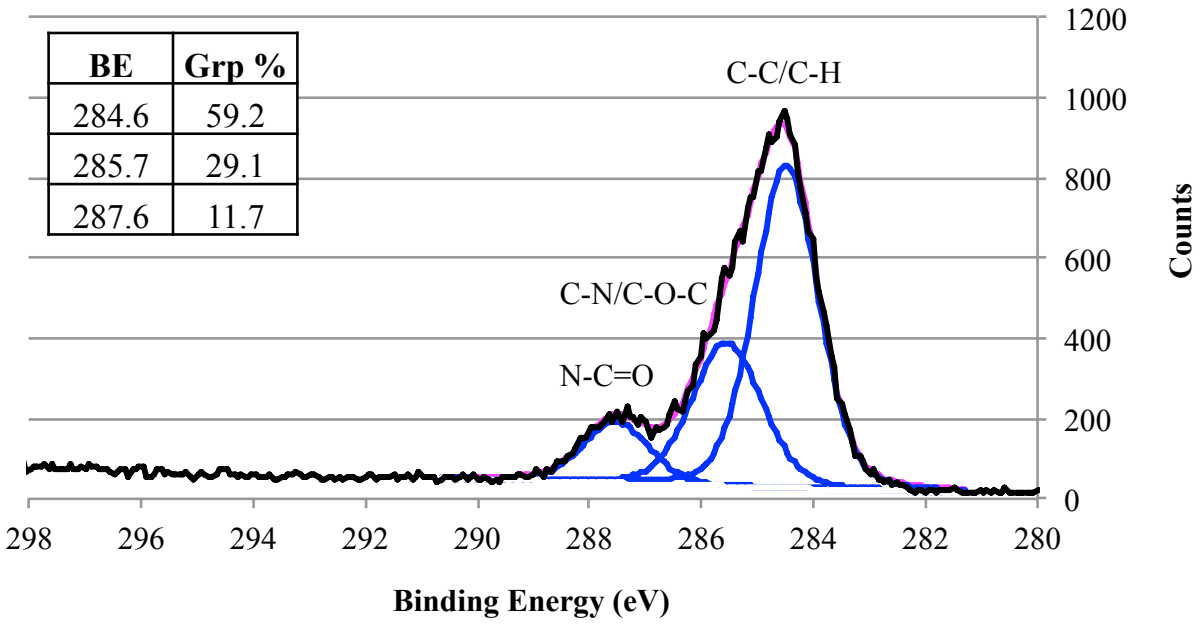

Figure 43. High-resolution carbon peak for *control 1* sample.

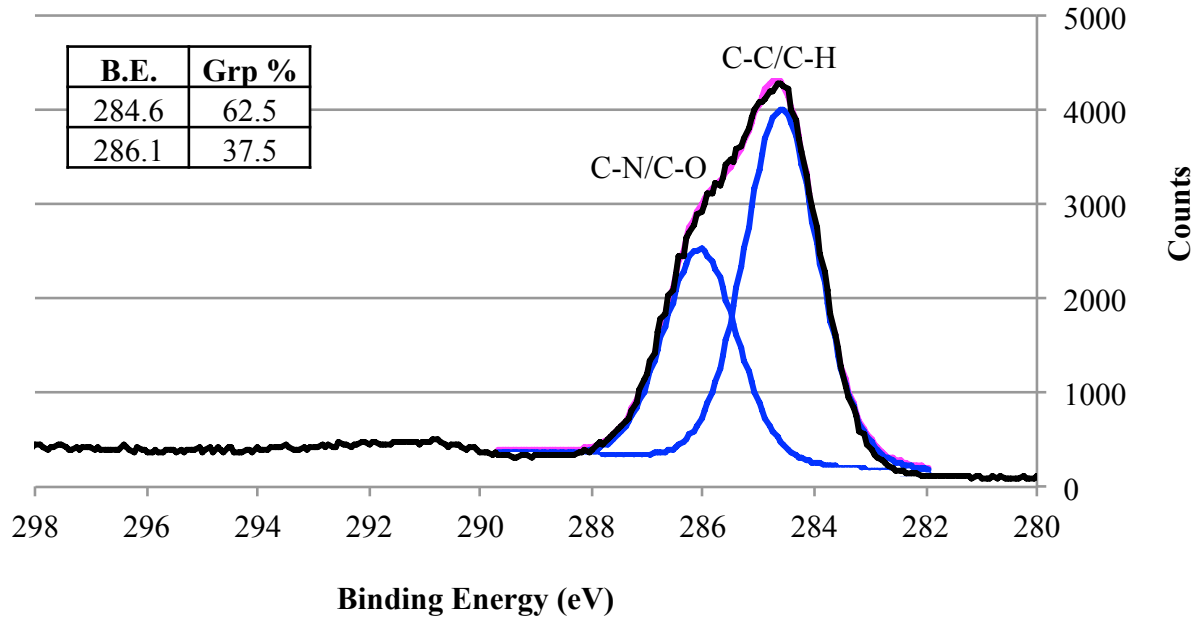

Figure 44. High-resolution carbon peak for Toray 3900 epoxy resin sample.

When a plasma treated substrate with hydroxyl or carboxyl functional groups on the surface is in contact with a curing epoxy, it is possible that some of the epoxides could react to form covalent

bonds with the cured surface. This notion was proposed by Zaldivar, et al. and is shown in Figure 45. [19]

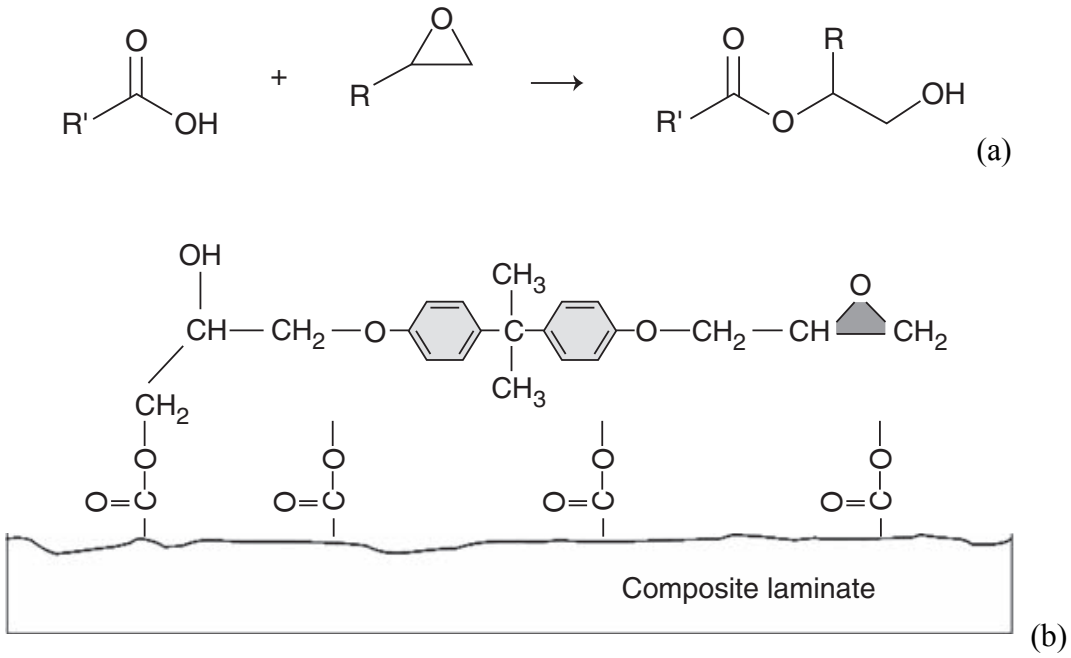

Figure 45. (a) Carboxyl group reacting with an epoxide and (b) suggested reaction between a plasma treated composite and a curing epoxy adhesive. **[19]**

Overall, XPS showed an increase in oxygen content on the surface of atmospheric pressure plasma treated samples. XPS survey scans also showed a decrease in nitrogen on plasma treated samples compared to control peel ply only samples. This observed decrease in nitrogen content on plasma treated samples suggest the nylon remnants/interphase could have been removed with plasma treatment. However, functionalization was supported as the chemistry of the plasma treated surfaces were not only different from *control 1* samples but also that of a pure epoxy, suggesting the remnants/interphase were not removed but rather functional groups were added to the surface. Further investigation would be necessary to determine if adhesion was due primarily to a functionalization or removal mechanism.

5.1.5 Relationship Among Surface Energy, Surface Chemistry, and Failure Mode

It was suggested that surface characteristics could be potentially used to predict bond quality. As shown in section 5.1.1, G_{IC} measurements did not vary significantly between levels of plasma treatment but failure mode did change. As shown in Figure 46, the average oxygen content was unable to differentiate between good and poor bond quality. Though not shown here, this held true for nitrogen and carbon contents as well. There was also no correlation between group percent of carbon bonding states (e.g. –COOH) and level of adhesion failure. Shown in Figure 47 is the relationship between polar surface energy and average adhesion failure. This plot suggests that polar surface energies for this specific system (Toray T800/3900-2 prepared with PFG 52006 peel ply and subsequent plasma treatment) below 27 mJ/m^2 were not sufficient for good bond quality.

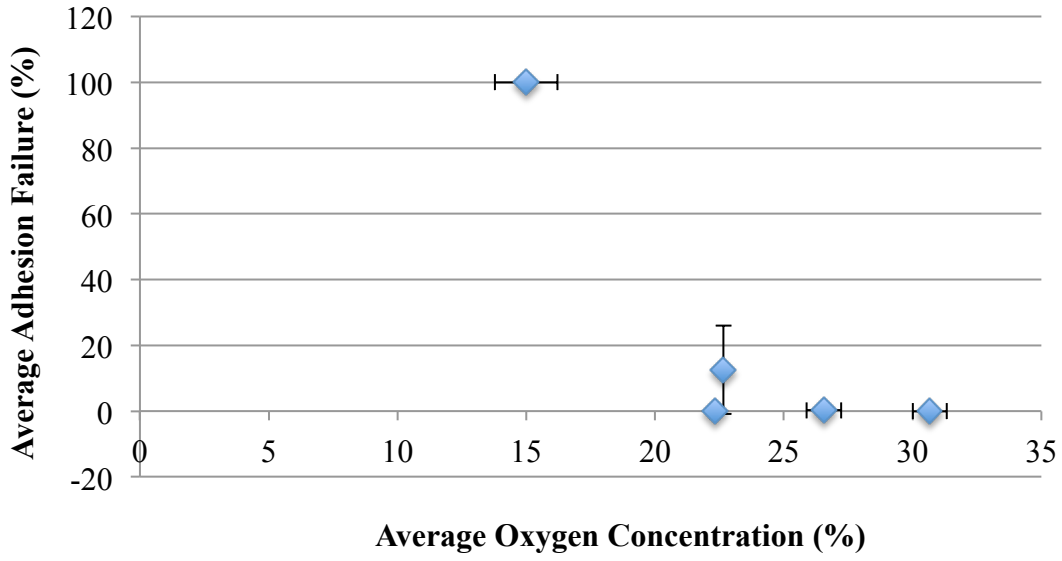

Figure 46. Average adhesion failure as a function of average oxygen content with standard deviation error bars.

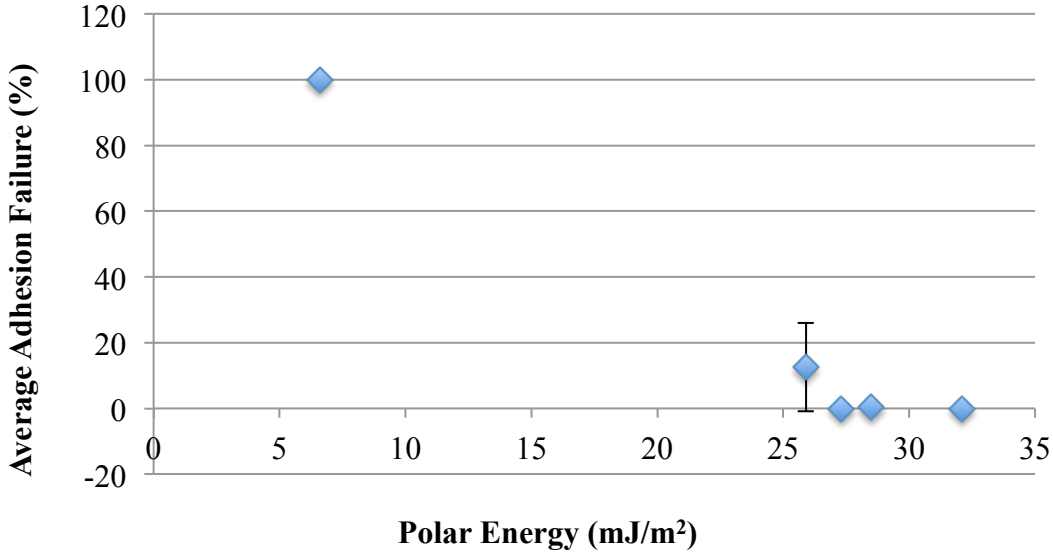

Figure 47. Average adhesion failure with standard deviation error bars as a function of polar surface energy.

5.1.6 SEM Images

Chemical and surface energy differences were detected on the plasma treated samples compared to the control peel ply only samples, though whether these changes were due to a functionalization or removal mechanism is still unclear. Thus, SEM was used to determine if there were any physical differences between the surfaces. *Control 1* surfaces (Figure 48) were compared to *high 1* samples (Figure 49) using SEM because if a physical difference were to exist, it would be most obvious in this case. As shown in Figure 48, it is apparent that nylon peel ply is transferred to the composite surface upon peel ply removal. This "onion skinning" effect of the peel ply fibers that supports peel ply transfer to the composite surface is shown in Figure 50. Peel ply fibers are extruded during fabrication, resulting in long chain molecules along the direction of the fiber. This construction of the fiber would suggest the fibers are stronger along the direction of the fiber rather than radially due to covalent bonds in the polymer chain backbone. The aligned chains would likely be held together by secondary forces, resulting in weaker bonds

between chains. This explains why the individual fibers could peel layer by layer similar to that of an onion, resulting in CFRP surfaces observed in Figure 48. Also shown in Figure 48 (c) and (d) is a mud crack-like morphology that has been observed on plasma treated samples. [19]

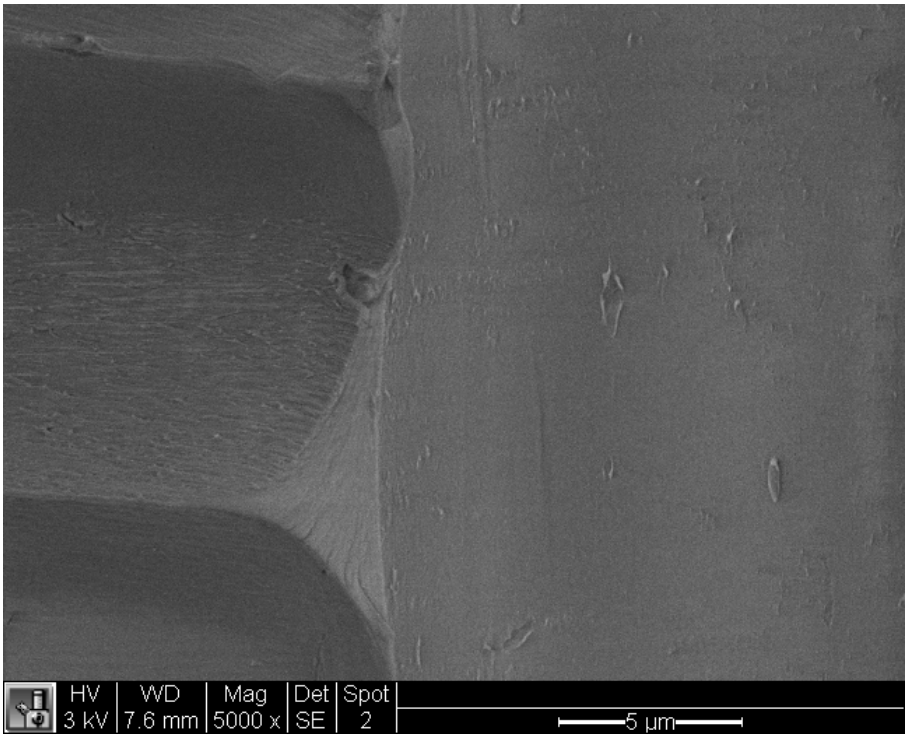

(a)

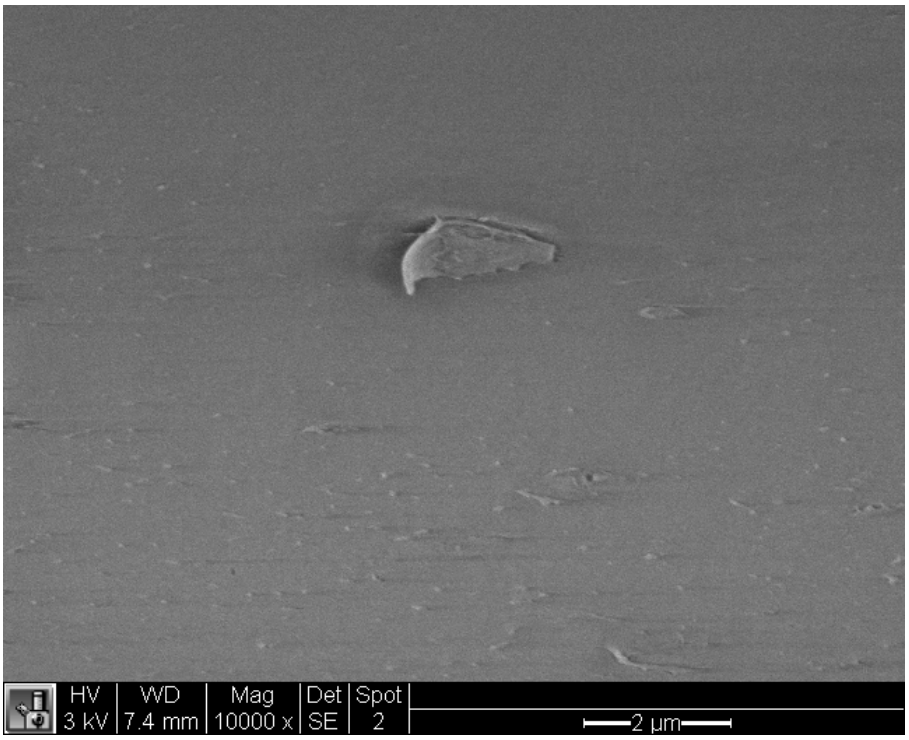
HV
3 kV
WD
7.4 mm
Mag
10000 x
Det
SE
Spot
2
2 µm

(b)

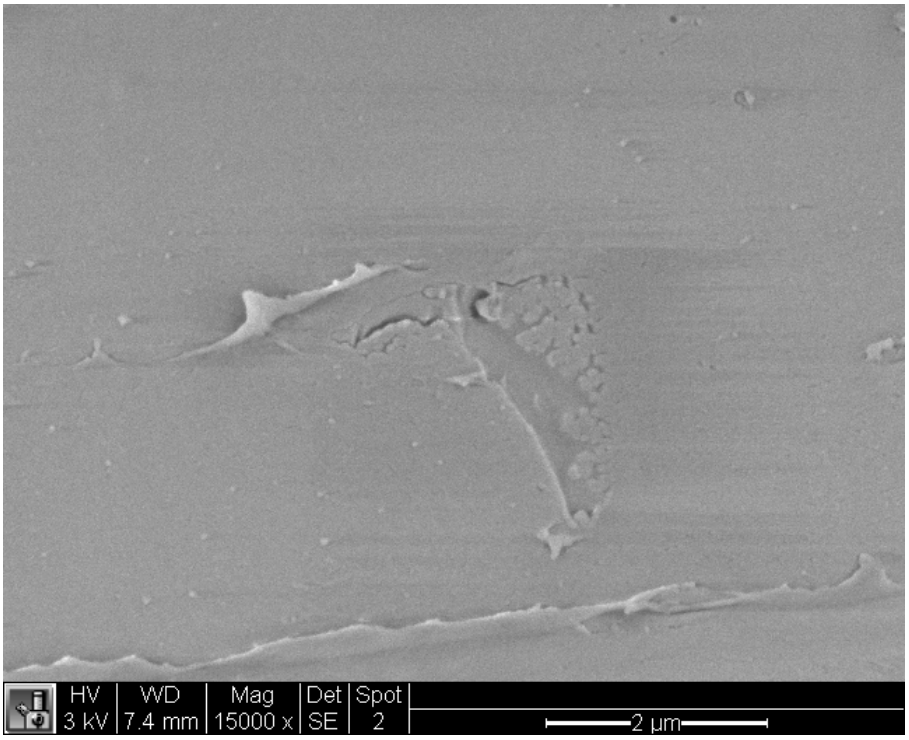
HV
3 kV
WD
7.4 mm
Mag
15000 x
Det
SE
Spot
2
2 µm

(c)

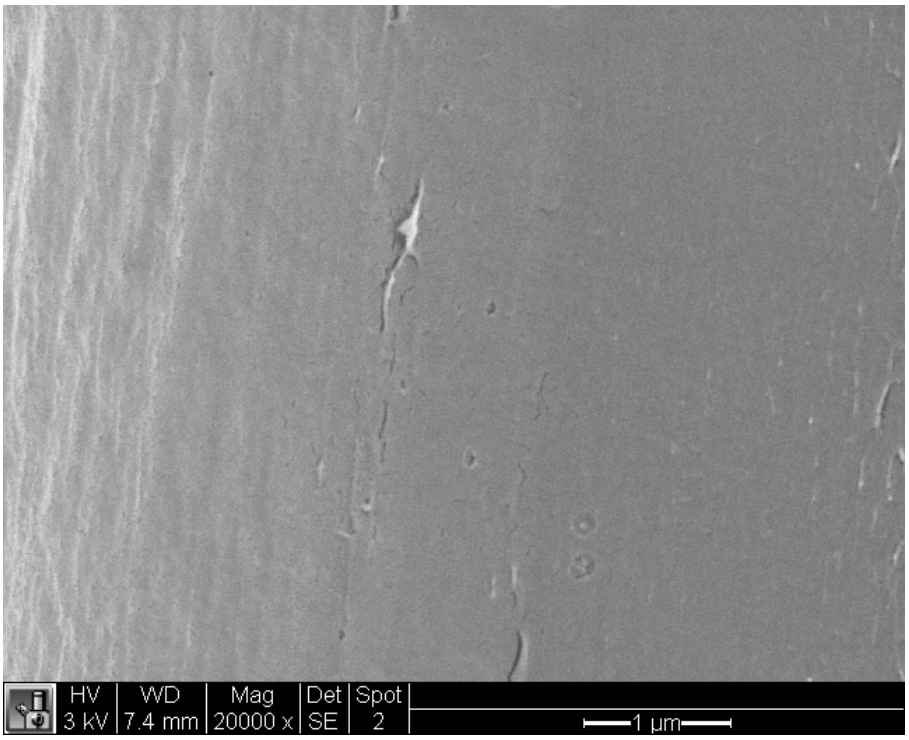

(d)

Figure 48. Electron micrographs of *control 1* surfaces at (a) 5000X, (b) 10,000X, (c) 15,000X, and (d) 20,000X magnifications.

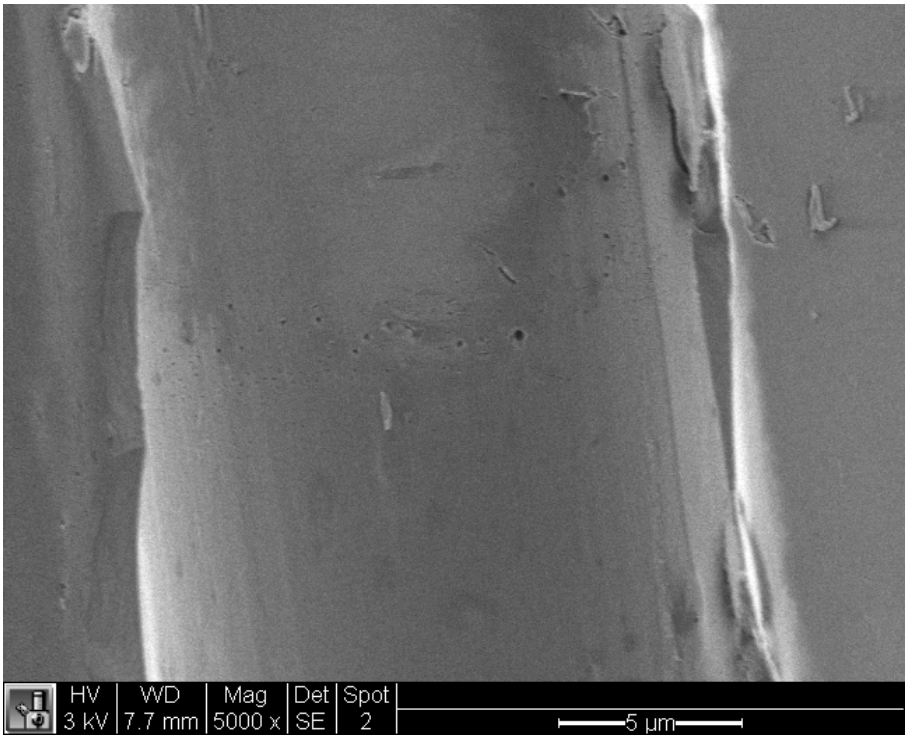

(a)

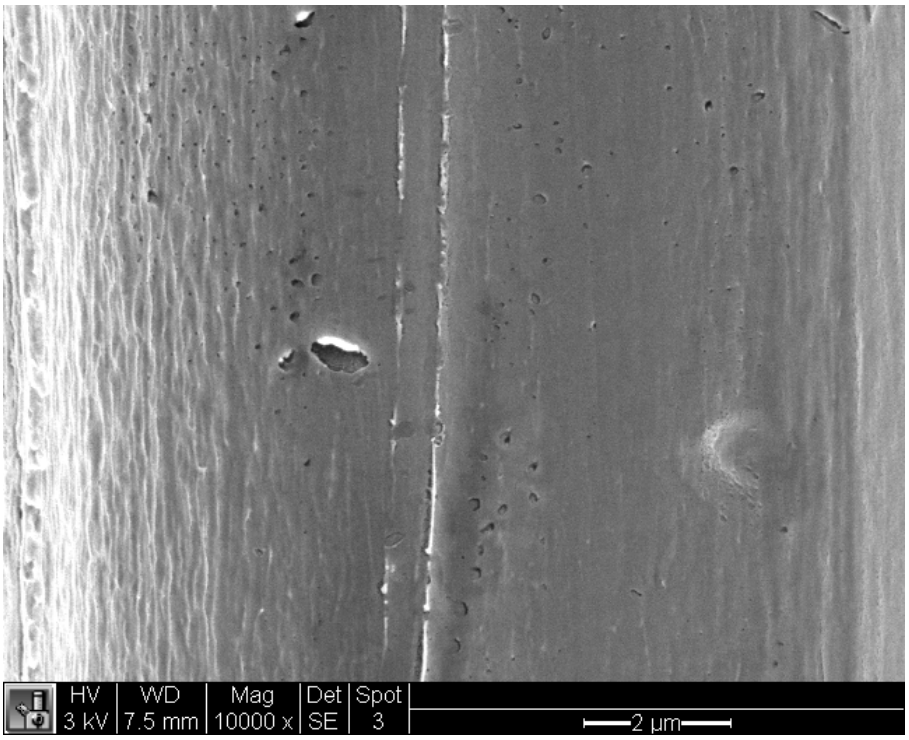
HV
3 kV
WD
7.5 mm
Mag
10000 x
Det
SE
Spot
3
2 µm

(b)

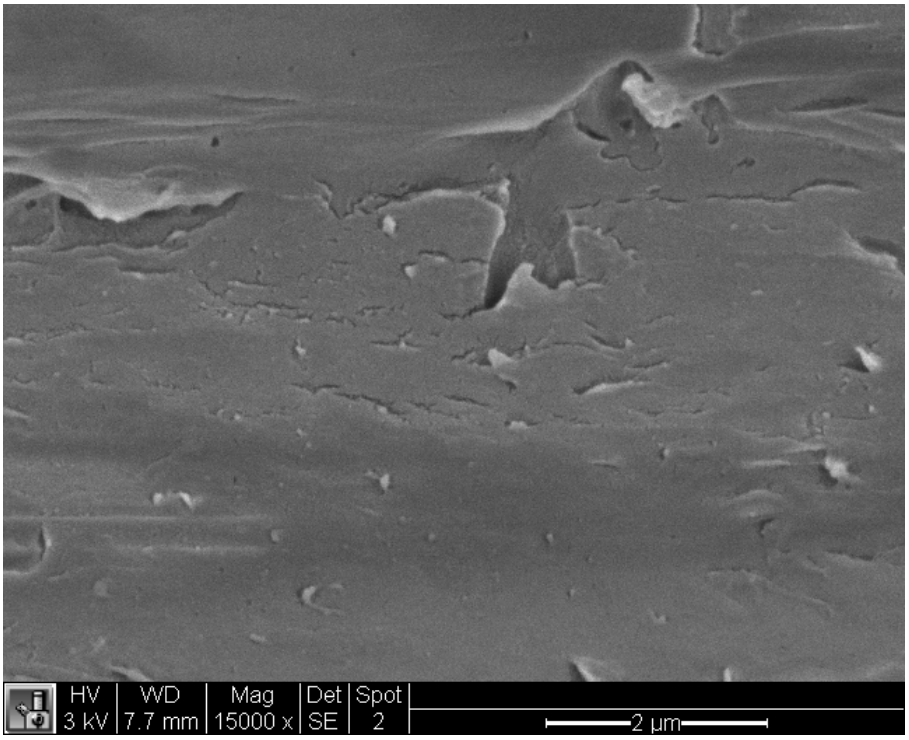
HV
3 kV
WD
7.7 mm
Mag
15000 x
Det
SE
Spot
2
2 µm

(c)

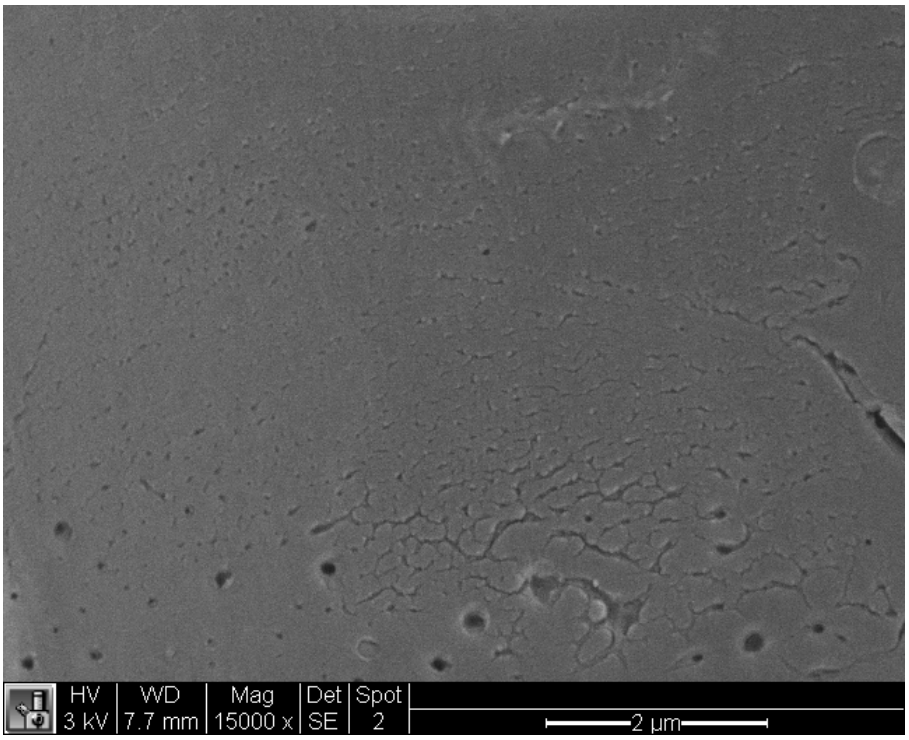

(d)

Figure 49. Electron micrographs of *high 1* surfaces at (a) 5000X, (b) 10,000X, (c) 15,000X, and (d) 20,000X magnifications.

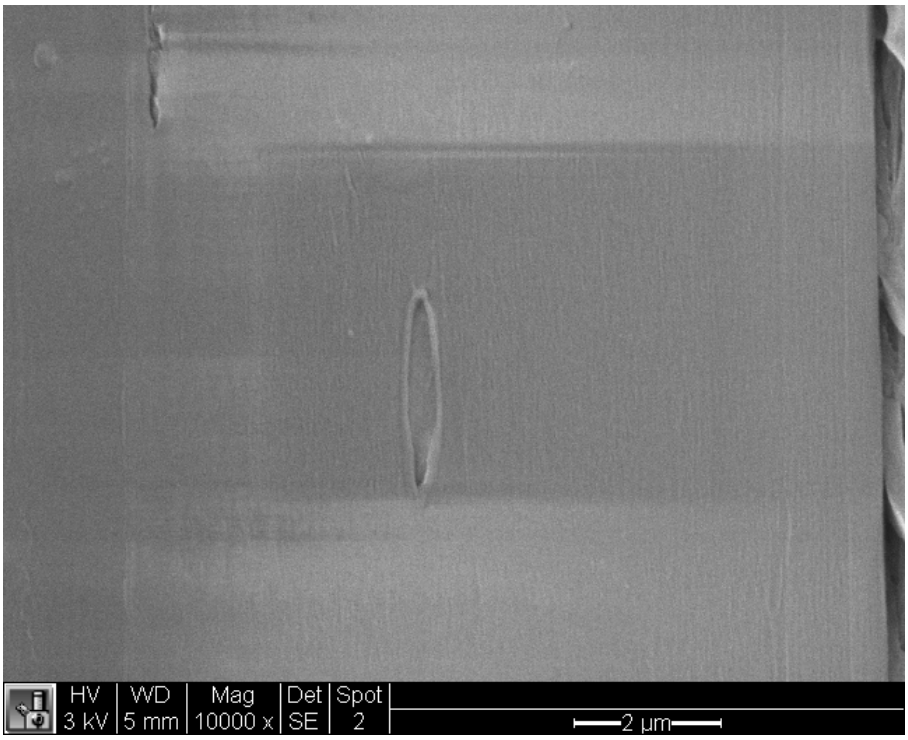

Figure 50. Electron micrograph at 10,000X of nylon peel ply removed from a Toray T800/3900-2 composite surface showing "onion skinning" effect.

Nylon peel ply remnants were also observed on *high 1* samples, as was a mud crack-like morphology (Figure 49). Initial observation of an apparent increase in this mud crack-like morphology on the *high 1* samples led to further examination of the *control 1* samples to confirm the increase. Figure 51 shows that *control 1* samples also exhibited significant amounts of a mud crack-like morphology. Because this morphology was observed on *control 1* and *high 1* samples, it could be due to the platinum sputtering process that all samples undergo to become conductive for SEM. Unlike *control 1* samples, however, "spot-like" features were prevalent (Figure 49). Previous research showed "spot-like" features on as-tooled composite surfaces cured against a release agent that was subsequently plasma treated. [31] As shown in Figure 51, "spot-like" features did exist on the *control 1* surface but not in a similar concentration to the *high 1* samples. These features could also be microporosity and not be a result of plasma treatment.

Microporosity would not necessarily be the same for all samples and could explain why it was observed in different concentrations on the *control 1* and *high 1* samples. These features could, however, be a result of the plasma interacting with the surface. Figure 52 is an image of an atmospheric pressure plasma flume on a composite surface. [31] There appear to be miniature explosions on the surface, which could also explain the "spot-like" features or craters on the surface, suggesting that atmospheric pressure plasma treatment is also potentially ablative and could remove some of the prepared composite surface.

These "spot-like" features were not observed on released peel ply prepared surfaces in previous research and the author suggested that vorticity prevented atmospheric pressure plasma from interacting directly with the CFRP surface within the individual peel ply channels (Figure 53). [31] The present research, however, suggests that plasma does in fact interact significantly with the CFRP surface within the individual channels as shown by the difference between *control 1* and *high 1* samples by SEM and fracture mode.

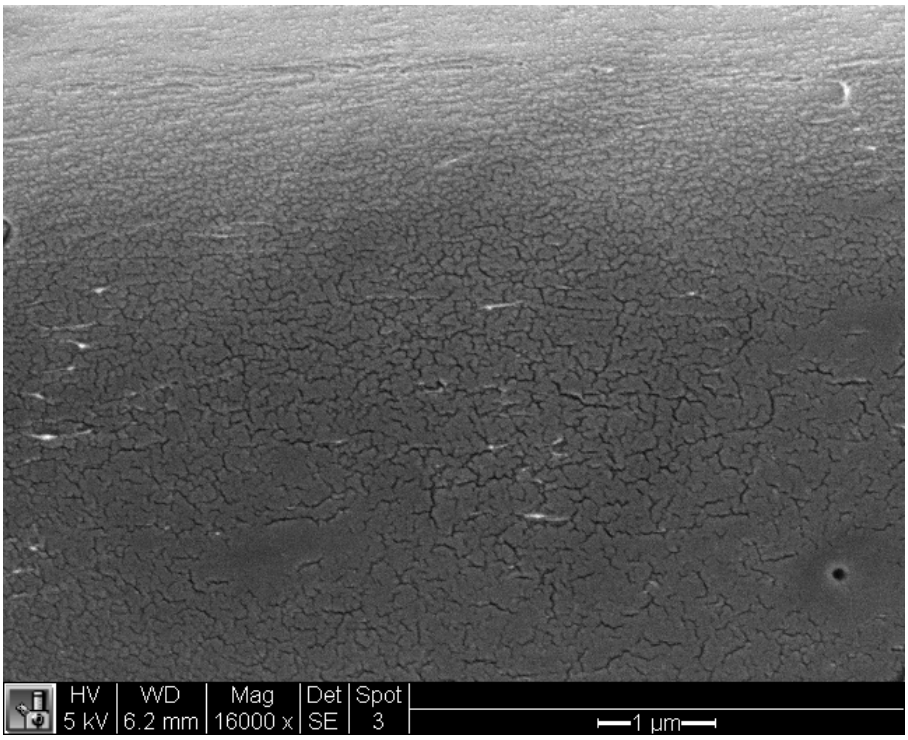

Figure 51. Electron micrograph of *control 1* sample at 16,000X showing significant mud cracking morphology but only one "spot-like" feature.

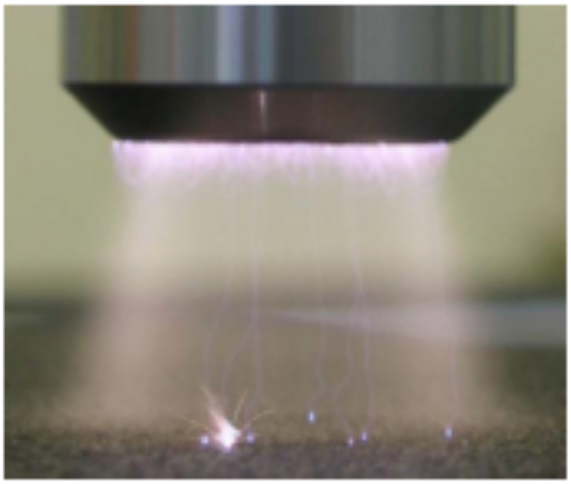

Figure 52. Image of plasma flume showing miniature explosions on a composite surface. [31]

Figure 53. Schematic of vorticity suggesting why atmospheric pressure plasma may not directly interact with the surface within the peel ply channels. [31]

Based on data to this point, it appears that bonding of plasma treated surfaces is mostly due to functionalization of the surface, as peel ply remnants are still present on the *high 1* surfaces. However, removal may still play a role as "spot-like" features were prevalent on the *high 1* surfaces and could have been areas where the peel ply interphase was removed from the surface. This encouraged further experiments, including the study of the interaction between the adhesive itself and the nylon peel ply as well as an additional material system that was known to result in adhesion failure. This system (Hexcel T300/F155 prepared with PFG 60001 peel ply) was of particular importance, because significant amounts of peel ply remnants have been observed on the peel ply prepared surface. If this material system were to bond well after atmospheric pressure plasma treatment, then examination of the plasma treated and control surface by SEM would render obvious if peel ply remnants were removed. Both of these experiments will be discussed in the following sections.

5.2 Hexcel F155/T300 + PFG 60001 Polyester Peel Ply + Atmospheric Pressure Plasma + EA 9696

5.2.1 DCB Testing

To determine if further examination of this material system would be warranted, DCB testing was performed first to find if a change in fracture energy and failure mode were observed after

plasma treatment. As shown in **Figure 54**, a change in failure mode was apparent from *control 2* samples to plasma treated samples. *Control 2* samples exhibited 100% adhesion failure whereas plasma treated samples exhibited mixed failure modes (adhesion, cohesive in the adhesive, cohesive in the substrate) that were confirmed with SEM. Previous research suggested that the thickness of the peel ply residue/remnants left behind on the composite surface were the cause of adhesion failure. [6] To determine if the observed adhesion failure on these samples was due to this, fracture surfaces were examined with SEM (**Figure 55**). The images in **Figure 55** are representative of the CFRP and adhesive side of adhesion failure regions, where peel ply remnants are present on both sides. It appeared that the regions experiencing adhesion failure fractured in the remnant phase, described by Moench and shown schematically in **Figure 56**. [6]

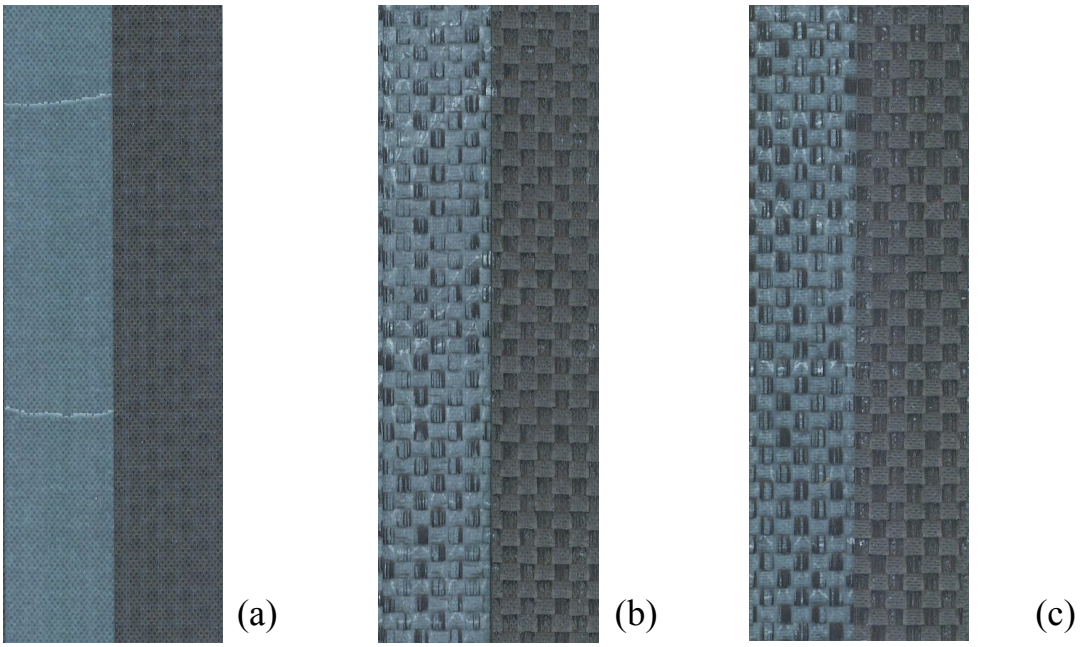

Figure 54. Representative images of (a) *control 2*, (b) *low 2*, and (c) *high 2* DCB fracture surfaces.

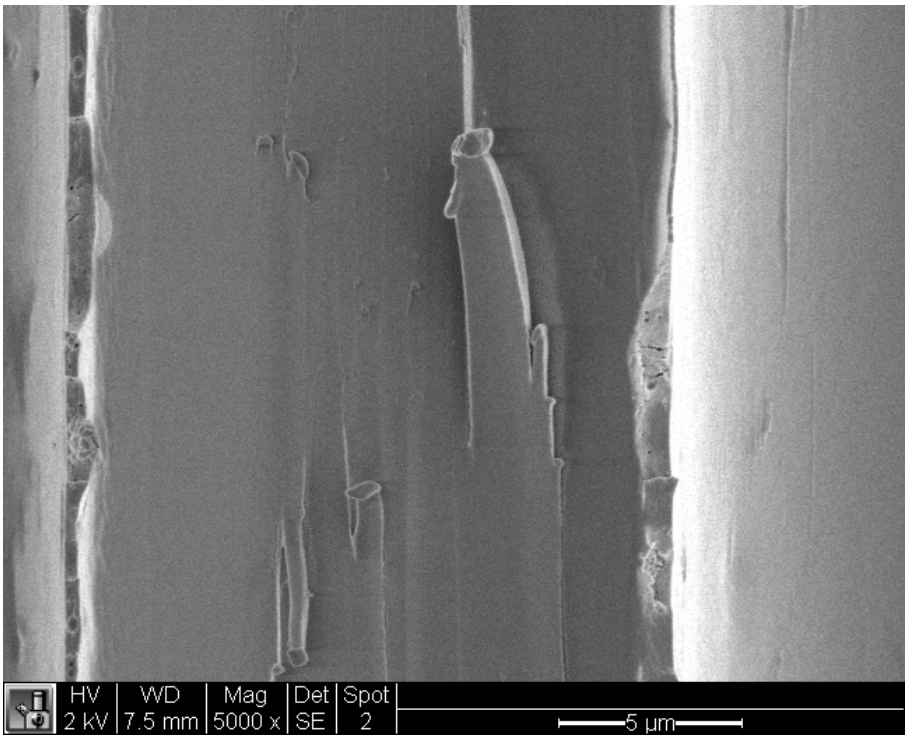
HV
2 kV
WD
7.5 mm
Mag
5000 x
Det
SE
Spot
2
5 µm
(a)

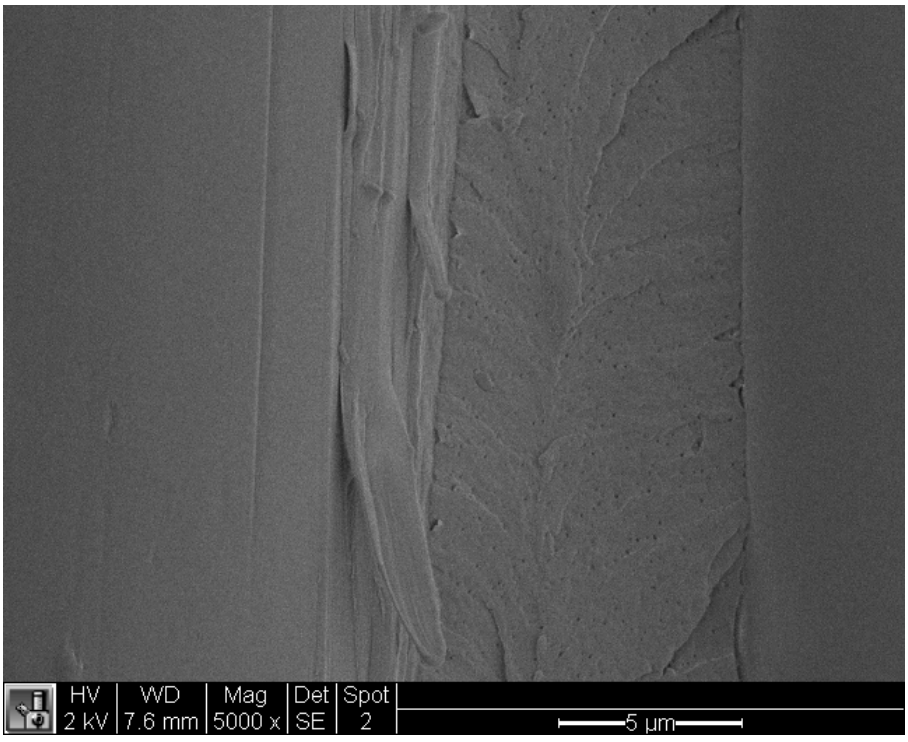
HV
2 kV
WD
7.6 mm
Mag
5000 x
Det
SE
Spot
2
5 µm
(b)

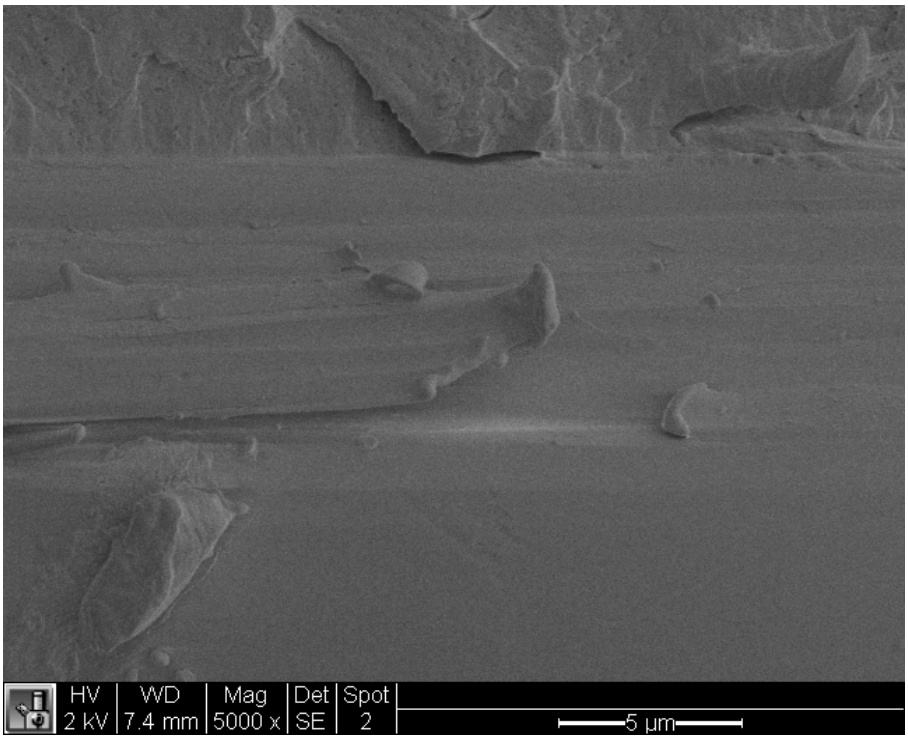

(c)

Figure 55. Electron micrographs of (a) *control 2* surface (b) *low 2* surface, and (c) *high 2* surface at 5000X.

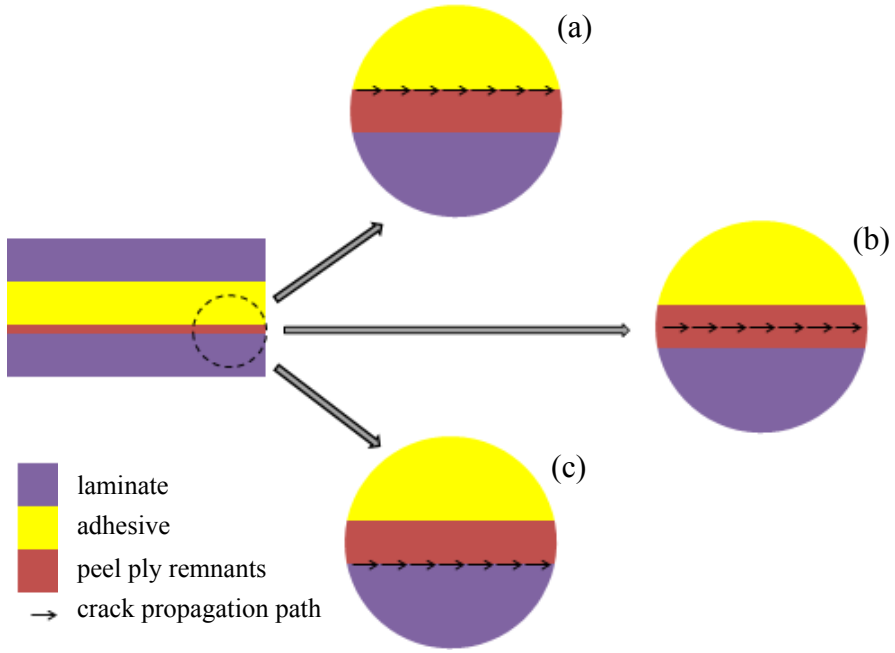

Figure 56. Three crack propagation paths with respect to peel ply remnants that are classified by adhesion failure, [6] where (a) describes crack propagation along the peel ply remnants and adhesive interface, (b) describes the crack propagation path within the peel ply remnants, which was observed in this study, and (c) describes crack propagation along the peel ply remnants and adherend interface.

Fracture energies for *control 2* samples were low (275 J/m^2 with a standard deviation of 93 J/m^2). Fracture energies (Figure 57) were not entirely valid for plasma treated samples, as ply bridging was observed during testing (Figure 58). Bridging occurs when fibers or lamina delaminate from both DCB adherend surfaces and results in a dual crack propagation (Figure 58). Previous research has shown G_{IC} to increase due to fiber bridging. [78] Other research at the University of Washington also supported this. [79] Equation [11] (4.3) assumes one crack is propagating through the DCB specimen during testing. As Hurley described, when two cracks propagate through the DCB, the denominator in Equation [11], the total crack area, is smaller than the

actual value, which would result in an apparent increase in fracture energy.[79] The crack is smaller because instead of the formation of two new surfaces upon fracture, four surfaces are actually created.

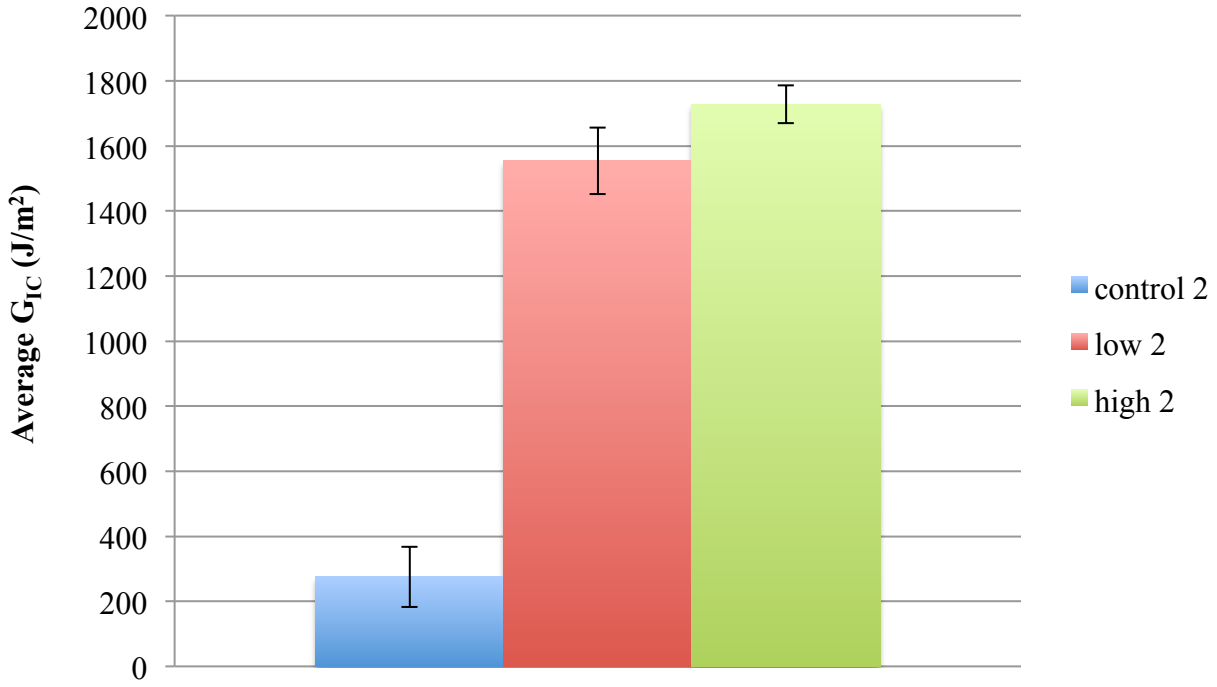

Figure 57. Average G_{IC} measurements for *control 2*, *low 2*, and *high 2* samples with standard deviation error bars.

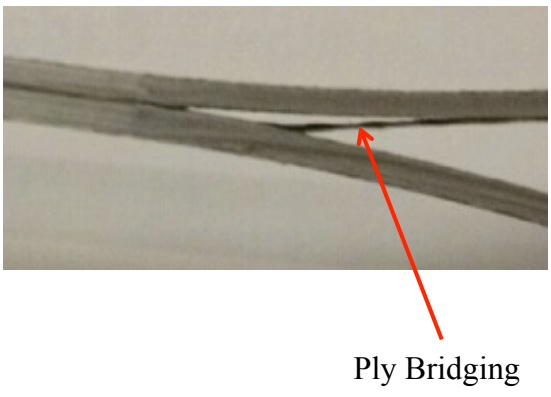

Figure 58. Ply bridging observed on all plasma treated samples.

From this data, it was obvious that atmospheric pressure plasma treatment changed failure from 100% adhesion failure to mixed failure modes as observed with SEM. Also, this initial examination of fracture surfaces suggested that peel ply remnants were not removed from the peel ply prepared surface prior to adhesion, as peel ply fibers were present on the fracture surfaces. These results warranted further characterization of the prebond surfaces, including CA measurements, FTIR, XPS, and SEM.

5.2.2 Contact Angle Measurements

Some unexpected results for *control 2*, *low 2*, and *high 2* samples, based off of materials system 1, were observed. Polar fluid CA measurements for plasma treated samples were lower than *control 2* surfaces, perhaps as expected (Figure 59). However, there were two unexpected observations: (1) DI H_2O CA increased with plasma treatment, and (2) DIM CA increased for plasma treated samples compared to *control 2* samples. This was not observed on material system 1 (Figure 34). To understand the first observation, surface chemistry and surface morphology information were needed as will be explained in the following sections.

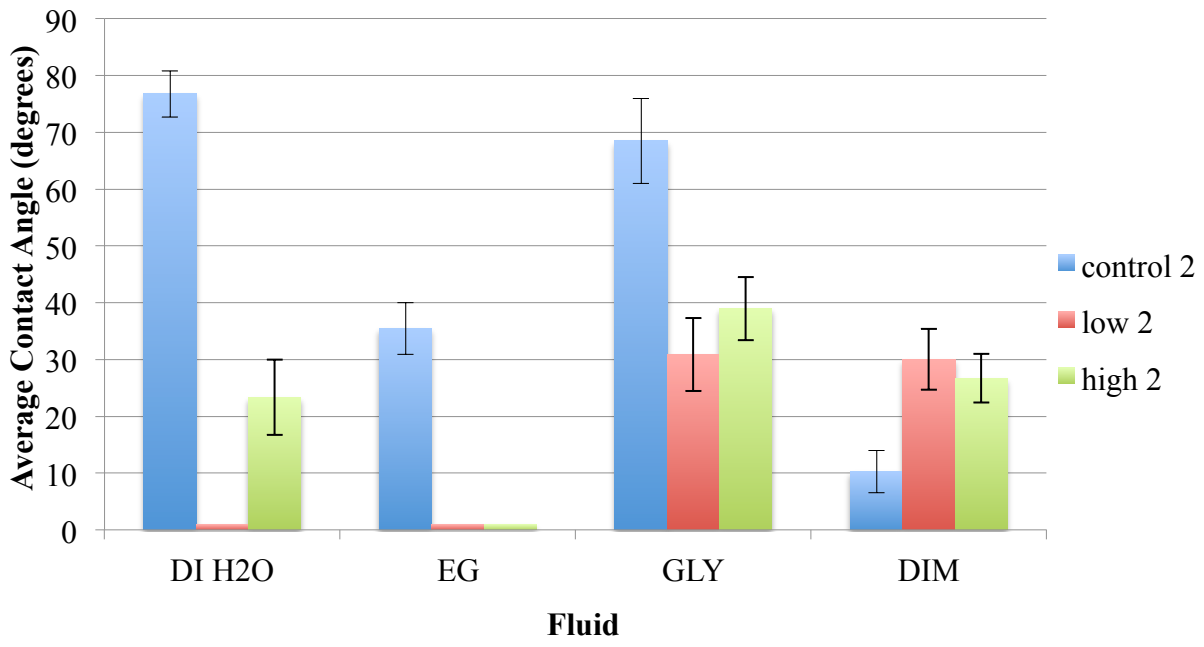

Figure 59. CA measurements for *control 2*, *low 2*, and *high 2* surfaces with standard deviation error bars.

From CA measurements, surface energies and wettability envelopes were calculated (Figure 60 and Figure 61). As shown in Figure 60, the polar surface energy increased significantly for plasma treated samples compared to *control 2* samples, causing a significant increase in total surface energy. Also shown in Figure 60 is a decrease in dispersive energy. It was interesting to observe that all surface energy components were similar to those calculated for material system 1. The trend of decreasing polar component and increasing dispersive component with plasma treatment was not intuitive and requires further investigation.

Unlike wettability envelopes for material system 1 (Figure 36), the significant change in wettability envelopes with plasma treatment does not explain why adhesion was observed for plasma treated samples but not *control 2* samples, as typical epoxy adhesives would be expected to wet all surfaces examined (Figure 61). This suggested that the difference in adhesion is likely

due to chemical or morphological differences that would need to be investigated with FTIR, XPS, and SEM.

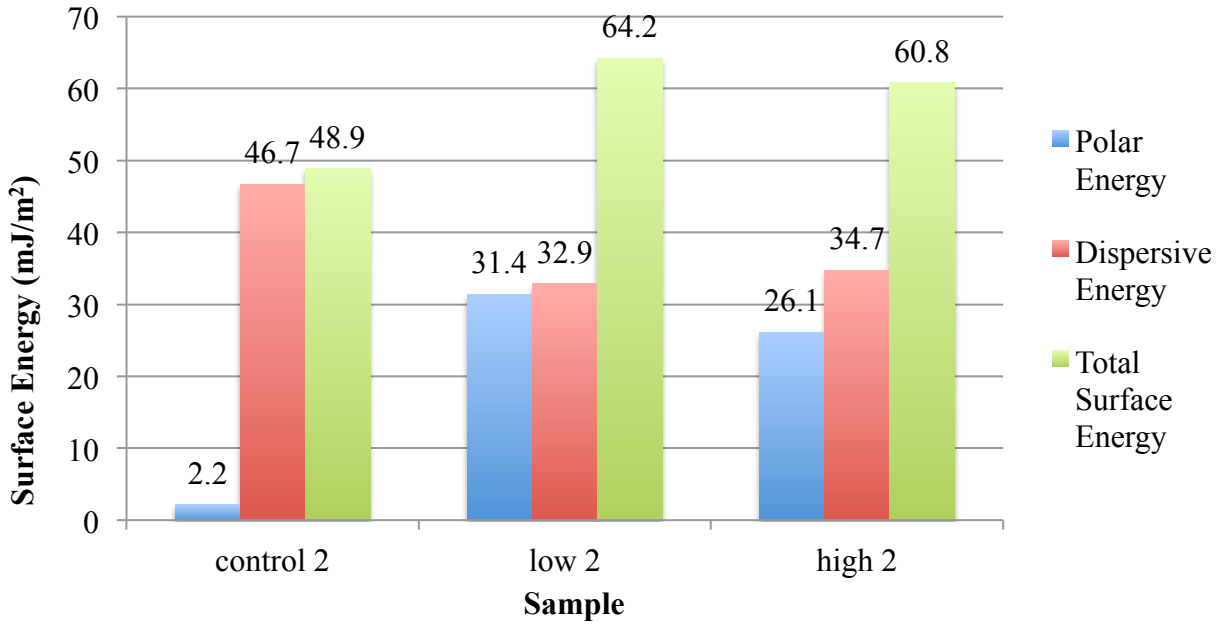

Figure 60. Surface energies for *control 2*, *low 2*, and *high 2* samples.

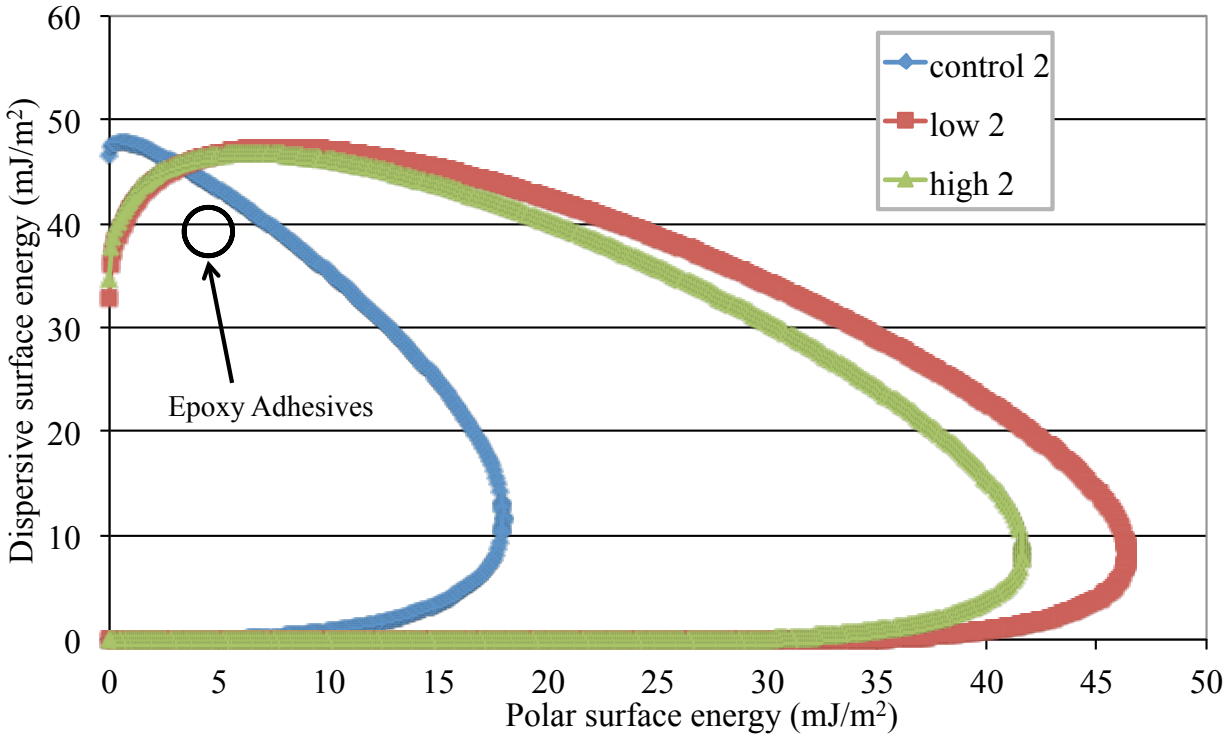

Figure 61. Wettability envelopes for *control 2*, *low 2*, and *high 2* samples with typical epoxy adhesive surface energy. [67]

Overall, there was a clear difference between surface energies of *control 2* and plasma treated samples with an apparent, though small, difference between *low 2* and *high 2* surfaces. Further characterization was necessary to discern these differences.

5.2.3 FTIR Measurements

Shown in Figure 62 are representative FTIR spectra from each substrate (*control 2*, *low 2*, and *high 2*), as well as a virgin PFG 60001 polyester peel ply spectrum. Some polyester peaks were identified on the peel ply spectrum. [80,81] As observed, there were nonobvious polyester peaks on the composite samples or changing peaks in those locations. From initial inspection, FTIR spectra for all samples were not noticeably different. MVA was thus used to highlight the subtle spectral differences between sample sets. As shown in Figure 63, *control 2*, *low 2*, and *high 2*

(with an identified potential outlier), grouped separately using 2 principal components, and thus were identified by the PLS model as different sample sets.

The difference detected between the samples could be due to the amount of oxygen and nitrogen on the surfaces of the substrates or other factors, such as reflectivity variations. It would be expected that the sample plasma treated with the slowest raster speed (*high 2*) would have the most oxygen and nitrogen on the surface while the *control 2* sample would have the least. As stated previously, diffuse reflectance FTIR samples to a depth up to about 10 μm.[64] This results in signal from the bulk of sample, which would be the same for all samples tested. Atmospheric pressure plasma only penetrates a small depth on the order of a few nanometers.[19] Thus, the surface would need to be sufficiently altered in order for the signal from FTIR measurements to be significantly different. To determine chemical differences at the scale that peel ply preparation and plasma treatment changes the composite surface, XPS was necessary.

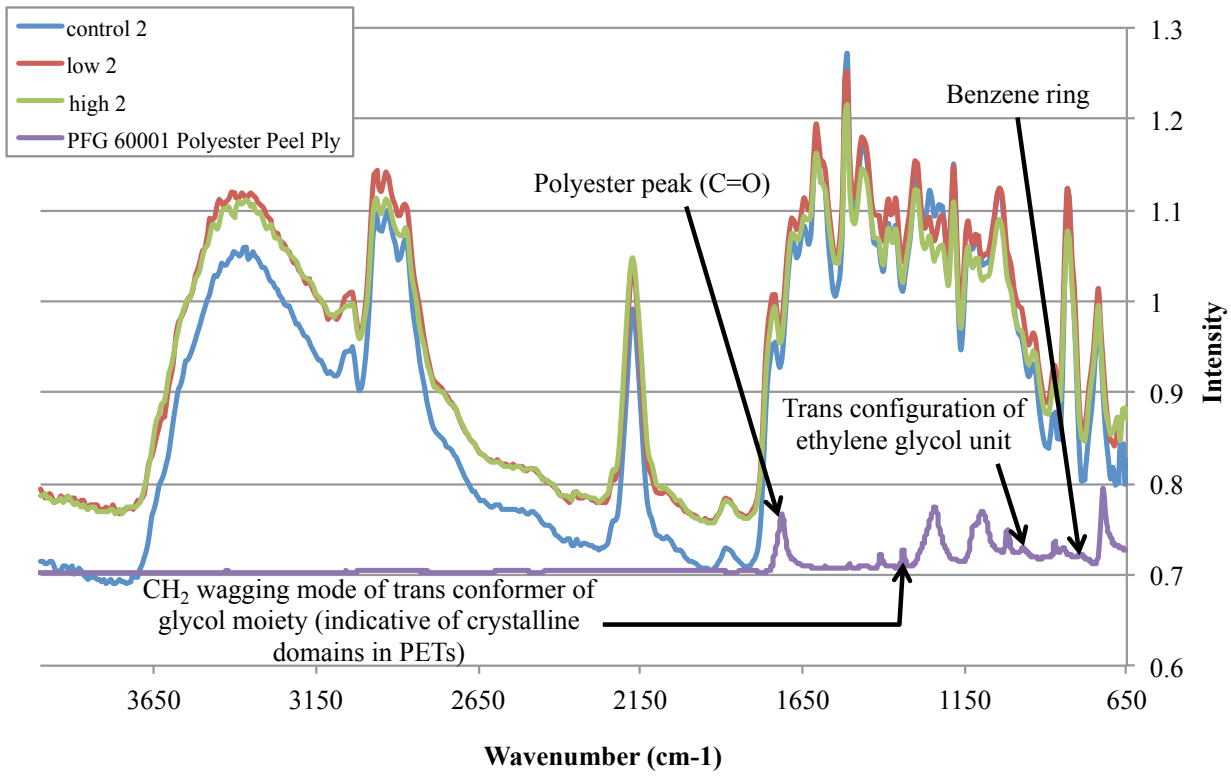

Figure 62. Representative FTIR spectra for *control 2*, *low 2*, *high 2*, as well as PFG 60001 polyester peel ply with some polyester peaks identified. [80,81]

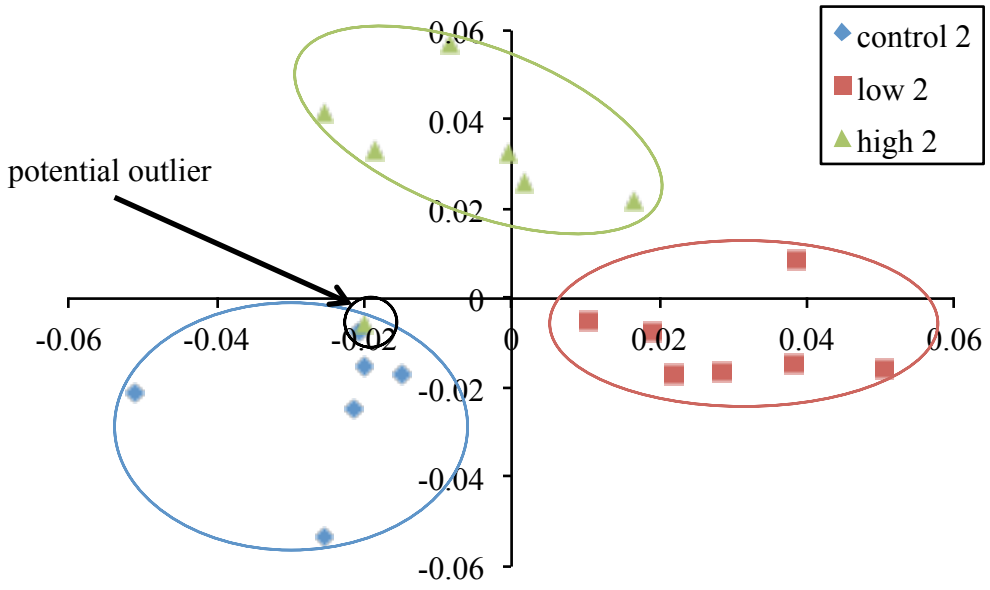

Figure 63. Scores plot from PLS analysis of *control 2*, *low 2* and *high 2* spectral data preprocessed with multiplicative scatter correction, a gap 1st derivative, and 5 smoothing points.

5.2.4 XPS Measurements

Survey and high-resolution scans were significantly different for *control 2* and plasma treated surfaces. Atomic percentages determined from survey scans are shown in Table 9. It was observed that the percentage of oxygen increased from approximately 25% to 33% and then decreased slightly to 28% for *control 2* to *low 2* to *high 2* treatments, respectively. An increase in oxygen on the surface of plasma treated surfaces compared to *control 2* surfaces was expected as previous results for material system 1 also showed an increase in oxygen on the plasma treated surfaces. This was also expected because the atmospheric pressure plasma was generated from air, which is composed of oxygen and nitrogen. Given this, it was also expected to observe a significant increase in nitrogen content on the surface. Nitrogen increased from approximately 1.5% to 5% to 18% for *control 2* to *low 2* to *high 2* surfaces. Though an increase in nitrogen content on material system 1 samples was not observed with plasma treatment, whereas it was

apparent here, this difference could be explained by the nitrogen on the surface from the nylon peel ply used with material system 1 and not used in material system 2.

Carbon content was shown to decrease with an increase in atmospheric pressure plasma treatment compared to *control 2* samples, also shown in Table 9. There was also fluorine observed on one spot on the *control 2* sample and was likely due to contamination found in the release film and other common release agents found in the laboratory. Sodium was observed on plasma treated samples (Table 9). This could potentially originate from contamination found in the laboratory or these analysis spots could have included fibers, which are known to have levels of sodium and other alkali metals present on the surface. [82] Peel ply on all samples was not fully infiltrated with epoxy matrix resin that ultimately resulted in fiber rich areas on the surface that could explain the sodium observed with XPS (Figure 64). Low levels of bromine were also present on all samples (Table 9). Epoxy resins are brominated to increase fire-retardance. [82,83,84] Though brominated resins are commonly used in the manufacture of printed circuit boards and much of the literature cites application in the electronics field, the composite studied here is brominated for fire-retardant properties. [82,83,84]

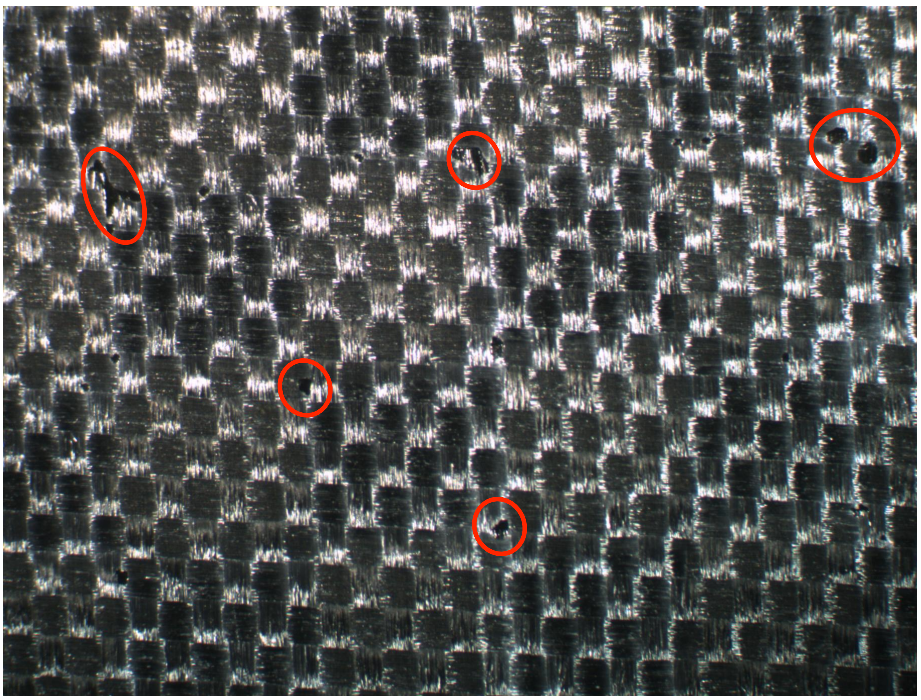

Figure 64. Stereomicroscope image at 10X of PFG 60001 prepared Hexcel T300/F155 composite highlighting fiber rich regions with red circles.

Table 9. Atomic percentages of carbon, nitrogen, oxygen, and potential contaminants on *control 2*, *low 2*, and *high 2* samples.

Element		**Sample**		
		control 2	***low 2***	***high 2***
C 1s	Average	72.877	60.972	53.127
	StDev	0.251	0.582	1.465
N 1s	Average	1.579	4.813	18.004
	StDev	0.395	0.293	2.672
O 1s	Average	25.089	33.453	27.963
	StDev	0.088	0.933	1.403
Br 3d	**Average**	0.186	0.357	0.412
	StDev	0.049	0.133	0.038
Na 1s	**Average**	N/A	0.405	0.494
	StDev	N/A	0.187	0.323
F 1s	**Average**	0.805	N/A	N/A
	StDev	N/A	N/A	N/A

Peak fitting of high-resolution XPS spectra showed an increase in oxygen and nitrogen containing functional groups after plasma treatment. Specifically, there appeared to be –COOH functional groups on plasma treated surfaces as shown in Figure 65 and Figure 66. Note that on the *high 2* sample, the –COOH could also be identified as –COON, shown in Figure 66. This peak could be attributed to either –COOH or –COON functional groups, or represent a combination of both. More research would be necessary to determine which functional group is

associated with that peak. It is sufficient to state, however, that oxygen-rich functionalities were identified as a result of plasma treatment. *Control 2* (no plasma, peel ply only) surface high-resolution peak fitting is shown in Figure 67 for comparison. No –COOH was observed on the *control 2* surface. The *control 2* sample showed polyester groups on the surface (–COOR, where the "*" on the figures denotes with which carbon the peak was associated). These polyester groups are chemically consistent with polyethylene terephthalate (PET) likely originating from the peel ply used.

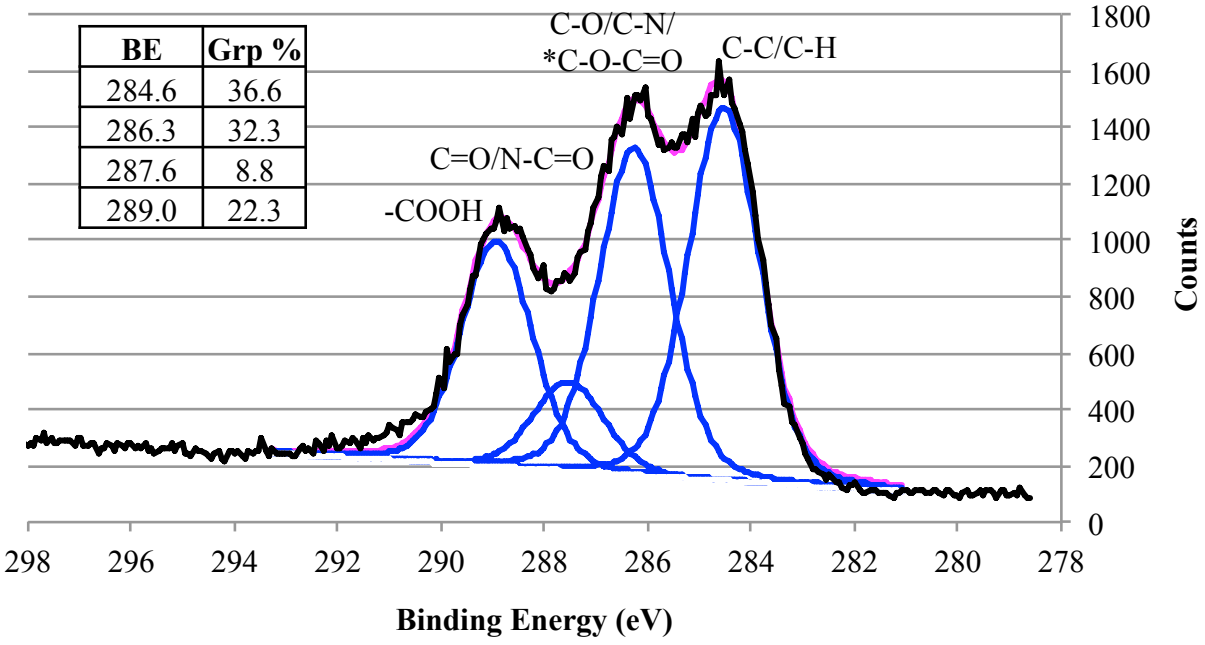

Figure 65. High-resolution carbon scan for the *low 2* surface.

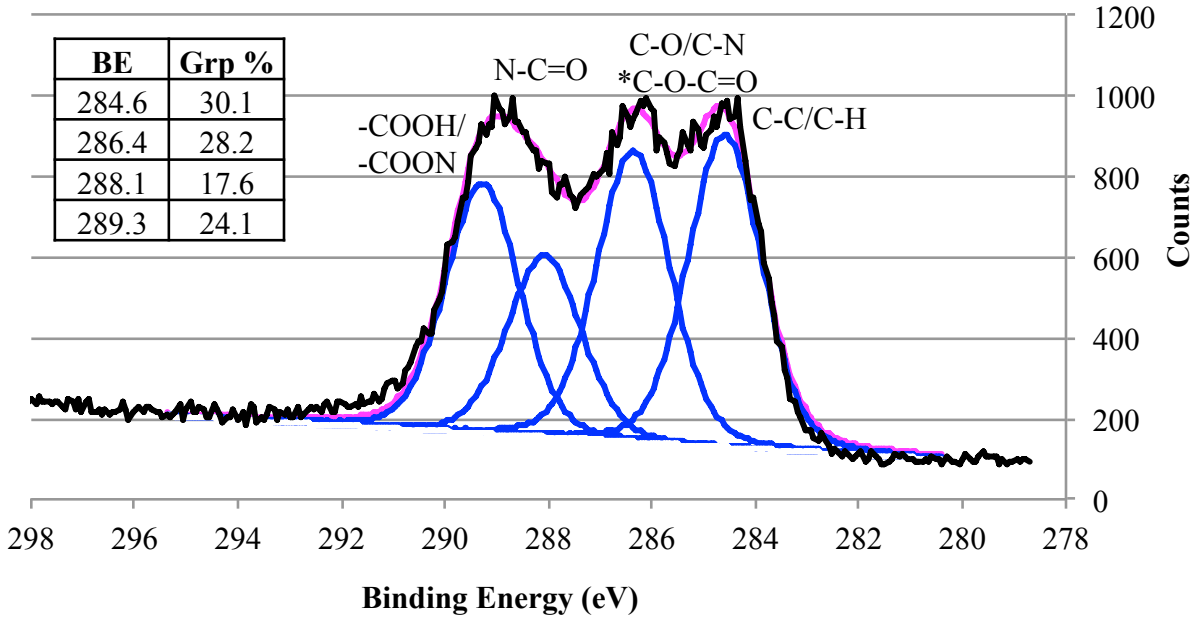

Figure 66. High-resolution carbon scan for the *high 2* surface.

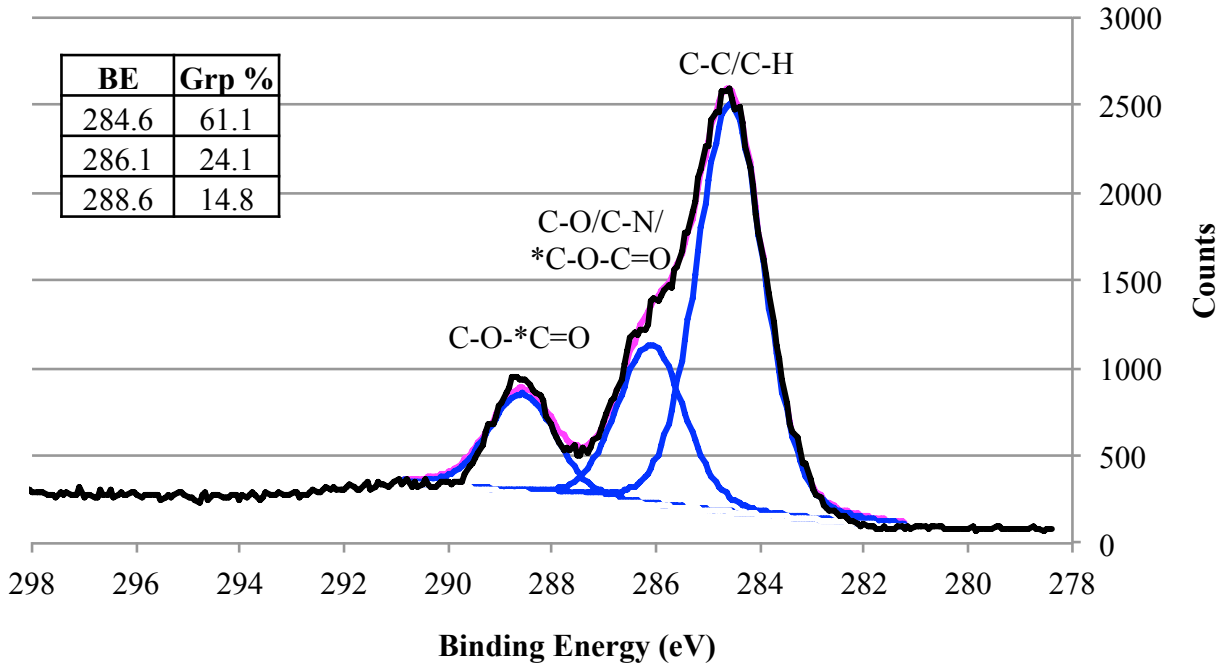

Figure 67. High-resolution carbon scan for the *control 2* surface.

Overall, XPS showed an increase in oxygen and nitrogen on the surface of atmospheric pressure plasma treated samples, as supported by high-resolution scans. Polyester groups were still identified on *low 2* and *high 2* specimens, so SEM was necessary to confirm the presence of peel ply remnants and also determine if there were any surface morphology changes. The present data suggested that the CFRP surfaces were functionalized in order to improve adhesion, as polyester groups were detected on all surfaces but only carboxyl groups were detected on plasma treated samples.

5.2.5 SEM Images

As expected from examination of the DCB fracture surfaces (Figure 68), significant levels of peel ply remnants were observed on the Hexcel T300/F155 CFRP surface. Examination of the peel ply removed from the CFRP surface also confirmed that the peel ply was transferred to the composite (Figure 69).

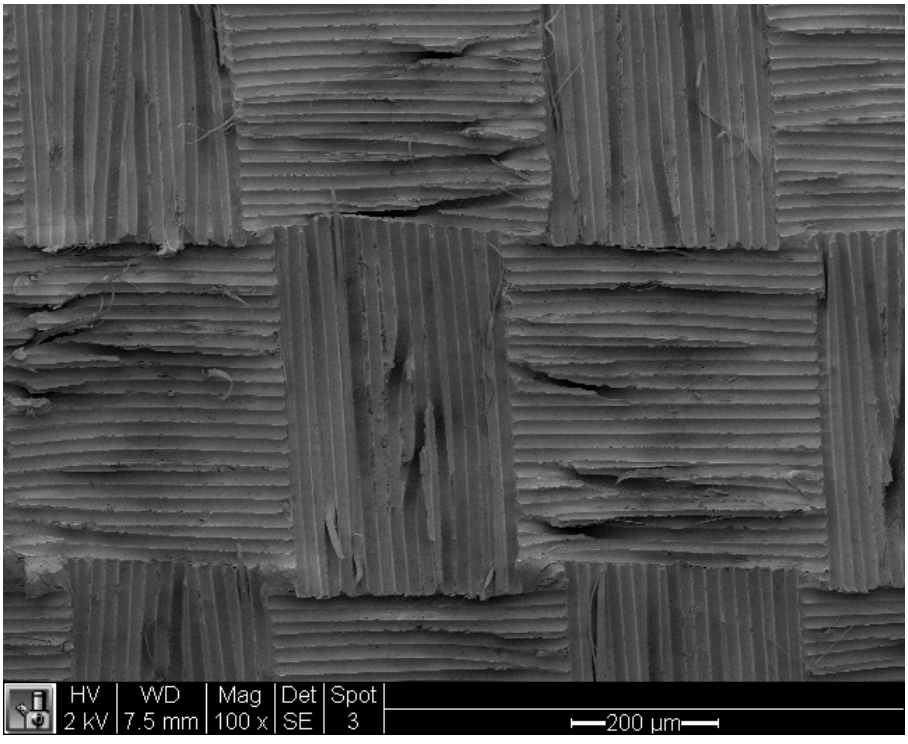

(a)

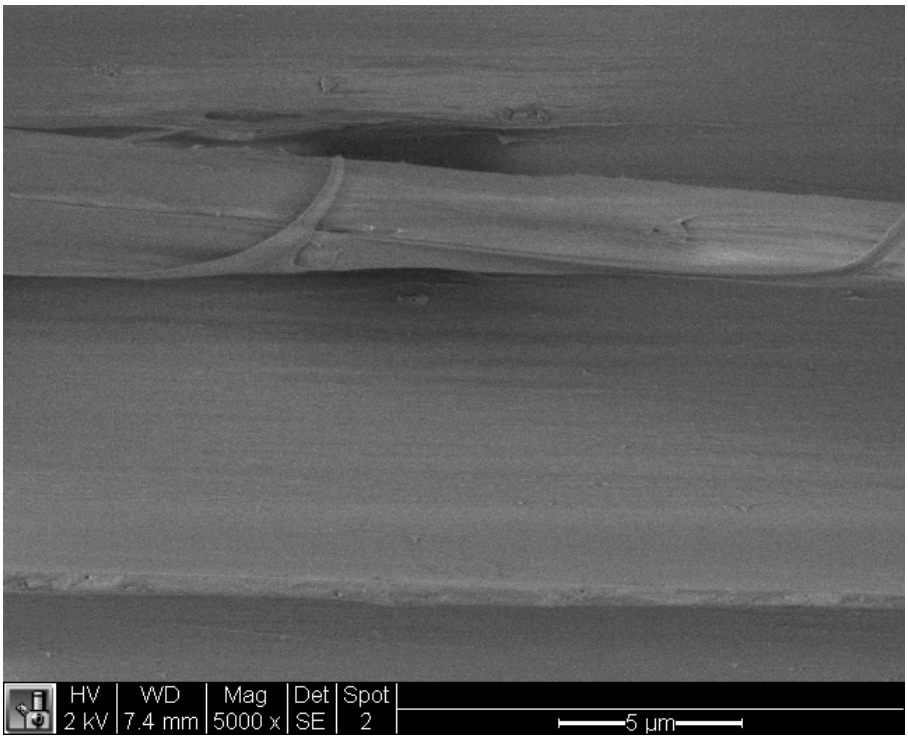

(b)

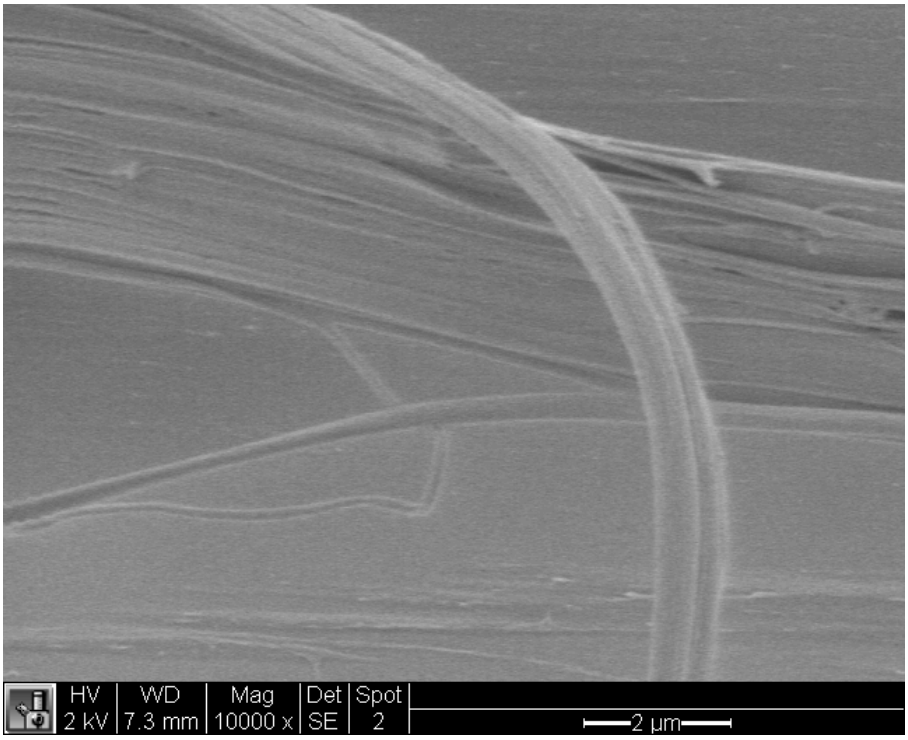

(c)

Figure 68. Electron micrographs of Hexcel F155/T300 prepared with PFG 60001 polyester peel ply at (a) 100X, (b) 5000X, and (c) 10,000X magnifications.

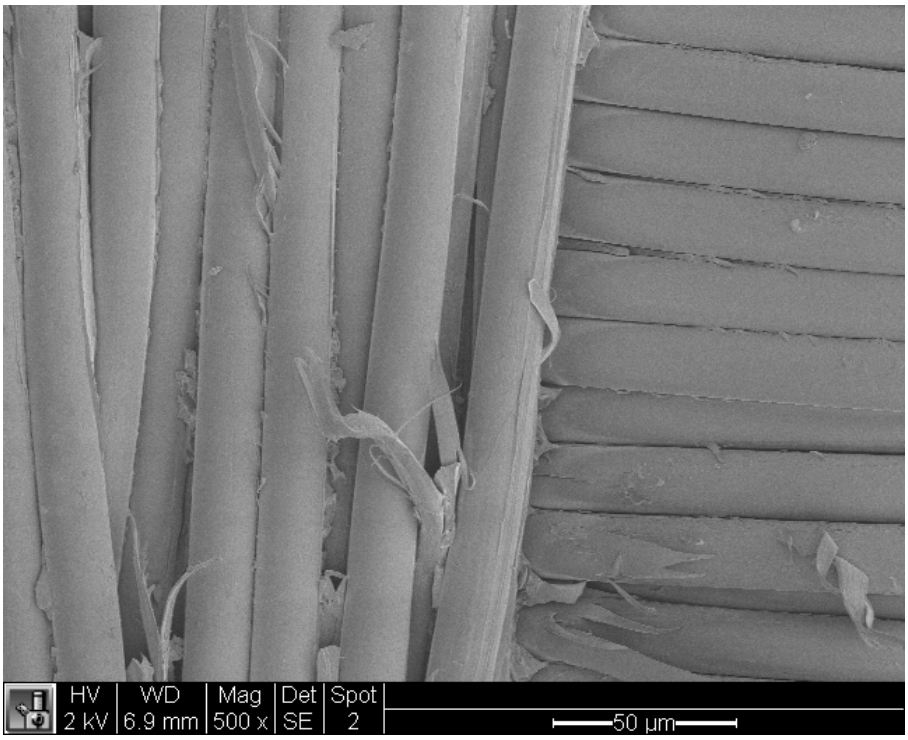

Figure 69. Electron micrograph of PFG 60001 peel ply removed from Hexcel T300/ F155 CFRP at 500X magnification.

Atmospheric pressure plasma treatment at 2.54 cm/s (*high 2*) was applied to the Hexcel T300/F155 surface and subsequently examined with SEM. Note that this is the same raster speed used for the Toray T800/3900-2 with PFG 52006 nylon peel ply for SEM analysis. As shown previously (5.2.1), *high 2* resulted in a mixed failure mode, most importantly showing that plasma treatment changed failure mode from 100% adhesion failure to a combination of cohesive within the composite, cohesive within the adhesive, and adhesion failure modes. Other surface characterization measurements confirmed that surface characteristics changed with plasma treatment. Examination of the electron micrographs at high magnifications post plasma treatment showed that peel ply remnants were still present on the surface and that the surface morphology of the peel ply remnants changed (Figure 70). This observation supports the hypothesis that the peel ply remnants/interphase were functionalized to promote adhesion.

However, the hypothesis that atmospheric pressure plasma treatment removes the peel ply remnants to promote adhesion could also be supported by these images. As observed in Figure 70, the morphology of the polyester peel ply surface changed. This could be due to restructuring of the polymer surface and/or partial removal of the peel ply remnants. It also could be due to localized heating due to the plasma or potentially relaxation. More research would be necessary to prove the observed surface morphology was due entirely to the atmospheric pressure plasma treatment. Considering, however, that there were significant amounts of peel ply remnants present on both *control 2* and plasma treated samples and the chemistry of the surface changed drastically with plasma treatment, it was suggested that the predominant reason for adhesion here was likely due to surface functionalization.

Also observed in Figure 70 (c) and (d) was a nano-scale "spot-like" surface morphology of the composite surface adjacent to the peel ply remnant. This type of morphology has been observed before on as-tooled composite surfaces but not on peel ply prepared composites.[31] Serrano had suggested that the atmospheric pressure plasma experienced vorticity and prohibited plasma from interacting with the surface at the bottom of the peel ply channels (Figure 53). Based on results on both material systems examined in this study, whether the plasma interacted directly or indirectly with the peel ply channels, there was significant interaction with these surfaces. Overall, these images coupled with XPS analysis suggested that functionalization of the peel ply prepared surface was the dominant factor for adhesion.

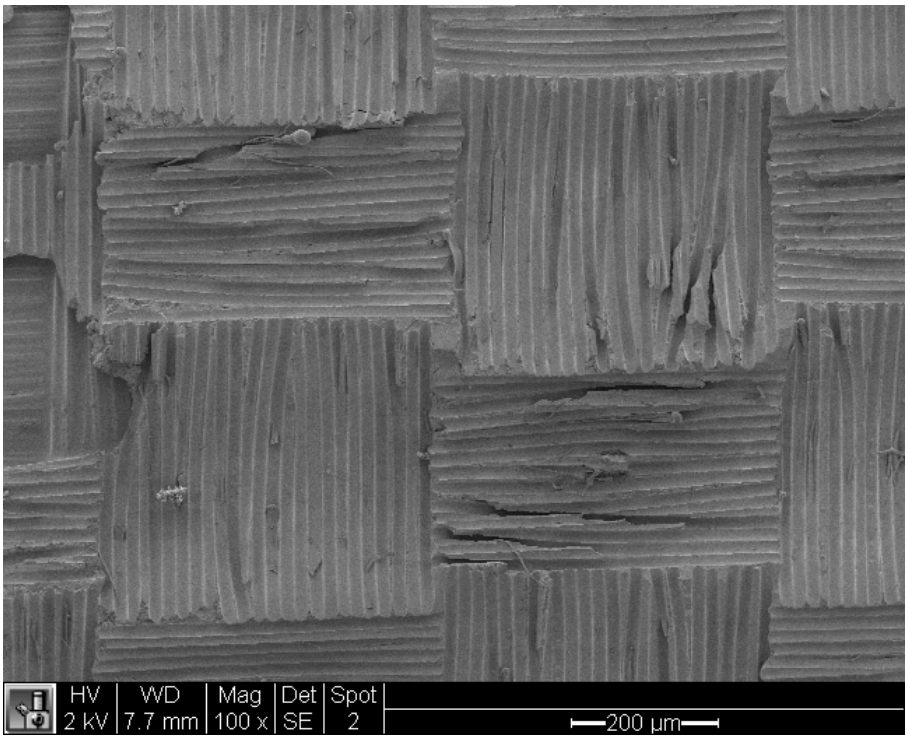
HV
2 kV
WD
7.7 mm
Mag
100 x
Det
SE
Spot
2
200 µm

(a)

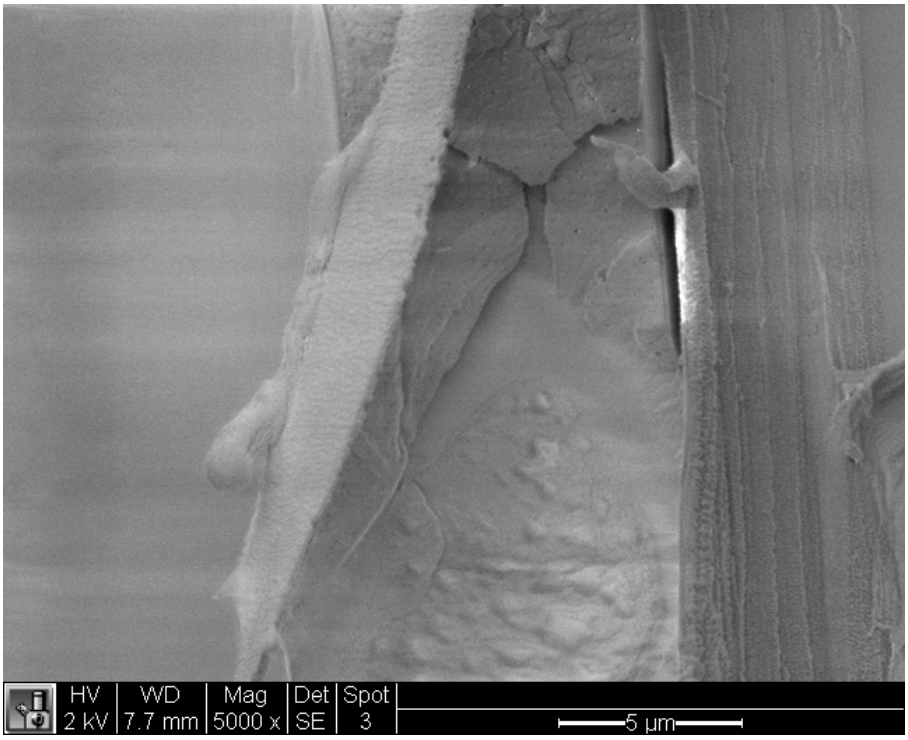
HV
2 kV
WD
7.7 mm
Mag
5000 x
Det
SE
Spot
3
5 µm

(b)

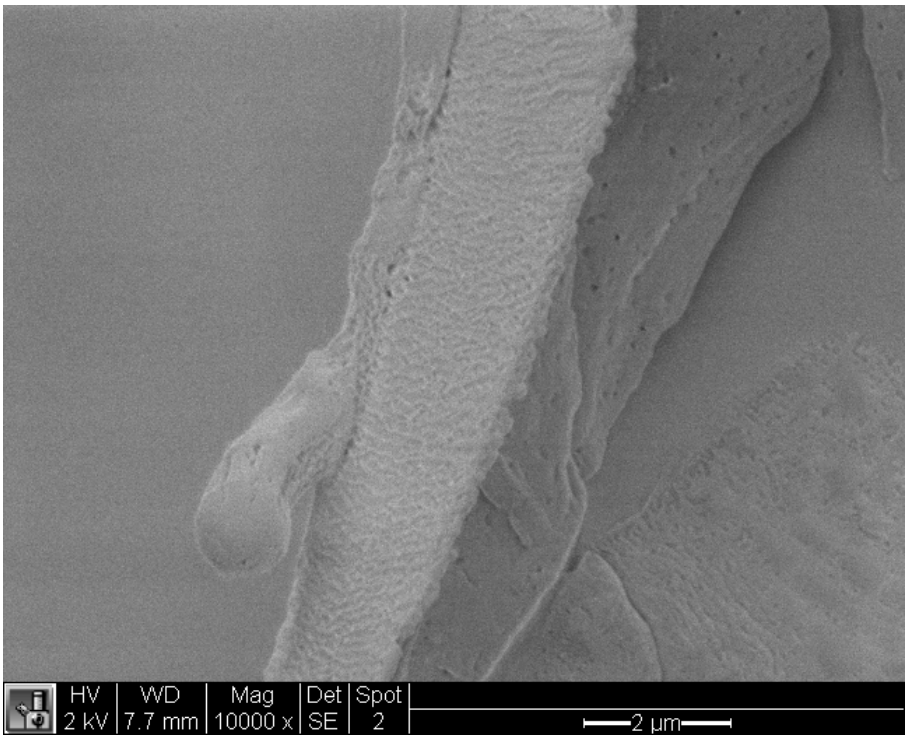

(c)

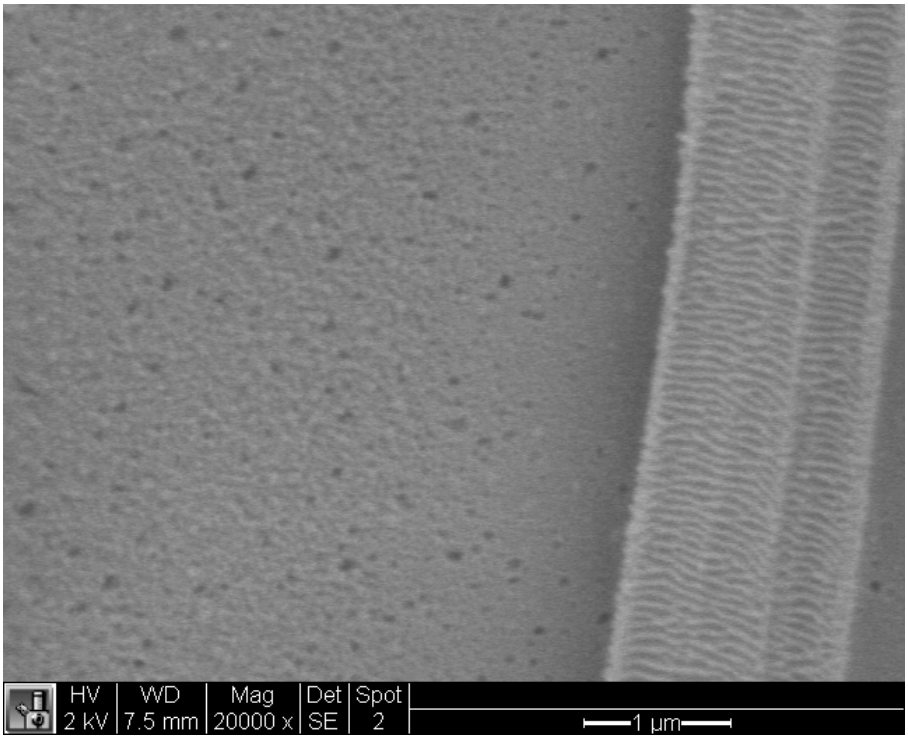

(d)

Figure 70. Electron micrographs of Hexcel F155/T300 prepared with PFG 60001 and 2.54 cm/s (*high 2*) plasma treatment at (a) 100X, (b) 5000X, (c) 10,000X, and (d) 20,000X magnifications.

5.3 Interaction of MetlBond 1515-3M with PFG 52006 Nylon Peel Ply

Examination of the interaction between both virgin peel ply and plasma treated peel ply and MB 1515-3M adhesive was examined as a simple way to determine if bonding was due to functionalization or removal of the nylon peel ply remnants/interphase for material system 1. CA measurements were used to determine if surface energy differences existed. XPS was used to determine if nylon was transferred to the adhesive surface during cure and SEM was used to confirm whether visible remnants were present on the adhesive surfaces.

5.3.1 Contact Angle Measurements

As shown by CA measurements and surface energy calculations (Figure 71 andFigure 72), there was little difference observed between MB 1515-3M prepared with virgin PFG 52006 nylon peel ply and those prepared with peel ply treated with atmospheric pressure plasma at 2.54 cm/s (1 in/s). It should be noted, however, that the plasma treated peel ply was more difficult to remove from the MB 1515-3M adhesive than the virgin peel ply, suggesting there was a stronger bond between the plasma treated peel ply and the adhesive than the virgin peel ply and the adhesive. Evidence of this is shown in Figure 73 as the plasma treated peel ply is curled more than the virgin peel ply upon removal. This is likely due to the peeling angle. In the case of the virgin peel ply being removed from the adhesive, only a shallow peeling angle was necessary to remove the peel ply. In the case of the plasma treated peel ply, a larger peeling angle was necessary which may have caused the tighter curvature of the removed peel ply.

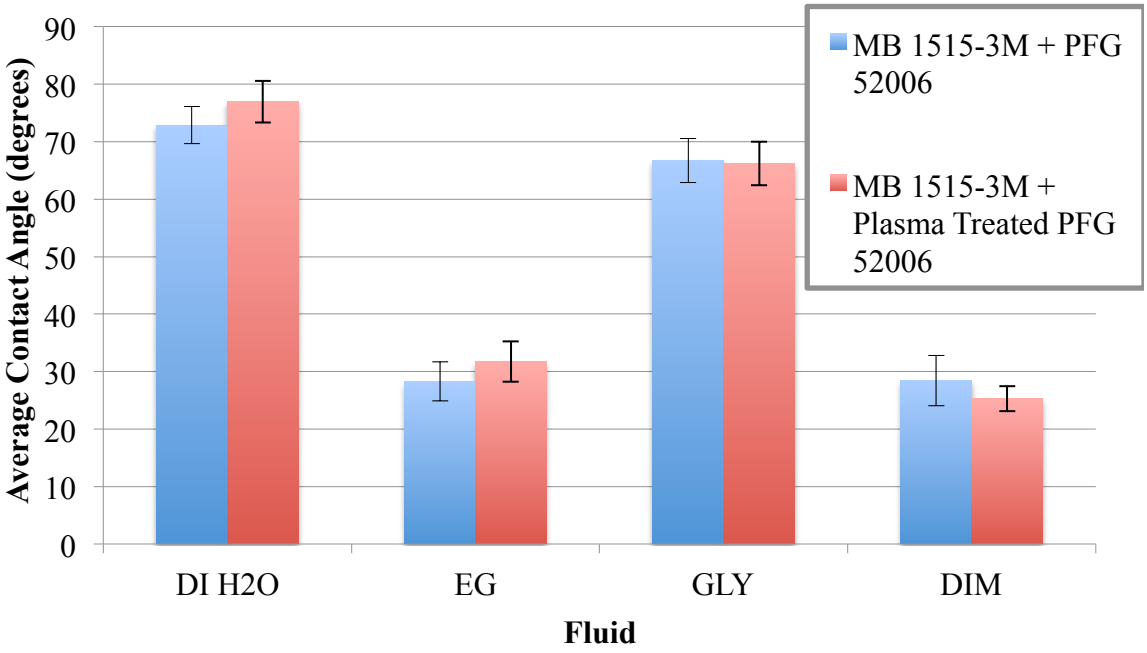

Figure 71. Average CA measurements on MB 1515-3M prepared with both virgin PFG 52006 peel ply and plasma treated PFG 52006 with standard deviation error bars.

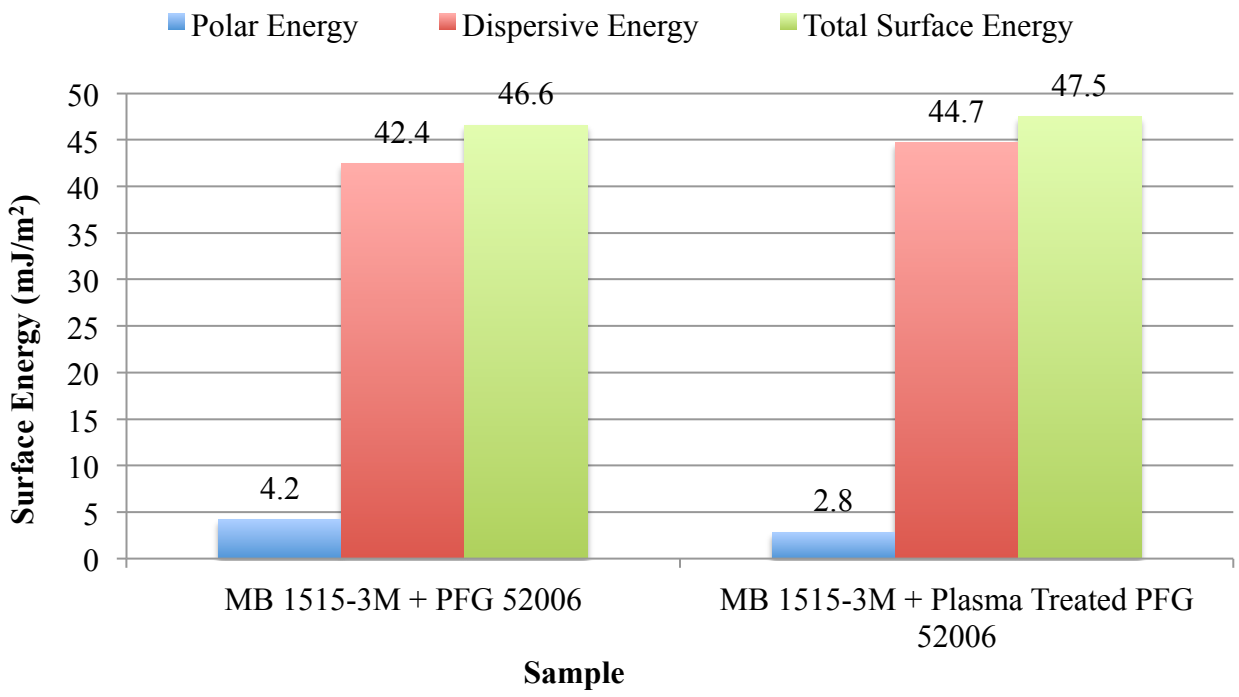

Figure 72. Surface energies of MB 1515-3M prepared with both virgin PFG 52006 peel ply and plasma treated PFG 52006.

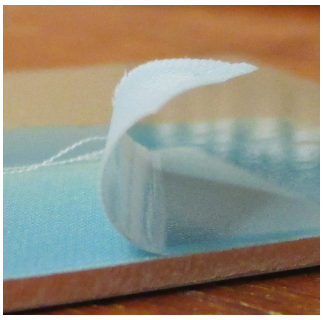 (a) 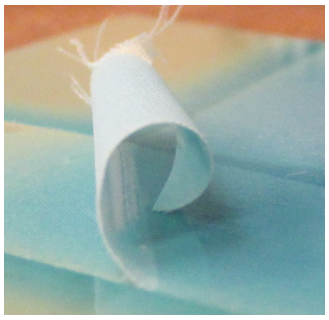 (b)

Figure 73. Images of (a) virgin peel ply being removed from MB 1515-3M and (b) plasma treated peel ply being removed from MB 1515-3M.

5.3.2 XPS Measurements

Survey scans were similar but did show slight differences between MB 1515-3M surfaces prepared with virgin PFG 52006 and those that were prepared with plasma treated PFG 52006. Atomic percentages determined from survey scans are shown in **Table 10**. Subtle atomic percentage variations between the MB 1515-3M surfaces prepared with virgin and plasma treated peel ply were the amount of nitrogen and oxygen present on the surface. Surfaces prepared with virgin peel ply have approximately 1.5% less nitrogen and 1.5% more oxygen than surfaces prepared with plasma treated peel ply (**Table 10**). The larger concentration of nitrogen on the MB 1515-3M surfaces prepared with the plasma treated peel ply could be due to more transfer of nylon to the surface compared to MB 1515-3M surfaces prepared with virgin peel ply. This could be confirmed with high-resolution XPS and/or SEM. Carbon and bromine concentrations were not significantly different. Compared to Hexcel T300/F155 composites prepared with PFG 60001 peel ply, the MB 1515-3M surfaces showed similar concentrations of bromine, which could be from brominating the epoxy adhesive to achieve fire-retardance properties. [82,83,84]

Table 10. Atomic percentages of carbon, nitrogen, oxygen, and bromine on MB 1515-3M surfaces prepared with PFG 52006 and MB 1515-3M surfaces prepared with plasma treated PFG 52006.

Element		Sample	
		MB 1515-3M + PFG 52006	**MB 1515-3M + 2.54 cm/s plasma treated PFG 52006**
C 1s	Average	77.774	77.429
	StDev	0.983	0.400
N 1s	Average	7.510	9.179
	StDev	0.741	0.494
O 1s	Average	14.370	12.839
	StDev	0.905	0.296
Br 3d	Average	0.345	0.553
	StDev	0.044	0.343

Like survey scans, high-resolution spectra were also similar for MB 1515-3M surfaces prepared with both virgin and plasma treated peel ply (Figure 74 and Figure 75). Both high-resolution carbon peaks were described with 3 peaks. Both surfaces showed carbon bonding states that could be attributed to both epoxy and nylon (C-N, C-O, C-O-C, N–C=O, C=O). The presence of amide groups (N–C=O) on the MB 1515-3M surfaces prepared with both virgin and plasma treated PFG 52006 was supported by SEM images that will be discussed in the next section.

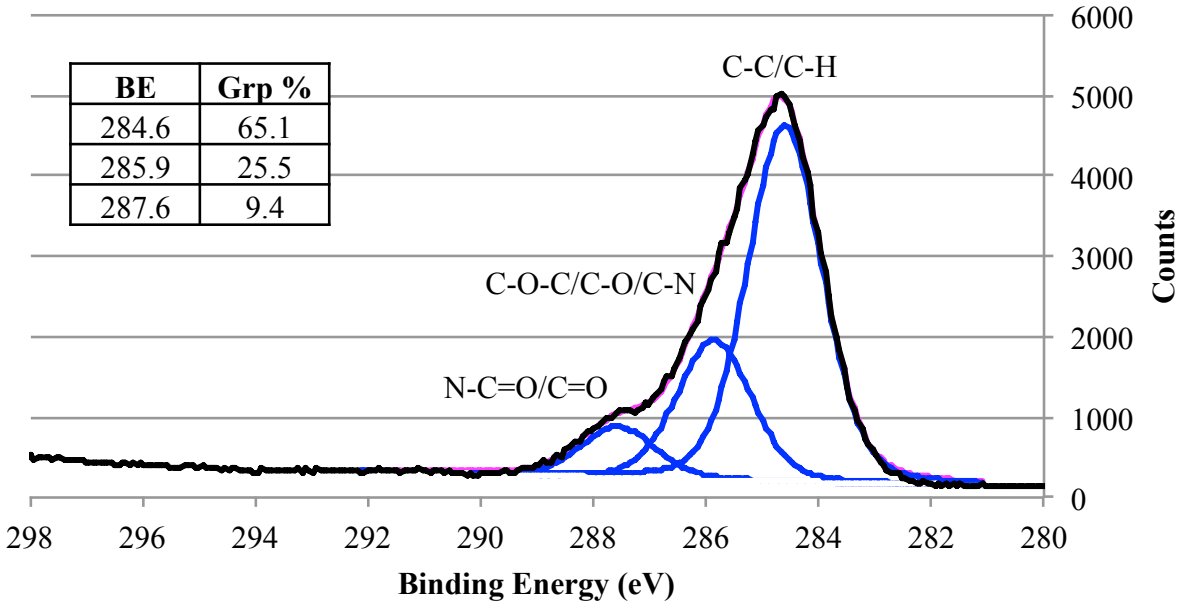

Figure 74. High-resolution carbon scan for MB 1515-3M prepared with virgin PFG 52006 nylon peel ply.

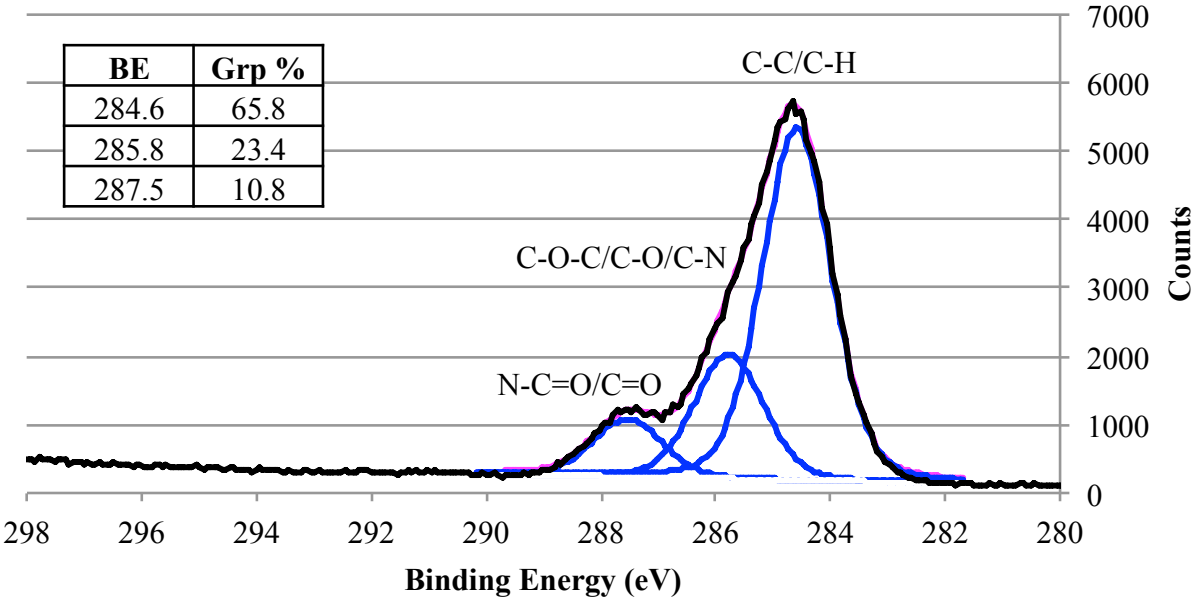

Figure 75. High-resolution carbon scan for MB 1515-3M prepared with plasma treated PFG 52006 nylon peel ply.

Also examined was virgin peel ply and plasma treated peel ply. Table 11 shows that plasma treatment resulted in an increase in oxygen (~14%) and nitrogen (~2.5%) and an approximate 17% decrease in carbon on the surface. This significant change in surface chemistry suggested that PFG 52006 was functionalized by atmospheric pressure plasma treatment. High-resolution spectra also supported functionalization. Figure 76 and Figure 77 are high-resolution carbon spectra of virgin and plasma treated peel ply, respectively. As expected, carbon bonding states were characteristic of nylon for virgin PFG 52006 peel ply (Figure 76). Plasma treated peel ply was better described with a four peak fit and showed the addition of carboxyl groups on the surface, supporting a functionalization mechanism (Figure 77).

Table 11. Atomic percentages of carbon, nitrogen, and oxygen on virgin PFG 52006 and PFG 52006 with 2.54 cm/s (1”/s) atmospheric pressure plasma treatment.

Element		**Sample**	
		Virgin PFG 52006	**PFG 52006 + 2.54 cm/s plasma**
C 1s	Average	80.918	63.864
	StDev	0.250	0.486
O 1s	Average	11.587	25.832
	StDev	0.460	0.525
N 1s	Average	7.495	10.053
	StDev	0.575	0.390
Na 1s	Average	0	0.252
	StDev	N/A	0.157

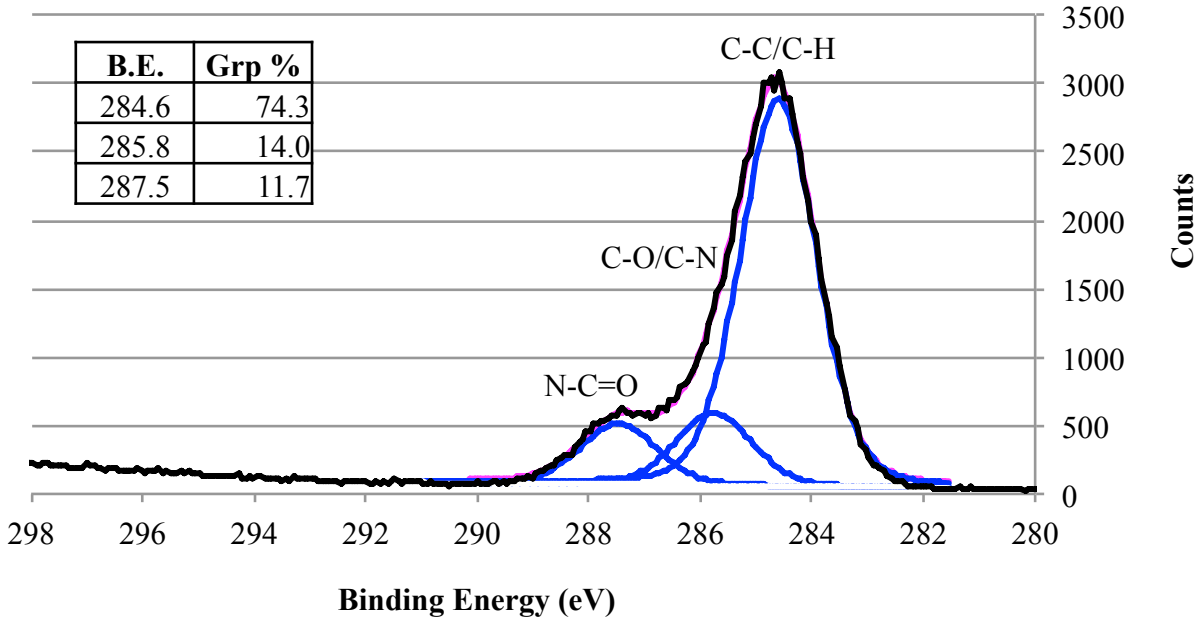

Figure 76. High-resolution carbon scan of virgin PFG 52006 nylon peel ply.

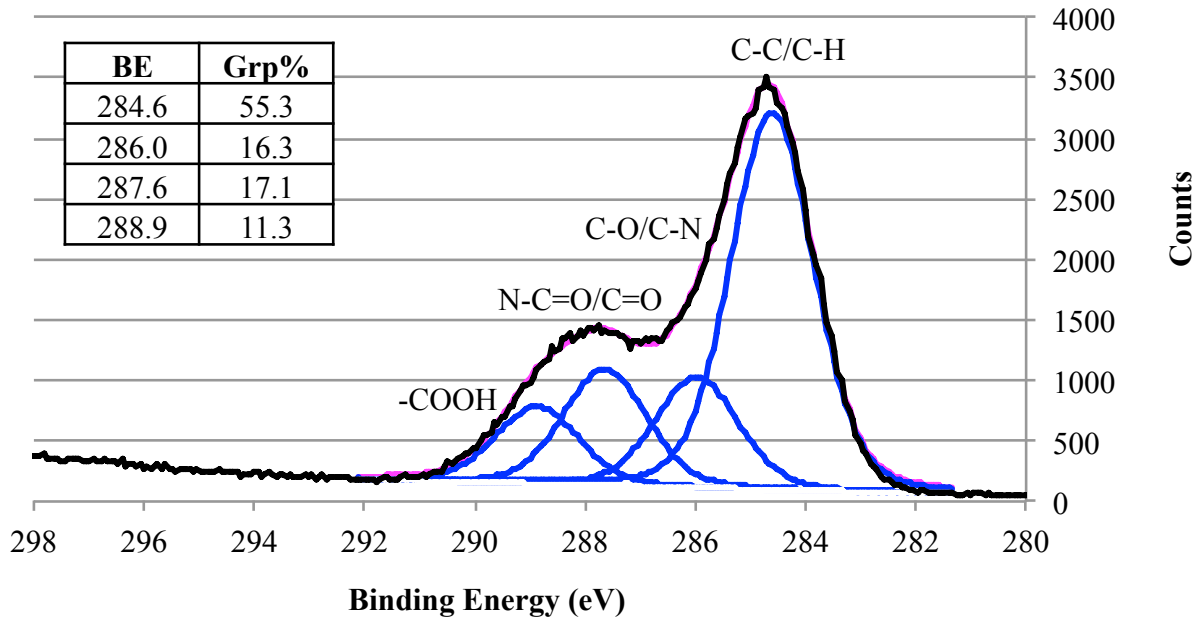

Figure 77. High-resolution carbon scan of plasma treated PFG 52006 nylon peel ply.

5.3.3 SEM Images

Initial inspection of MetlBond 1515-3M adhesive surfaces prepared with PFG 52006 nylon peel ply suggested there may be some peel ply remnants transferred to the surface (Figure 78). Examination of virgin peel ply fibers, however, could help explain this surface morphology (Figure 79). Peel ply that was removed from the MetlBond 1515-3M surface was thus examined with SEM (Figure 80). These images suggest that some of the peel ply did exhibit "onion skinning" and transferred to the surface. The presence of nylon on the surface was supported by XPS.

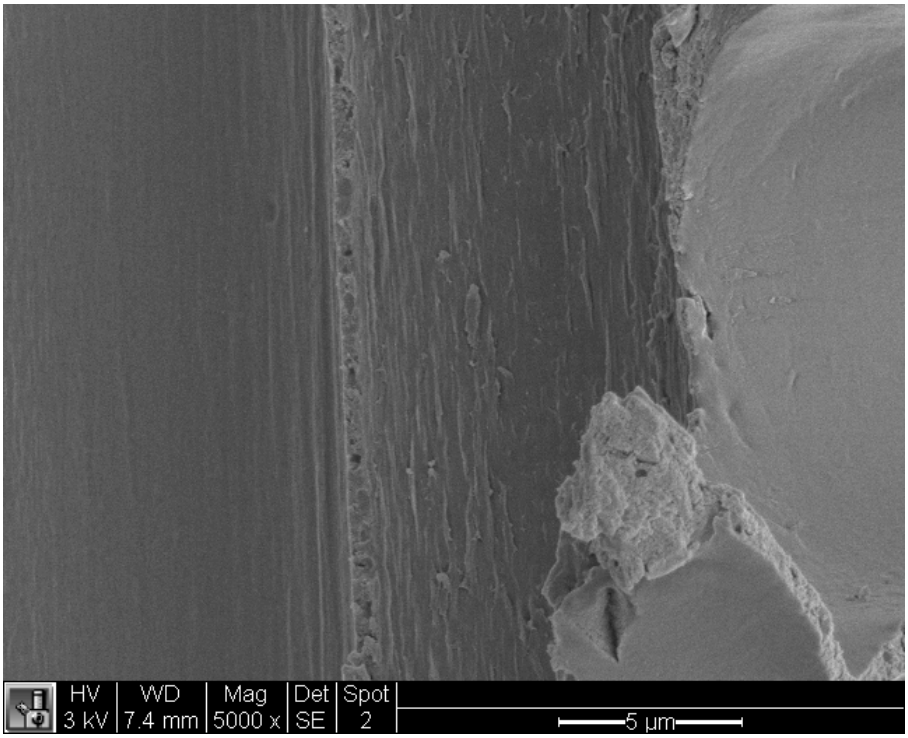

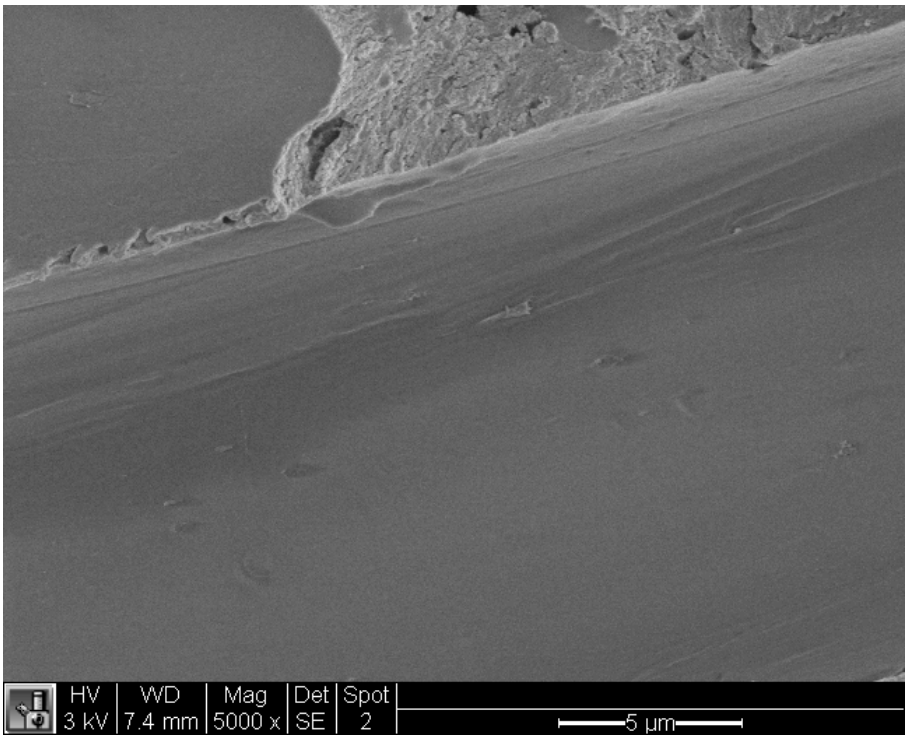

Figure 78. Electron micrographs at 5000X of MB 1515-3M surface prepared with PFG 52006.

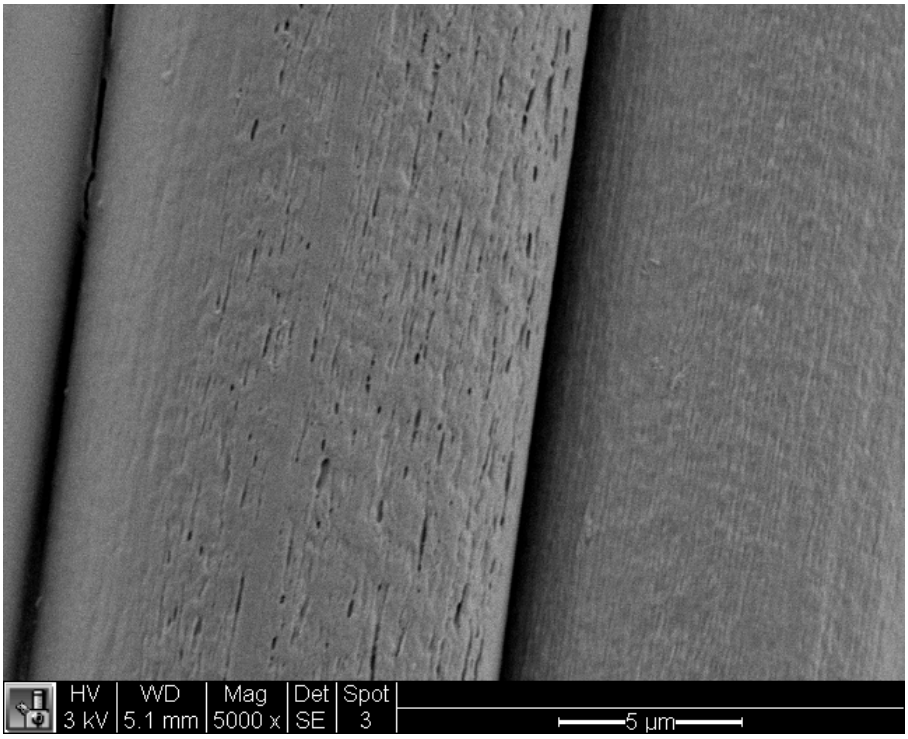

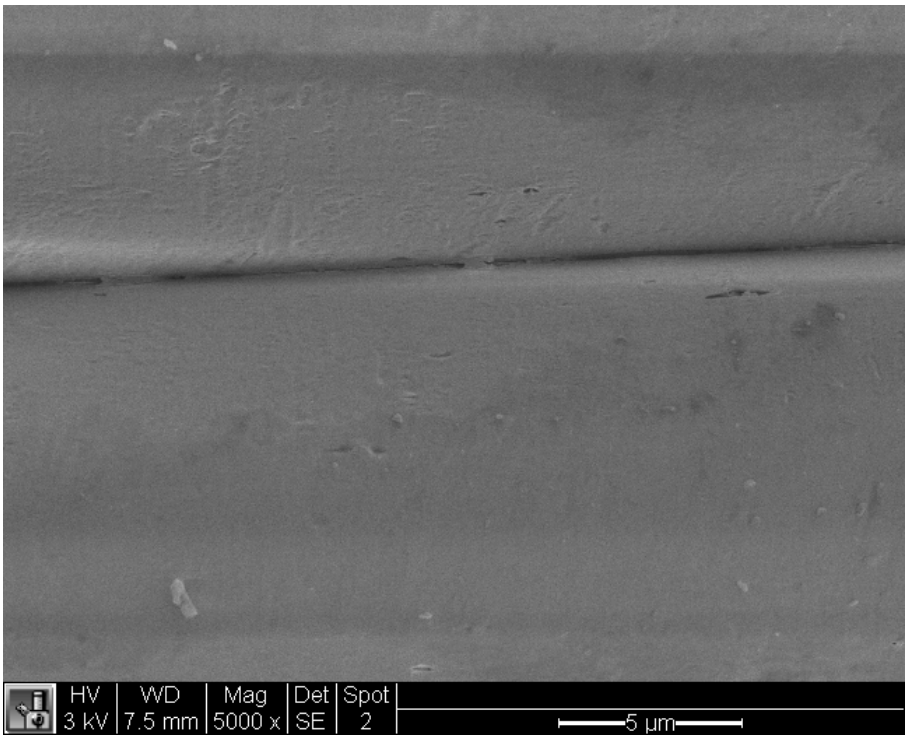

Figure 79. Electron micrographs at 5000X of virgin PFG 52006 peel ply showing various surface morphologies.

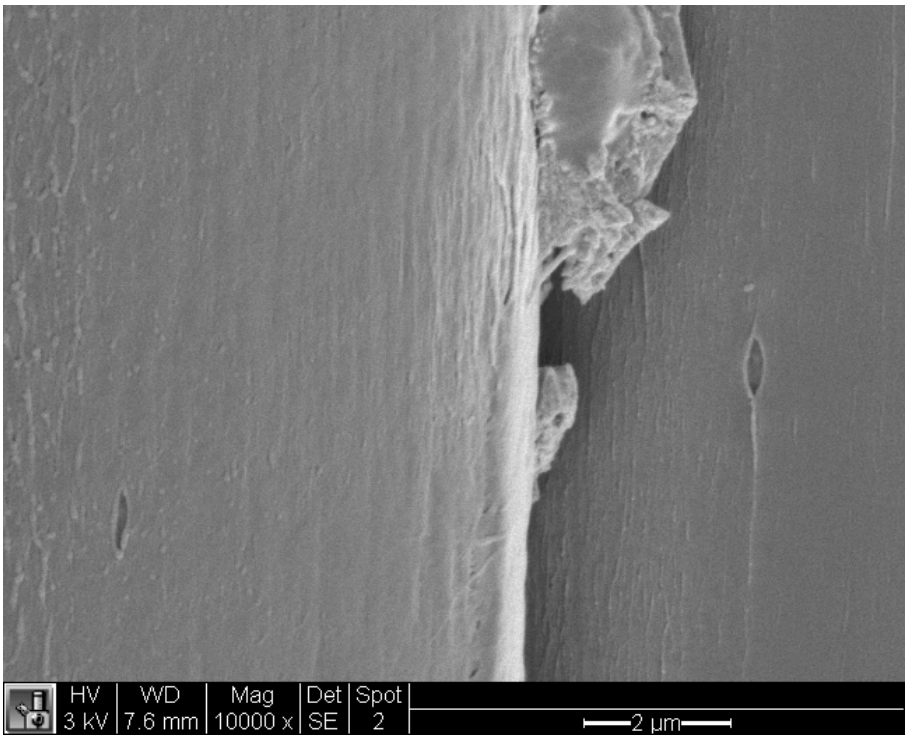

Figure 80. Electron micrograph of peel ply removed from MB 1515-3M showing "onion skinning" effect.

Examination of MetlBond 1515-3M prepared with plasma treated PFG 52006 nylon peel ply showed that significant amounts of peel ply remnants were left on the surface upon peel ply removal (Figure 81). Inspection of the plasma treated peel ply fibers showed a similar morphology to the fiber remnants on material system 2 that were exposed to atmospheric pressure plasma treatment (Figure 82). The change in surface morphology of the fibers supported the interaction of plasma with the nylon peel ply surface. The increased peel ply transfer to the MB1515-3M surface after plasma treatment of the peel ply suggested the primary reason for adhesion was a functionalization mechanism, as removal of nylon would only reveal more nylon and greater peel ply transfer to the adhesive surface was observed when the peel ply plasma treated first.

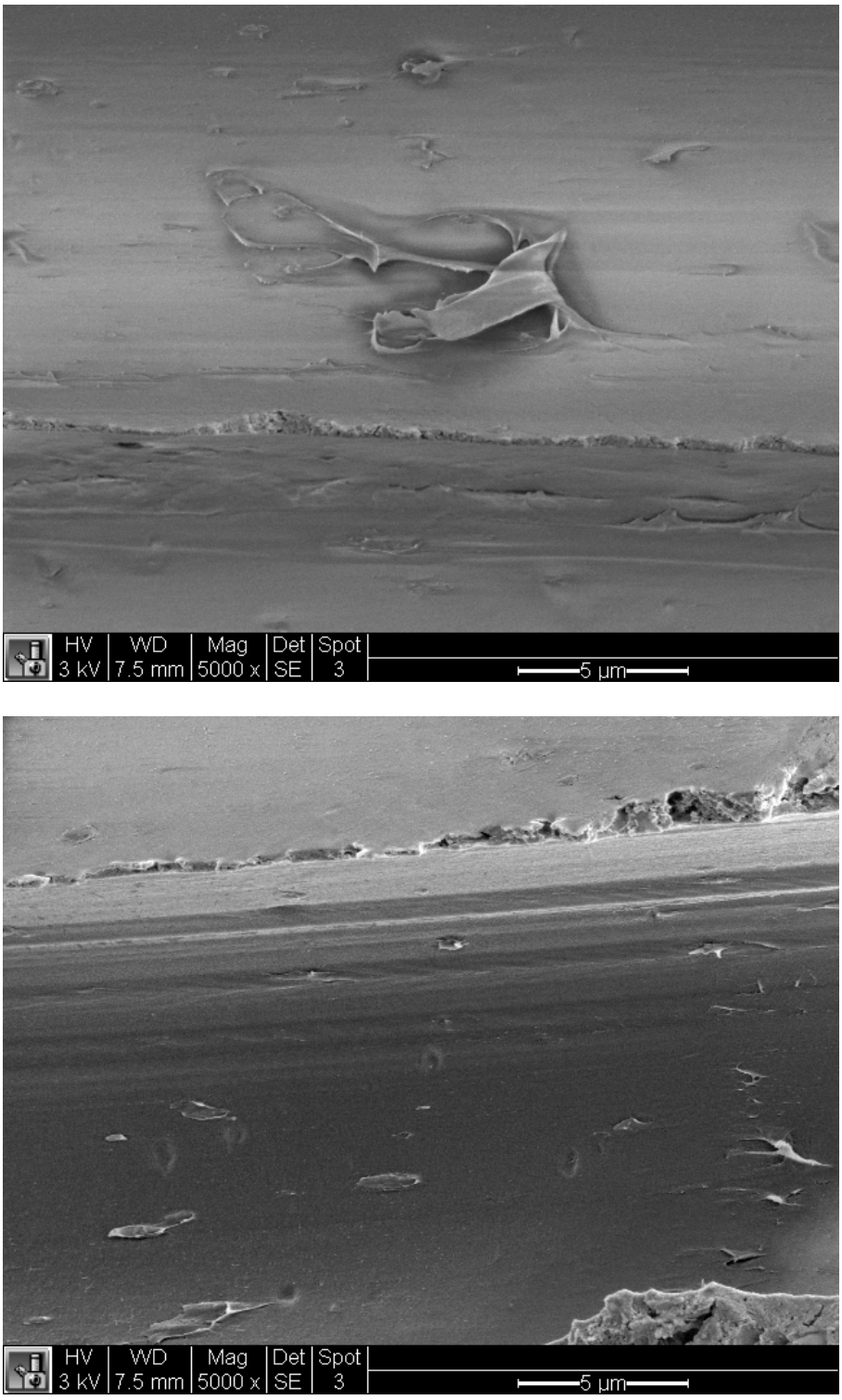

Figure 81. Electron micrographs at 5000X of MB 1515-3M prepared with plasma treated PFG 52006 nylon peel ply, showing significant amounts of peel ply remnants.

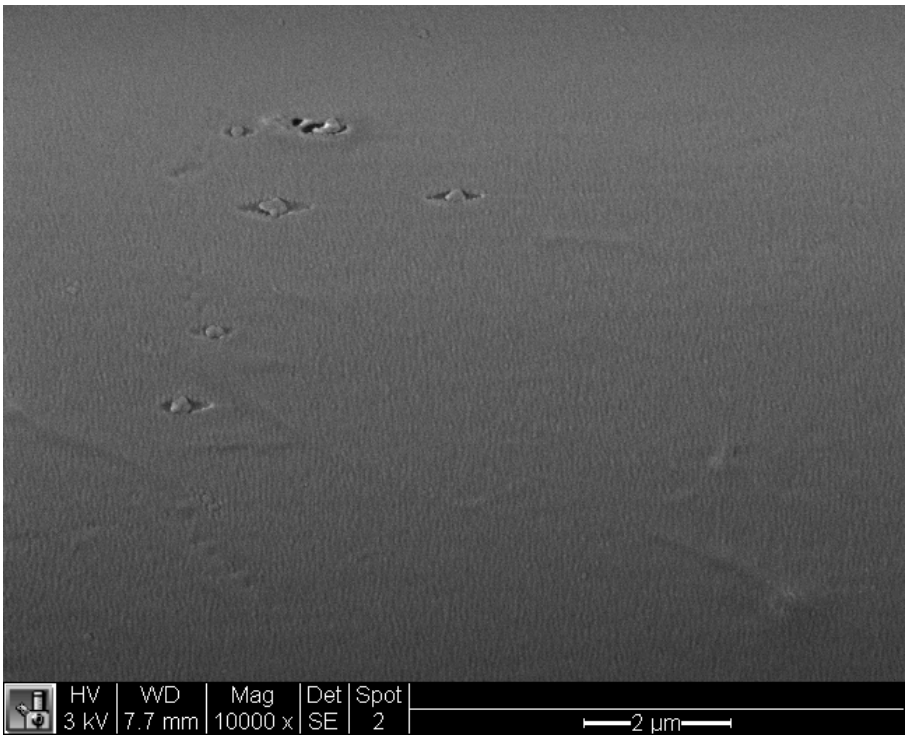

(a)

(b)

Figure 82. Electron micrograph of atmospheric pressure plasma treated PFG 52006 nylon peel ply at (a) 10,000X and (b) 20,000X.

5.4 Time Exposure to a Constant Environment – Material System 1

There were two objectives for this study: (1) whether bond quality and surface characteristics change with time, and (2) the robustness of atmospheric pressure plasma treatment. Determination of if and how surface characteristics and bond quality change with time can provide information regarding whether adhesion of plasma treated surfaces was due to a functionalization or removal mechanism. Additionally, for the aerospace industry, robust processes, including surface preparation, are desired. Thus far, atmospheric pressure plasma treatment has been shown to be a promising surface preparation method that can reverse the negative effects of incorrect peel ply usage. Robustness of how long for which the surface is activated after plasma treatment was examined. Samples were exposed to a constant environment as defined in 4.2.1. Note that times even up to one week after surface preparation would not occur at an aerospace OEM.

5.4.1 DCB Testing

From G_{IC} measurements, plasma treatment was shown to maintain fracture energy up to 168 h exposure but decreased slightly at 408 h and 720 h exposure (Figure 83). This slight decrease was shown to be significant by a student t-test. However, compared to *control 1* samples, the fracture energies for all DCB specimens tested in this study were significantly higher. The high fracture energies were supported by cohesive and interlaminar failure modes (Figure 84). Failure modes were the same for all exposure times examined in this study.

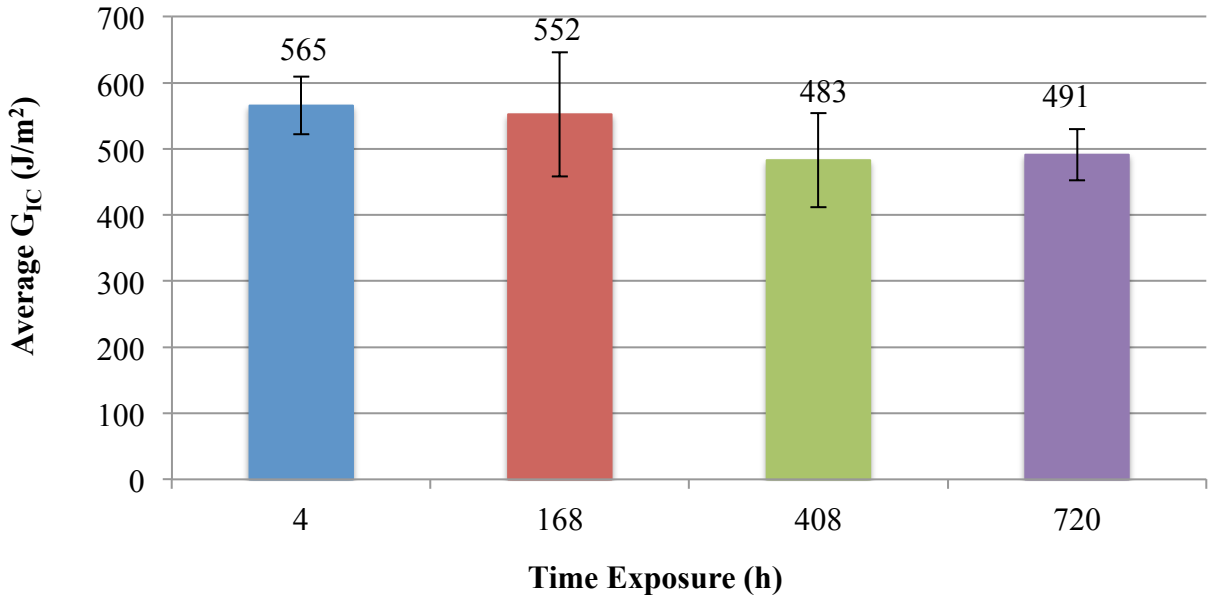

Figure 83. Fracture energies for time exposure DCB specimens with standard deviation error bars.

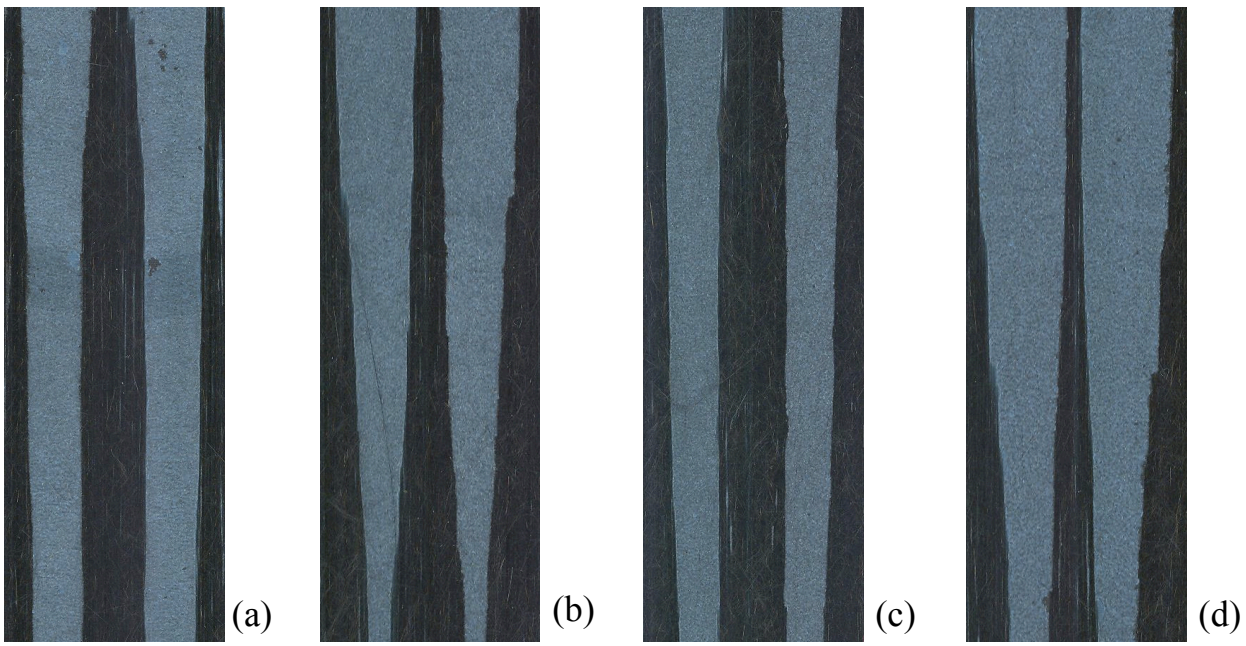

Figure 84. Representative DCB fracture surfaces for (a) 4 h, (b) 168 h, (c) 408 h, and (d) 720 h exposure times.

5.4.2 Contact Angle Measurements

CA measurements were shown to detect a difference in wetting and surface energy characteristics with increased exposure time to a constant environment (Figure 85-Figure 87). DI H_2O CAs increased gradually with exposure time. GLY increased significantly at 168 h exposure time and then remained constant to 720 h exposure. EG spontaneously wetted all surfaces and DIM remained unchanged from 4 h to 720 h exposure. The trends for DI H_2O, EG, and DIM CAs were consistent with previous research. [72]

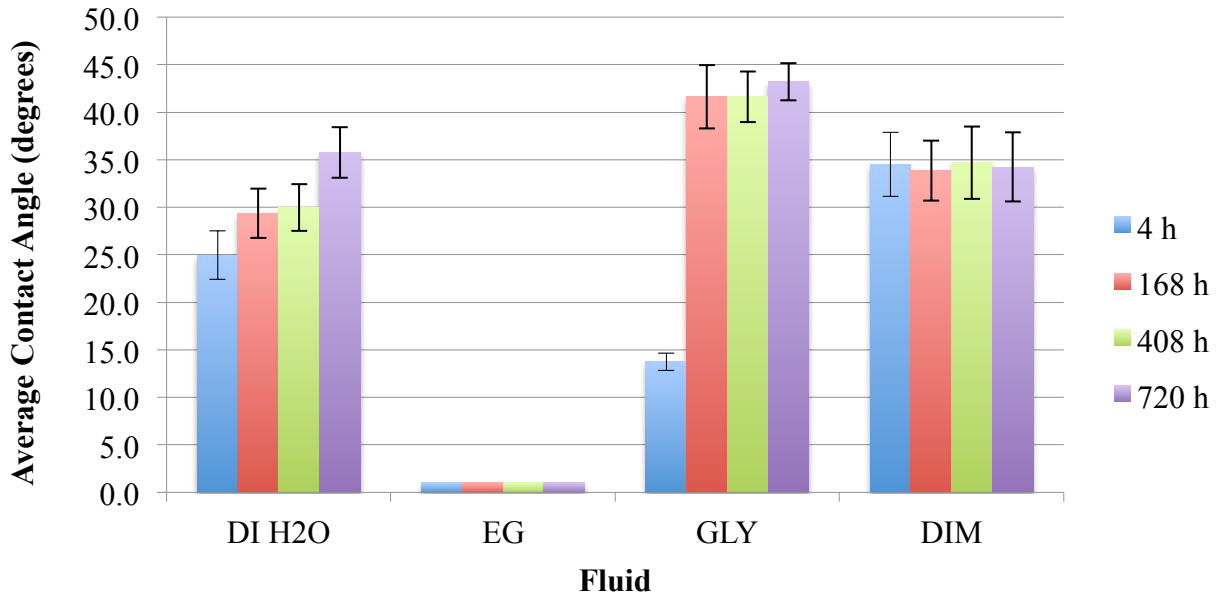

Figure 85. Average CA measurements for time exposure samples with standard deviation error bars.

Surface energies were again calculated from CA measurements. Overall, a slight decrease in polar surface energy and thus total surface energy was observed with exposure time (Figure 86). Wettability envelopes also showed a slight decrease in surface energy with exposure time, though epoxy adhesives would be expected to wet all out time samples (Figure 87). This could help explain why G_{IC} values remained high and failure modes were acceptable for samples

exposed to a constant environment for up to 720 h. This result was consistent with previous research. [72] The decrease in polar energy suggested that polar functional groups detected by XPS could be consumed upon interaction with a constant environment. This suggested that the surfaces were functionalized by atmospheric pressure plasma treatment and that the functional groups were consumed with time. In particular, carboxyl groups could react with water and thus reduce in concentration with time. However, because the change was slight, removal was not eliminated. If the remnants/interphase were removed, the surface would not be expected to change significantly with out time. Analysis of these samples by XPS was necessary to confirm if functional groups were consumed.

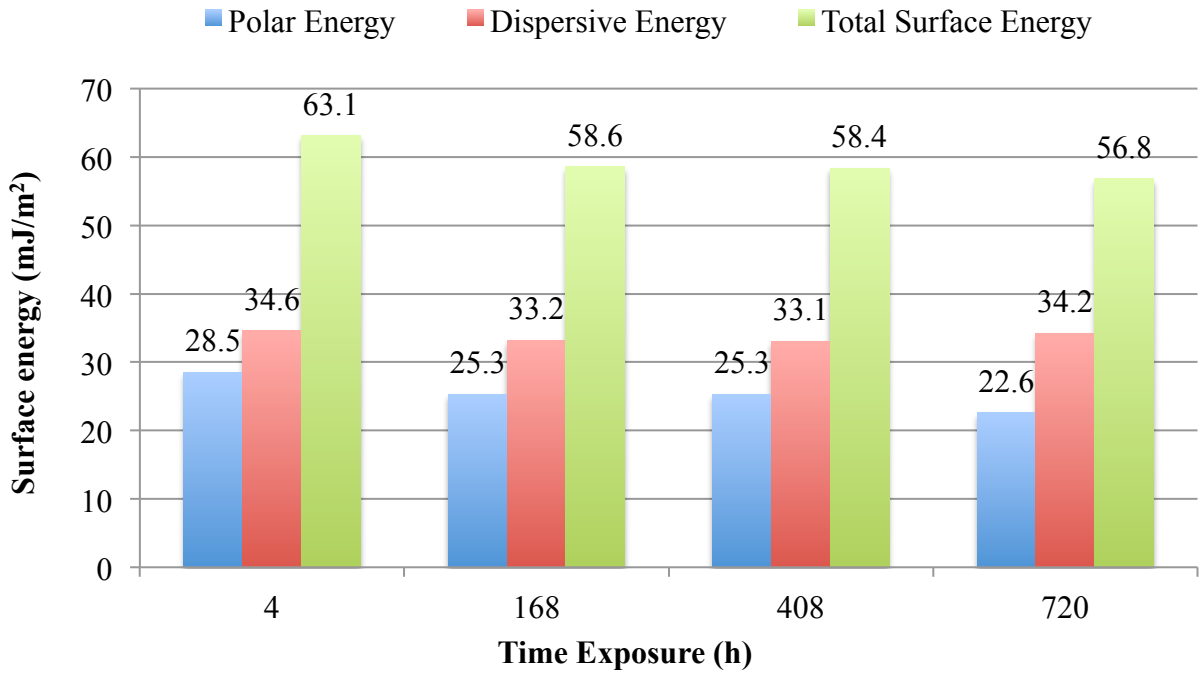

Figure 86. Surface energies for time exposure samples.

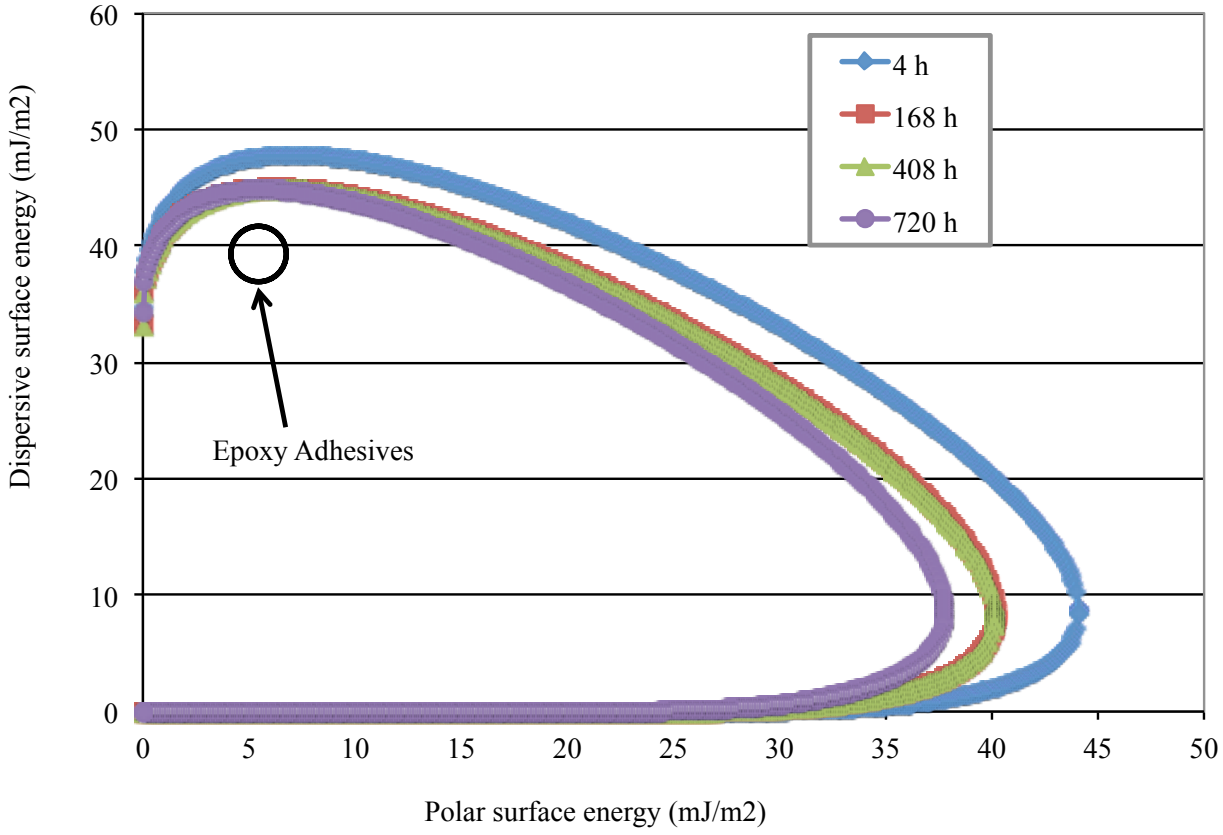

Figure 87. Wettability envelopes for time exposure samples.

5.4.3 FTIR Measurements

Shown in Figure 88 are representative spectra from each time exposure substrate (4, 168, 408, and 720 h). From initial inspection, FTIR spectra for all samples were not noticeably different. Thus, MVA was used to determine spectral differences. A PLS model using polar surface energy showed slight differences between sample sets. As shown in Figure 89, 4 h samples were grouped separately from all other out time samples. There was significant overlap between 168, 408, and 720 h samples (Figure 89). As described previously, these differences could be due to physical or chemical changes and XPS was necessary to determine surface chemistry modifications among the time exposure samples.

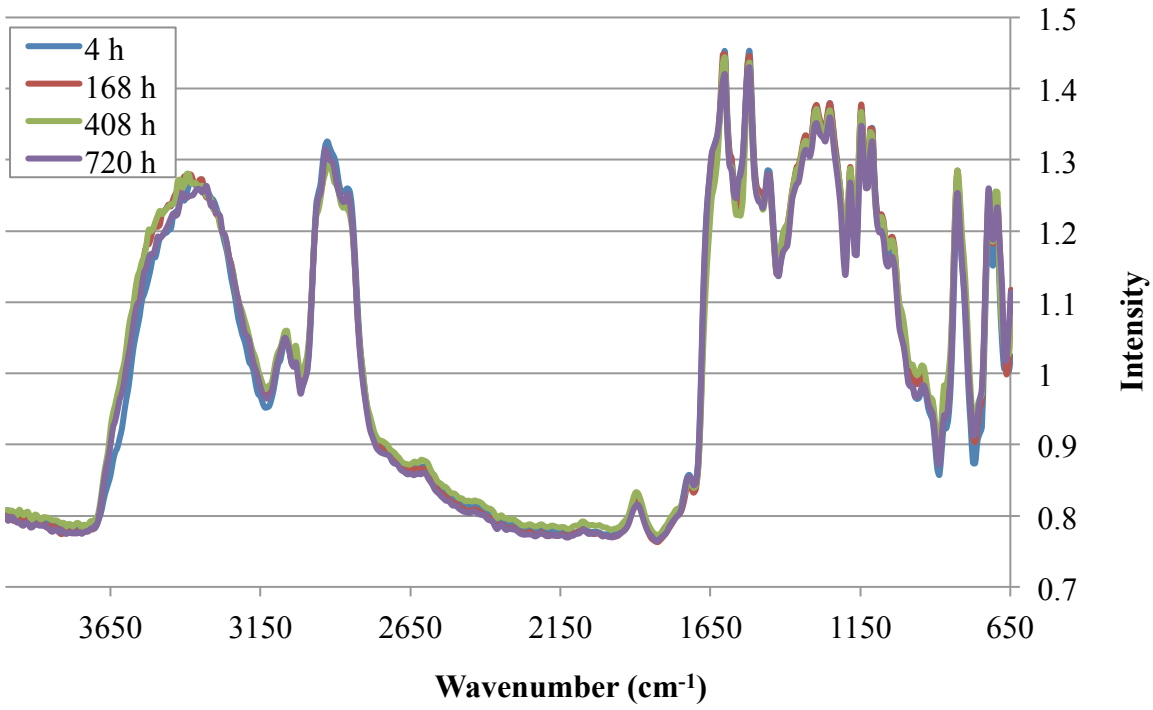

Figure 88. Representative FTIR for time exposure samples.

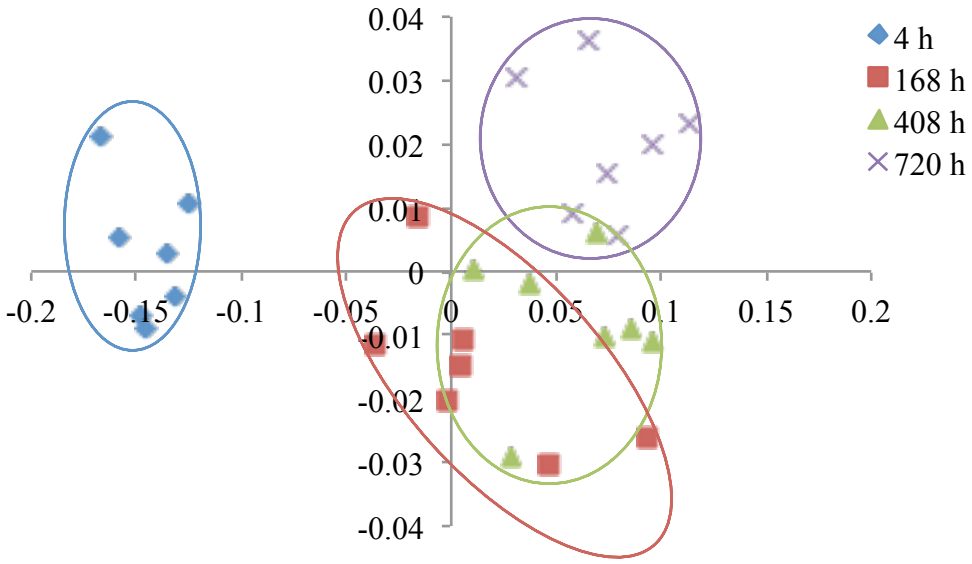

Figure 89. PLS scores plot for time exposure samples.

5.4.4 XPS Measurements

Survey and high-resolution scans were similar for all time exposure samples, which supported CA measurements. Atomic percentages determined from survey scans are shown in **Table 12**. It was observed that the percentage of carbon and nitrogen remained constant for time exposure samples. Some variations were observed but when standard deviations were considered, the differences were not significant. A slight decrease was observed in oxygen content with exposure time, suggesting that possibly some oxygen containing functional groups were consumed with time. This supports the slight decrease observed in polar surface energy described previously. Other differences that were observed among exposure samples were concentrations of sulfur, silicon, and sodium. Sulfur content increased with exposure time. Silicon and sodium were only observed on 168, 408, and 720 h samples. All of these elements could be contaminants found in a laboratory situation and could be partly responsible for a reduction in oxygen containing functional groups.

Table 12. Atomic percentages for time exposure samples.

Element		Sample			
		4 h	**168 h**	**408 h**	**720 h**
C 1s	Average	64.831	65.856	65.689	67.669
	StDev	0.760	1.299	2.812	0.562
N 1s	Average	8.279	8.126	7.204	7.511
	StDev	0.850	0.500	1.676	0.110
O 1s	Average	26.559	23.929	25.158	22.309
	StDev	0.673	0.209	1.146	0.511
S 2p	Average	0.331	0.980	1.027	0.882
	StDev	0.238	0.268	0.428	0.164
Si 2s	Average	N/A	0.749	0.401	1.120
	StDev	N/A	0.292	0.694	0.339
Na 1s	Average	N/A	0.360	0.521	0.509
	StDev	N/A	0.145	0.033	0.225

High-resolution spectra showed little differences among out time samples. All samples (4, 168, 408, 720 h) showed oxygen containing functional groups (C-O-C/C-O, C=O, and –COOH) (Figure 90-Figure 93). There was a slight decrease in the percentage of carboxyl groups on the 148, 408, and 720 h samples (Figure 91Figure 93) compared to the 4 h samples (Figure 90). This too supports functionalization. Also supporting a functionalization mechanism was the fact that

the surface chemistry was not characteristic of an untreated epoxy, which would be expected if the peel ply remnants/interphase were removed.

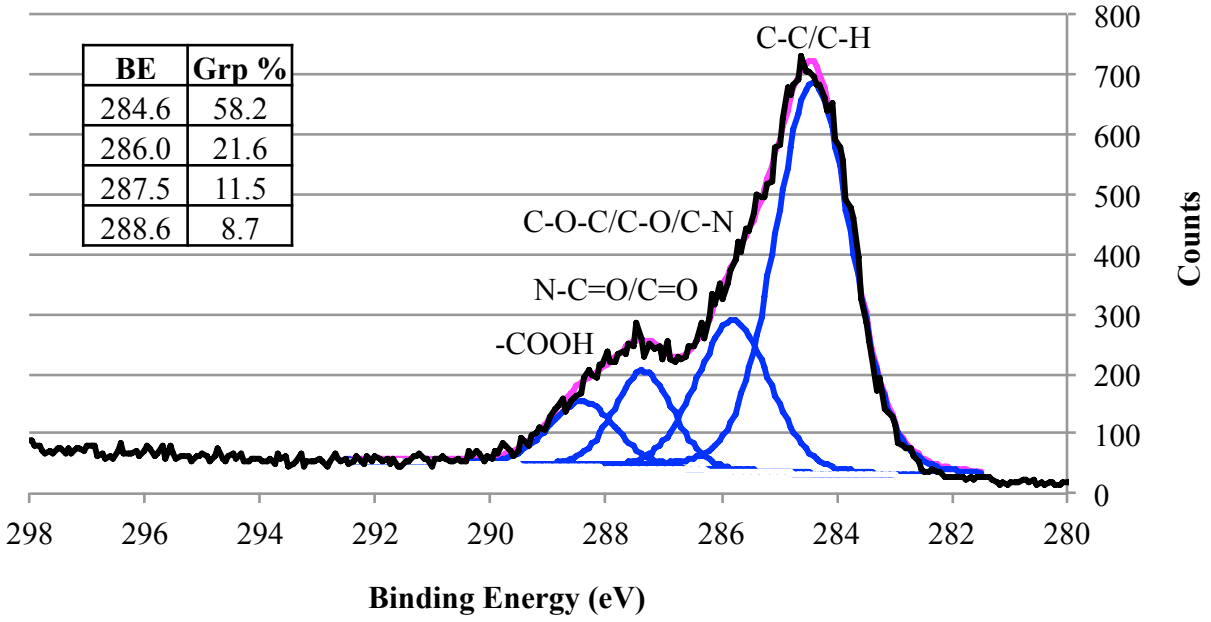

Figure 90. High-resolution carbon peak for 4 h sample.

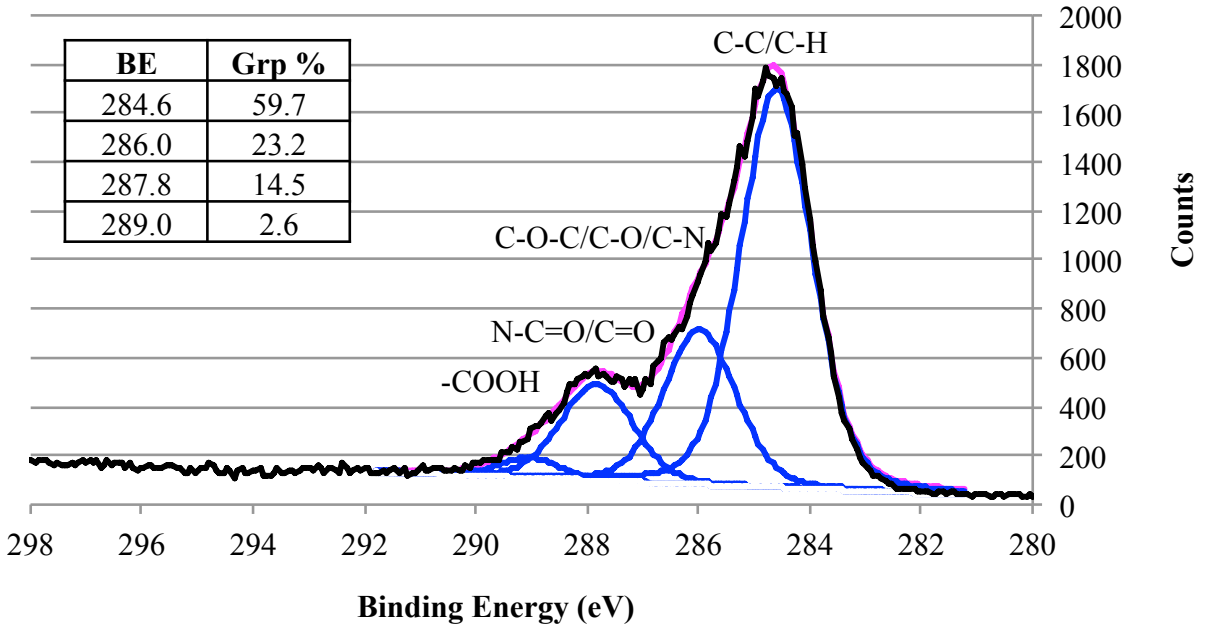

Figure 91. High-resolution carbon peak for 168 h sample.

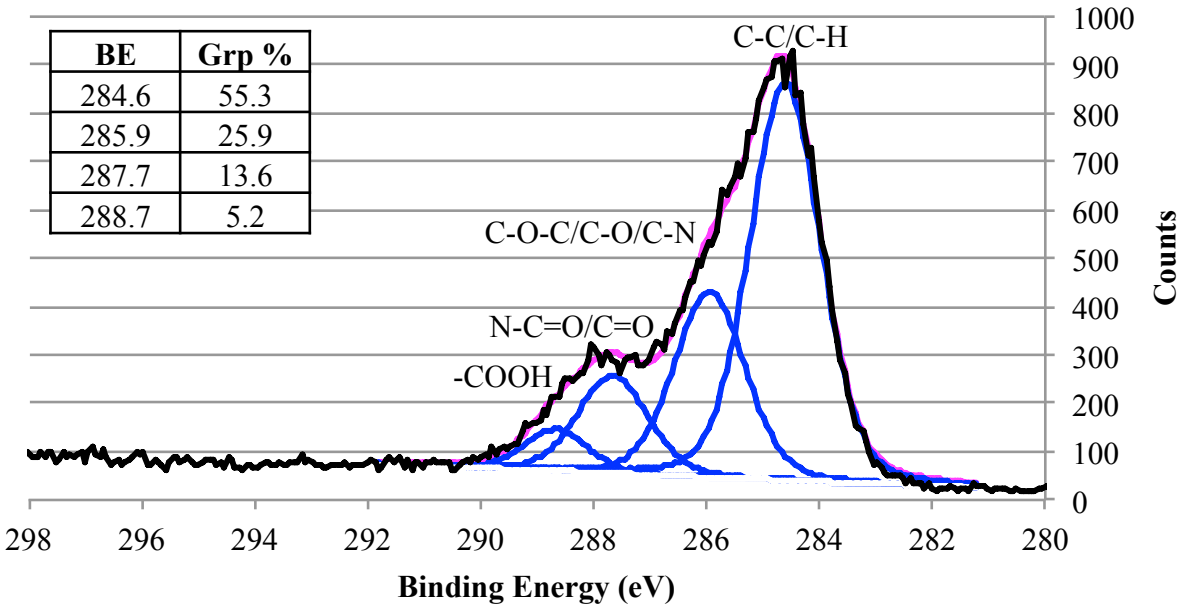

Figure 92. High-resolution carbon peak for 408 h sample.

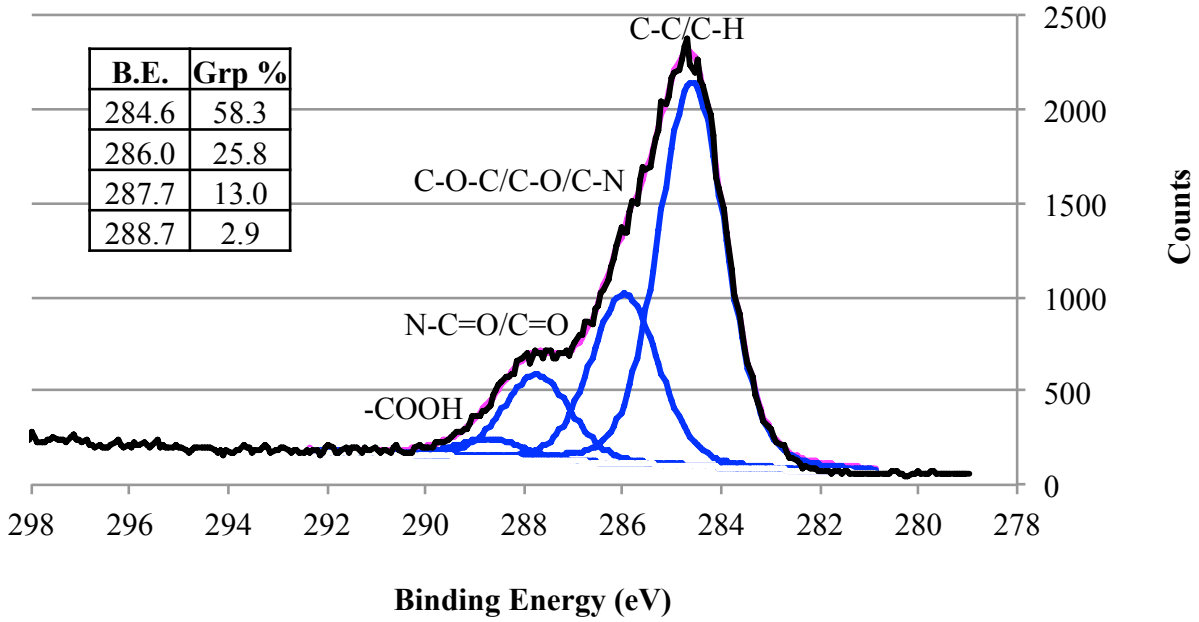

Figure 93. High-resolution carbon peak for 720 h sample.

CHAPTER 6: SUMMARY OF KEY FINDINGS

Table 13 is a summary table for surface characterization measurements to determine if the primary reason for improved adhesion was functionalization and/or removal of peel ply residue. Overall, improved adhesion was shown to be primarily due to a functionalization mechanism though removal was not entirely disproven. These results are further summarized and described in the following sections as well as the robustness of atmospheric pressure plasma treatment with respect to exposure to a controlled environment.

Table 13. Summary table

Experiment		Hypothesis Supported	Justification
Toray T800/3900-2 + PFG 52006 + plasma (different levels of plasma treatment)	CA	Functionalization and/or Removal	Surface energy changes were detected and likely due to functionalization but removal was not rejected.
	FTIR	Functionalization and/or Removal	Changes were detected which could be attributed to surface morphology changes and/or chemical changes.
	XPS	Functionalization	Nylon groups were detected on all samples but carboxyl groups were only detected on plasma treated samples, supporting functionalization. Plasma treated samples did not have a chemistry that matched that of epoxy, also supporting functionalization.
	SEM	Functionalization and Removal	Peel ply remnants were detected before and after plasma treatment that suggested functionalization but "spot-like" morphology on plasma treated surfaces suggested removal.
Toray T800/3900-2 + PFG 52006 + plasma (time exposure study)	CA	Functionalization and/or Removal	Surface energy decreased with time exposure though the decrease was slight.
	FTIR	Functionalization and/or Removal	Changes were detected which could be due to surface

			morphology changes and/or chemical changes.
	XPS	Functionalization	Carboxyl group percentages decreased with time, suggesting functional groups were consumed. At no point was the surface chemistry characteristic of that of an untreated epoxy.
Hexcel T300/F155 + PFG 60001 + plasma	CA	Functionalization and/or Removal	Surface energy changes were detected that were likely due to functionalization but removal was not eliminated.
	FTIR	Functionalization and/or Removal	Changes were detected which could be due to surface morphology changes and/or chemical changes.
	XPS	Functionalization	Polyester groups were detected on both peel ply only and plasma treated surfaces and an increase in oxygen and nitrogen containing functional groups was also detected that suggested the peel ply prepared surface was functionalized. The surface energy of plasma treated surfaces was also not characteristic of an untreated epoxy.
	SEM	Functionalization	Though the morphology of plasma treated peel ply tendrils suggested that part of the remnants could have been removed, significant amounts of peel ply remnants were detected before and after plasma treatment that suggested functionalization was the primary reason for adhesion.
MB 1515-3M + virgin and plasma treated PFG 52006	CA	Neither	No surface energy differences were detected.
	XPS	Functionalization	Nylon groups were identified on MB 1515-3M surfaces prepared with both virgin and plasma treated peel ply. However, survey scans showed more nitrogen and a higher percentage of nylon groups on MB 1515-3M surfaces prepared plasma treated peel ply compared to those

			prepared with virgin peel ply. This suggested that more nylon was transferred to the surface prepared with plasma treated peel ply, suggesting functionalization.
	SEM	Functionalization	Peel ply remnants were detected on surfaces prepared with both virgin and plasma treated peel ply, however, greater transfer of remnants was observed on MB 1515-3M prepared with plasma treated peel ply.

This work showed that atmospheric pressure plasma could change poor bonding surfaces to good bonding surfaces, primarily attributed to a functionalization mechanism. This work also supported previous research on peel ply prepared surfaces hypothesizing that weak adhesion is due to either chemical incompatibility or the thickness of a weak boundary layer proposed to form during cure. [6] From the present research, chemical incompatibility was shown to be a primary driver for weak adhesion as atmospheric pressure plasma treatment changed surface chemistry and did not entirely remove weak boundary layers, especially in the case of material system 2. However, it should be stated that although atmospheric pressure plasma treatment improved bond quality of material system 2, some adhesion failure was still observed, and thus weak adhesion due to the thickness of a weak boundary layer was not entirely disproven.

6.1 Toray T800/3900-2 + PFG 52006 Nylon Peel Ply + Atmospheric Pressure Plasma Treatment + MetlBond 1515-3M

Bond quality and surface characteristics supported a significant difference between peel ply only and plasma treated surfaces. DCB results showed that atmospheric pressure plasma treatment improved poor bonding surfaces. Overall, surface characteristics were different for *control 1* surfaces compared to those that were plasma treated after peel ply removal. These variations

could have been attributed to either functionalization or removal as shown in Table 13, though functionalization was identified as the primary reason for improved adhesion. Polar surface energy (Figure 47) displayed the potential for predicting adhesion where polar energies above 27.3 mJ/m^2 exhibited good bond quality (high G_{IC} values and < 1% adhesion failure) and those below exhibited significant amounts of adhesion failure. XPS data collected to date does not show potential to predict adhesion though future studies could further explore this.

6.2 Time Exposure to a Constant Environment – Material System 1

Atmospheric pressure plasma treatment of Toray T800/3900-2 CFRP prepared with PFG 52006 supported both functionalization and removal mechanisms. The slight changes in surface energy measurements suggested functionalization though they did not rule out removal. XPS measurements suggested functionalization as carboxyl functional groups reacted and were thus consumed with time exposure to a constant environment. Additionally, none of the plasma treated surfaces had chemistries that were characteristic of an untreated epoxy, which would have supported a removal mechanism. Atmospheric pressure plasma treatment of Toray T800/3900-2 CFRP prepared with PFG 52006 was also shown to be a robust surface preparation method for bonding with MB 1515-3M. Acceptable failure modes and high G_{IC} values were observed up to 720 h after plasma treatment. Surface characteristics changed slightly with out time (lower surface energy and detection of contaminants [Si, Na] on 168, 408, and 720 h samples), however, surface energies remained high and oxygen containing functional groups were still present on all exposure samples, in contrast to *control 1* specimens that had lower surface energies and no carboxyl groups. Overall, atmospheric pressure plasma treatment has shown potential as a robust surface preparation method for composite bonding.

6.3 Hexcel T300/F155 + PFG 60001 Polyester Peel Ply + Atmospheric Pressure Plasma Treatment + EA 9696

Similar to material system 1, plasma treatment had a significant effect on bond quality and surface characteristics. Compared to material system 1, PFG 60001 polyester preparation of Hexcel T300/F155 resulted in significantly more peel ply remnants upon peel ply removal. Because adhesion occurred after plasma treatment, even though significant amounts of peel ply remnants were still present, functionalization was supported. Though removal was not entirely disproven, these results supported that the primary reason for improved adhesion of composites prepared with the incorrect peel ply was due to functionalization of the surface.

6.4 Interaction of MetlBond 1515-3M and PFG 52006 Nylon Peel Ply

CA measurements were inconclusive in determining a difference between MB 1515-3M surfaces prepared with virgin and plasma treated PFG 52006 nylon peel ply. XPS survey scans showed more nitrogen and a higher percentage of nylon groups on MB 1515-3M surfaces prepared with plasma treated peel ply compared to those prepared with virgin peel ply. The nitrogen could be ascribed to more nylon transfer to the surface. SEM supported that more nylon peel ply remnants were present on surfaces prepared with plasma treated peel ply compared to ones prepared with virgin peel ply. XPS also showed that plasma treated PFG 52006 had carboxyl functional groups present on the surface, whereas virgin PFG 52006 did not, further supporting a functionalization mechanism. XPS and SEM supported that the primary reason for improved adhesion of composites after plasma treatment that were originally prepared with the incorrect peel ply was due to functionalization of the surface.

CHAPTER 7: FUTURE WORK

Future work could include further examination of how atmospheric pressure plasma treatment changes the surface of composite materials to promote adhesive bonding. This involves application to other material systems with and without peel ply preparation. In the case of peel ply prepared composites treated with subsequent atmospheric pressure plasma, additional surface characterization techniques could be used to determine variations in thickness of interphases/remnants created upon peel ply removal. These techniques may include dynamic SIMS, XPS coupled with an ion etch gun, and angle dependent XPS. Additionally, for as-tooled surfaces prepared with release agents and films prior to atmospheric pressure plasma treatment, atomic force microscopy (AFM) could be of interest. Not only would traditional AFM be of interest for morphological information, but also AFM modified with epoxy-functionalized tips could offer information about the interaction between an epoxy adhesive in contact with a plasma treated composite surface. Profilometry measurements or confocal microscopy would also be useful to measure surface roughness both attributed to peel ply as well as to atmospheric pressure plasma treatment.

Time exposure studies examining the Toray T800/3900-2 CFRP prepared with PFG 52006 and atmospheric pressure plasma treatment supported a functionalization mechanism. Also primarily supporting a functionalization mechanism was Hexcel T300/F155 CFRP prepared with PFG 60001 and plasma treatment, because significant amounts of peel ply remnants were still present after plasma treatment. Examining the Hexcel T300/F155 CFRP prepared with PFG 60001 peel ply in terms of a similar out time study would further support whether functionalization or removal is the primary mechanism for adhesion. It would be interesting to determine how these time exposure results compare to those of the present research.

Also relevant and important for future study is examining the long-term durability of adhesive bonds, particularly those where the composite is prepared with peel ply and subsequent atmospheric pressure plasma treatment. All bonded samples studied in this research were tested at ambient conditions within a couple of weeks of bonding operations. Hot/wet conditioning or thermal cycling could help understand what type of bonding (e.g. chemical, mechanical, etc.) is responsible for adhesion. If bonds maintain their toughness after environmental and/or thermal cycling, that would support the formation of covalent chemical bonds between the adhesive and the composite.

Ultimately, future studies further examining peel ply and atmospheric pressure plasma treatment as surface preparation methods for composite bonding would help fundamentally determine why improved adhesion occurs. These studies would contribute to the overall understanding of how polymer matrix composites and adhesives interact during bonding in terms of surface energy, surface chemistry, and morphological properties of the materials.

REFERENCES

[1] L. J. Hart-Smith, D. Brown, and S. Wong, "Surface Preparations for Ensuring that the Glue will Stick in Bonded Composite Structures," *10th DoD/NASA/FAA Conference on Fibrous Composites in Structural Design*, November 1993.

[2] J. Bardis and K. Kedward, in *DOT/FAA/AR-03/53*, 2004.

[3] W. N. Delgass and R. G. Cooks, "Focal Points in Mass Spectroscopy," *Science*, pp. 545-53, 1987.

[4] D. A. Jesson and J. F. Watts, "The interface and interphase in polymer matrix composites: effect on mechanical properties and methods for identification," *Polymer Reviews*, vol. 52, pp. 321-354, 2012.

[5] A. J. Kinloch, *Adhesion and Adhesives Science and Technology*. New York: Chapman and Hall, 1987.

[6] M. K. Moench, "The Effect of Nylon and Polyester Peel Ply Surface Preparation on the Bond Quality of Composite Laminates," Materials Science and Engineering, University of Washington, Seattle, Ph. D. Dissertation 2013.

[7] Joel R. Fried, *Polymer Science & Technology*. Upper Saddle River, NJ, USA: Pearson Education, Inc., 2003.

[8] R. B. Prime, "Chapter 6: Thermosets," in *Thermal Characterization of Polymeric Materials*, Edith A. Turi, Ed. San Diego, CA, USA: Academic Press, 1997.

[9] Ryan E. Toivola, "Mechanochromic Fluorescent Probe Molecules for Damage Detection in Aerospace Polymers and Composites," Materials Science and Engineering, University of Washington, Seattle, PhD Thesis 2013.

[10] Massachusetts Institute of Technology. (2003) MIT OpenCoursWare. [Online]. http://ocw.alfaisal.edu/OcwWeb/Materials-Science-and-Engineering/3-064Polymer-EngineeringFall2003/CourseHome/index.htm

[11] Flake C. Campbell, *Manufacturing Processes For Advanced Composites*. New York, NY, USA: Elsevier Inc., 2004.

[12] K. C. Cole, "A New Approach to Modeling the Cure Kinetics of Epoxy Amine Thermosetting Resins," *Macromolecules*, vol. 24, pp. 3093-97, 1991.

[13] Leon Shechter, John Wynstra, and Raymond P. Kurkjy, "Glycidyl Ether Reactions with Amines," *Industrial and Engineering Chemistry*, vol. 48, no. 1, pp. 94-7, January 1956.

[14] R. Bossi, R. Carlsen, F. J. Boerio, and G. Dillingham, "Composite Surface Preparation QA for Bonding," in *SAMPE 2005*, Long Beach, 2005.

[15] F. J. Boerio, B. Roby, R. G. Dillingham, R. H. Bossi, and R. L. Crane, "Effect of Grit Blasting on the Surface Energy and Composition of Graphite/Epoxy Composites," in *37 ISTC*, Seattle, 2005.

[16] Kay Y. Blohowiak, Peter J. Van Voast, Paul H. Shelley, and Jake W. Grob, "Nonchemical Surface Treatments Using Energetic Systems for Structural Adhesive Bonding," in *SAMPE 2010*, Seattle, 2010.

[17] M. A. Belcher, C. J. Wohl, J. W. Hopkins, and J. W. Connell, "Laser Surface Preparation and Bonding of Aerospace Structural Composites," in *SAMPE 2010*, Seattle, 2010.

[18] C. David Warren, Felix L. Paulauskas, and Raymond G. Boeman, "Laser Ablation Assisted Adhesive Bonding of Automotive Structural Composites," in *12th International Conference on Composite Materials*, Paris, France, 1999.

[19] R. J. Zaldivar, J. Nokes, G. L. Steckel, H. I. Kim, and B. A. Morgan, "The Effect of Atmospheric Plasma Treatment on the Chemistry, Morphology and Resultant Bonding Behavior of a Pan-Based Carbon Fiber-Reinforced Epoxy Composite," *Journal of Composite Materials*, vol. 44, no. 2, pp. 137-56, 2010.

[20] B. Clark and B. Flinn, "Evaluation of Nylon and Polyester Peel Plies Using the Rapid Adhesion Test," in *SAMPE 2007*, Baltimore, 2007.

[21] M. Kanerva and O. Saarela, "The peel ply surface treatment for adhesive bonding of composites: A review," *International Journ. of Adhesion & Adhesives*, vol. 43, pp. 60-69, 2013.

[22] L. J. Hart-Smith, G. Redmond, and M. J. Davis, "The Curse of the Nylon Peel Ply," in *41st SAMPE International Syposium and Exhibition*, 1996.

[23] M. Phariss and B. Flinn, "The Effect of Peel-Ply Surface Preparation Variables on Bond Quality," in *DOT/FAA/(AR)-06/28*, 2006.

[24] B. D. Flinn and C. W. Hickmott, "Effect of Surface Preparation Technique on Bond Quality of AGATE Composite Laminates," in *SAMPE 2009*, Baltimore, MD.

[25] B. D. Flinn, B. K. Cark, J. Satterwhite, and P. J. Van Voast, "Influence of Peel Ply Type on Adhesive Bonding of Composites," in *SAMPE 2007*, Baltimore, MD, 2007.

[26] ASTM D5573 Standard Practice for Classifying Failure Modes in Fiber-Reinforced-Plastic (FRP) Joints, 2012, www.astm.org.

[27] M. A. (Tony) Belcher, K. L. Krieg, P. J. Van Voast, and K. Y. Blohowiak, "Nonchemical Surface Treatments Using Atmospheric Plasma Systems for Structural Adhesive Bonding," in *SAMPE 2013*, Long Beach, CA, 2013.

[28] R. A. Wolf, *Atmospheric Pressure Plasma for Surface Modification*. Hoboken: Wiley, 2012.

[29] Alexander Fridman and Lawrence A. Kennedy, *Plasma Physics and Engineering*, 2nd ed. Boca Raton, FL: CRC Press, 2011.

[30] Plasmatreat - Plasma Technology. [Online]. http://www.plasmatreat.ca/

[31] Javier Sanchez Serrano, "Surface Modifications of Composite Materials by Atmospheric Pressure Plasma Treatment," Materials Science and Engineering, Universidad Rey Jaun Carlos, PhD Thesis 2011.

[32] Claire Tendero, Christelle Tixier, Pascal Tristant, Jean Desmaison, and Philippe Leprince, "Atmospheric pressure plasmas: A review," *Spectrochimica Acta Part B*, vol. 61, pp. 2-30, 2006.

[33] M. Noeske, J. Degenhardt, S. Strudthoff, and U. Lommatzsch, "Plasma jet treatment of five polymers at atmospheric pressure: surface modifications and the relevance for adhesion," *International Journal of Adhesion & Adhesives*, vol. 24, pp. 171-7, 2004.

[34] N. Encinas, B. Diaz-Benito, J. Abenojar, and M. A. Martinez, *Surf. & Coat. Technol.*, vol. 205, no. 2, pp. 396-402, 2010.

[35] N. Encinas, J. Abenojar, and M. A. Martinez, *International Journal of Adhesion & Adhesives*, vol. 33, pp. 1-6, 2012.

[36] B. Boschmans et al., "Static secondary ion mass spectrometry (S-SIMS) analysis of atmospheric plasma treated polypropylene films," *Applied Surface Science*, vol. 252, pp. 6660-3, 2006.

[37] N. Encinas et al., "Surface modification of aircraft used composties for adhesive bonding," *International Journal of Adhesion & Adhesives*, vol. 50, pp. 157-63, April 2014.

[38] R. Crossley, S. Ratchev, and A. Smith, "Emerging Technologies for Use in Aerospace Bonded Assemblies," *SAE Int. J. Aerosp.*, vol. 6, no. 2, 2013.

[39] Prof. Allan S. Hoffman, Liquid and Solid Surface Energies: Liquid Contact Angles on Solid Surfaces, April 27, 2012, Modified Slide.

[40] I. Hatsuo, *Characterization of Composite Materials*. New York, NY: Momentum Press, 2010, eBook.

[41] D. A. Skoog, J. Holler, and S. R. Crouch, *Principles of Instrumental Analysis*, 6th ed.: Thomson Brooks/Cole, 2007.

[42] J. C. Vickerman, *Surface Analysis, The Principle Techniques*. New York, NY: Wiley, 1997.

[43] J. C. Vickerman and D. Briggs, Eds., *TOF-SIMS: Materials Analysis by Mass Spectrometry*, 2nd ed. UK: IM Publications LLP and SurfaceSpectra Limited, 2013.

[44] Joseph Goldstein et al., *Scanning Electron Microscopy and X-Ray Microanalysis*, 3rd ed. New York, NY, USA: Springer, 2003.

[45] E. M. Slayter and H. S. Slayter, *Light and Electron Microscopy*. New York, NY: Cambridge Univ. Pr., 1993.

[46] J. Satterwhite, J. Aubin, and B. D. Flinn, "Partial Laminate Curing for use in Peel Ply-Prepared Adhesive Bonding," in *SAMPE 2009*, Baltimore, 2009.

[47] Arthur W. Adamson, *Physical Chemistry of Surfaces*, 3rd ed. New York, NY, USA: John Wiley & Sons, 1976.

[48] Mark Strobel and Christopher S. Lyons, "Thoughts on Contact Angles and Wettibility," 3M Company Corporate Process Research Laboratory, 3M, St. Paul, MN,.

[49] D. K. Owens and R. C. Wendt, "Estimation of the Surface Free Energy of Polymers," *Journ.*

of Appl. Poly. Sci., vol. 13, pp. 1741-47, 1969.

[50] M. E. Petrie, *Handbook of Adheisves and Sealants*. New York, NY: McGraw-Hill Professional, 2000.

[51] M. Zenkiewicz, *Journ. of Achieve. in Mater. and Mfg.*, vol. 24, no. 1, 2007.

[52] C. J. van Oss, R. J. Good, and M. K. Chaudhury, "Additive and Nonadditive Surfae Tension Components and the Interpretation of Contact Angles," *Langmuir*, vol. 4, pp. 884-91, March 1988.

[53] W. A. Zisman, "Relation of the Equilibrium Contact Angle to Liquid and Solid Constitution," *Advances in Chemistry Series*, vol. 43, pp. 1-51, 1964.

[54] M. E. R. Shanahan Greiveldinger, *Surf. Inter. Films*, vol. 327, no. II, 1999.

[55] Amer Al-Shareef, P. Neogi, and Baojun Bai, "Force based dynamic contact angles and wetting kinetics on a Wilhelmy plate," *Chemical Engineering Science*, vol. 99, pp. 113-17, 2013.

[56] Russell Stacy, "Contact Angle Measurement Technique for Rough Surfaces," Mechanical Engineering, Michigan Technilogical University, MS 2009.

[57] S. A. Page, J. C. Berg, and J.-A. E. Manson, "Characterization of epoxy resin surface energetics," *Journal of Adhesion Science and Technology*, vol. 15, no. 2, pp. 153-70, 2001.

[58] H. Balard, A. Saada, J. Hartmann, O. Aouadj, and E. Papirer, *Macrom. Symp.*, vol. 108, 1996.

[59] H. J. Busscher, A. W. J. Van Pelt, P. de Boer, H. P. de Jong, and J. Arends, *Coll. and Surf.*, vol. 9, 1984.

[60] Y. H. Mori, G. M. van de Ven, and S. G. Mason, *Coll. and Surf.*, vol. 4, 1982.

[61] J. F, Oliver, C. Huh, and S. G. Mason, "Coll. and Surf.," vol. 1, 1980.

[62] R. G. Dillingham and B. R. Oakley, "Surface Energy and Adhesion in Composite-Composite Adhesive Bonds," *The Journal of Adhesion*, vol. 82, pp. 407-26, 2006.

[63] A. C. Tracey, B. D. Flinn, K. Blohowiak, P. Van Voast, and W. Grace, "Effect of Variables on Contact Angle Measurements for Peel Ply Composite Sufaces," in *SAMPE 2010*, Seattle, 2010.

[64] B. C. Smith, *Fundamentals of Fourier Transform Infrared Spectroscopy*. Boca Raton, FL: CRC Press, Inc., 1996.

[65] J. Seelenbinder, Rapid identification of o-rings, seals and gaskets using the handheld Agilent 4100 ExoScan FTIR, 2012.

[66] A. C. Ferrari, S. E. Rodil, and J. Robertson, *Phys. Rev. B.*, vol. 67, no. 15, 2003.

[67] A. V. Pocius, *Adhesion and Adhesives Technology, An Introduction*, 2nd ed. Cincinnati, OH: Hanser Gardner Publications, Inc., 2002.

[68] ASTM D5528 Standard Test Method for Mode I Interlaminar Fracture Toughness of Unidirectional Fiber-Reinforced Polymer Matrix Composites, 2012, www.astm.org.

[69] Donald Adam, "Mixed-mode fracture toughness of composites," *High Performance Composites*, September 2009.

[70] P. J. Van Voast et al., "Effect of Varying Levels of Peel Ply Contamination on Adhesion Threshold," in *SAMPE 2010*, Seattle, WA, 2010.

[71] Peter J. Van Voast, Kay Y. Blohowiak, John C. Osborne, and M. A. (Tony) Belcher, "Rapid Test Methods for Adhesives and Adhesion," in *SAMPE 2013*, Long Beach, CA, 2013.

[72] Nina R. Gerber, Ashley C. Tracey, and Brian D. Flinn, "Effect of Time After Atmospheric

Pressure Plasma Treatment on Surface Characteristics and Bond Quality," in *CAMX 2014*, Orlando, FL, 2014.

[73] J. R. Chamberlain and V. L. Robertshaw, Wettability of Swellable Nonwovens: Determination of Contact Angle Against Swellable Nonwoven Material, 2004.

[74] C. Rulison, "So You Want to Measure Surface Energy?," in *Technical Note #306*, 1999.

[75] M. Tuttle, WET v 1.0, 2005, personally distributed executable for generating wetting envelopes.

[76] E. M. Enlow, J. L. Kennedy, A. A. Nieuwland, J. E. Kendrix, and S. L. Morgan, "Discrimination of Nylon Polymers Using Attenuated Total Reflection Mid-Infrared Spectra and Multivariate Statistical Techniques," *Applied Spectroscopy*, vol. 59, no. 8, 2005.

[77] Tucker Layne Howie, "Detection of Incipient Thermal Damage Of Carbon Fiber/Epoxy Composites Using Fluorescent Thermal Damage Probes," Materials Science and Engineering, University of Washington, Seattle, PhD Thesis 2013.

[78] J. H. Hwang, C. S. Lee, and W. Hwang, "Effect of Crack Propagation Directions on the Interlaminar Fracture Toughness of Carbon/Epoxy Composite Materials," *Applied Composite Materials* , vol. 8, no. 6, pp. 411-33, 2001.

[79] Kelsi M. Hurley and Brian D. Flinn, "Effect of Fiber Orientation on the Fracture of Woven Composite Laminates," in *SAMPE 2010 Student Research Symposium*, Seattle, WA, 2010.

[80] K. de la Caba, P. Guerrero, I. Mondragon, and J. M. Kenny, "Comparative Study by DSC and FTIR Techniques of an Unsaturated Polyester Resin Cured at Different Temperatures," *Polymer International*, vol. 45, no. 4, pp. 333-38, 1998.

[81] J. P. Hobbs, C. S. P. Sung, K. Krishnan, and S. Hill, "Characterization of Surface Structure

and Orientation in Polypropylene and Poly (ethylene terephthalate) Films by Modified Attenuated Total Reflection IR Dichroism Studies," *Macromolecules*, vol. 16, no. 2, pp. 193-99, 1983.

[82] F. U. Buehler and J. C. Seferis, "Effect of reinforcement and solvent content on moisture absorption in epoxy composite materials," *Composites Part A: Applied Science and Manufacturing*, vol. 31, no. 7, pp. 741-48, July 2000.

[83] Hemi N. Nae, "Cure and Thermal Properties of Brominated Epoxy Systems," *Journal of Applied Polymer Science*, vol. 33, no. 4, pp. 1173-85, March 1987.

[84] A. I. Balabanovich, A. Hornung, D. Mertz, and H. Seifert, "The effect of a curing agent on the thermal degradation of fire retardant brominated epoxy resins," *Polymer Degradation and Stability* , vol. 85, no. 1, pp. 713-23, July 2004.

[85] L. M. Galantucci, A. Gravina, G. Chita, and M. Cinquepalmi, "Surface treatment for adhesive-bonded joints by excimer laser," *Composites Part A*, vol. 27A, no. 11, pp. 1041-49, 1996.